12-2014

Wear Resistant Polydopamine/PTFE Nanoparticle Composite Coating for Dry Lubrication Applications

Samuel George Beckford
University of Arkansas, Fayetteville

Wear Resistant Polydopamine/PTFE Nanoparticle Composite Coating for Dry Lubrication Applications

Wear Resistant Polydopamine/PTFE Nanoparticle Composite Coating for Dry Lubrication Applications

A dissertation submitted in partial fulfillment
of the requirements for the degree of
Doctor of Philosophy in Microelectronics-Photonics

by

Samuel Beckford
John Brown University
Bachelor of Science in Mechanical Engineering, 2003
University of Arkansas
Master of Science in Mechanical Engineering, 2011

December 2014
University of Arkansas

This dissertation is approved for recommendation to the Graduate Council.

Dr. Min Zou
Dissertation Director

Dr. Andrew Wang
Committee Member

Dr. Jingyi Chen
Committee Member

Dr. Keith Roper
Committee Member

Professor Ken Vickers
Ex-Officio Member

The following signatories attest that all software used in this dissertation was legally licensed for use by Samuel Beckford for research purposes and publication.

Samuel Beckford, Student	Dr. Min Zou, Dissertation Director

This dissertation was submitted to http://www.turnitin.com for plagiarism review by the TurnItIn company's software. The signatories have examined the report on this dissertation that was returned by TurnItIn and attest that, in their opinion, the items highlighted by the software are incidental to common usage and are not plagiarized material.

Dr. Rick Wise, Program Director	Dr. Min Zou, Dissertation Director

Abstract

This dissertation presents an investigation into the effect of nanoparticle fillers and a polydopamine adhesive primer on the tribological performance of thin PTFE films. The principal objective of this investigation was to reduce wear in PTFE films, an issue which precludes the use of PTFE films in tribological applications requiring high durability. The friction and wear of the composite films were evaluated using a ball-on-flat configuration in linear reciprocating motion. It was found that the use of a polydopamine adhesive primer reduces the wear of PTFE films more than 600 times. X-ray photoelectron spectroscopy (XPS) results show that a tenacious layer of PTFE remains adhered to the polydopamine primer, which enables the durability of the polydopamine/PTFE film. Furthermore, the combination of a polydopamine primer, Cu nanoparticle fillers in the PTFE film, and optimal fabrication processes provided a collective effect that increased the wear life of PTFE films by more than 940 times. Because of the relatively low thickness of the film, it shows great potential for use in applications where durable, thin films are desirable.

Acknowledgements

Philippians 4:13 states, “I can do all things through Christ who strengthens me”. It is only through Him that I have achieved this accomplishment and I am forever thankful.

I would like to thank my mother, Fidelia Beckford, for her love and support; her encouragement has given me the motivation I needed to see this through to the end.

Also, a special thanks to Dr. Min Zou, my graduate advisor, for her mentorship and patience the last five years. It has been a long road, but the lessons learned are invaluable to me. Thank you for giving me the opportunity to work with you and my fellow lab mates, Corey Thompson, Drew Fleming, and Justin Carter.

To my lab mates, I can’t say that I will miss our weekly meetings, but without a doubt those discussions were very instrumental in my research. A special thanks to each of you for your collaboration and feedback when I needed it.

Finally, I would like to acknowledge the Electron Optics Facility (EOF) of the University of Arkansas for granting us access to their facility and equipment. Surface characterization using SEM and XPS was carried out in this facility.

This work was supported in part by the National Science Foundation under Grants CMS-0645040 and EPS-1003970, and in part by the Arkansas Biosciences Institute. Any opinions, findings, and conclusions or recommendations expressed in this material are those of the author and do not necessarily reflect the views of the National Science Foundation or Arkansas Biosciences Institute.

Dedication

This dissertation is dedicated to my mother, Fidelia Beckford.

Table of Contents

List of Figures

List of Tables

List of Published Material

Chapter 6. Wear Resistant PTFE/Silica Nanoparticle Composite Film:

This chapter is derived in part from an article published in Tribology Transactions on 20 September 2011, available online: http://www.tandfonline.com/10.1080/10402004.2011.606962.

Chapter 7. Use of gold Nanoparticle filled PTFE films to produce low friction and low wear surface coatings:

This chapter is derived in part from an article published in Tribology Letters on 11 September 2014. The final publication is available at Springer via http://dx.doi.org/ 10.1007/s11249-014-0402-4

Chapter 8. Wear resistant PTFE thin Film Enabled by a Polydopamine Adhesive Layer:

This chapter is derived in part from an article published in Applied Surface Science, Vol 292, on 15 February 2014, DOI# 10.1016/j.apsusc.2013.11.143. The final publication is available at Science Direct via http://www.sciencedirect.com/science/article/pii/S0169433213022320

Chapter 1

Introduction

It is estimated that at least one third of all energy produced is lost to friction and wear annually [1]. These losses include energy required to overcome friction during machine operation, as well as energy spent in the maintenance of part failure resulting from wear [2]. Traditionally, petroleum based oils and greases have played a dominant role in applications requiring lubrication. However, with new technology needing lubrication in extreme conditions such as high temperature, high pressure, maintenance free systems, low emission systems, and use in high vacuum [3], much emphasis has been placed on the development of effective solid lubricants. Using recent advances in coating technology, it is now possible to apply these solid lubricants as thin film coatings possessing low friction and wear resistant properties. These films have the potential of being used for applications in MEMS devices, biomedical devices, and machine components in general to reduce energy losses due to friction and wear.

Polytetrafluoroethylene (PTFE), which is used as a non-stick coating in cookware and commonly known by its brand name Teflon, has particularly drawn much attention. PTFE is attractive as a lubricant thin film because of its exceptionally low coefficient of friction (COF). However, PTFE is highly susceptible to wear, and as such, PTFE alone cannot be used in most applications. Because of this, many investigations have focused on creating PTFE composites that possess a greater wear resistance.

Table 1.1 presents a list of five PTFE composite coatings that have been studied in the past [4-8]. Some of these show significant wear reduction; however, there is still much room for improvement. Of these films, the most common coating seen in industry today is electroless Ni-P-PTFE [7]. It is mainly used in the prevention of galling in screws, splines and clutches.

However, its uses as a lubricant are limited because of its relatively high COF. PTFE alone typically exhibits a COF that ranges between 0.03 and 0.15 and a wear rate between 10^{-3} and 10^{-5} $mm^3/(N \cdot m)$ [9], depending on the testing conditions. In Table 1.1, it can be seen see that the COFs of the majority of the composite films are outside the typical range for pure PTFE. The coatings listed in Table 1.1 will be discussed in detail in Chapter 2.

Table 1.1: State-of-the-Art PTFE and PTFE composites coatings [4-8].

Film composition	Counterface	Sliding speed	Load	Film thickness	Coefficient of Friction		Wear		
					w/o filler	w/ filler	w/o filler	w/ filler	% change
PTFE + nanodiamond	Si_3N_4 ball (5.6 mm ø)	1 cm/s	0.8 N	30 µm	0.21	0.16	0.85 mm wear width	0.44 mm wear width	-48.2
Al_2O_3-TiO_2/PTFE	100C6 steel (6 mm ø)	50 cm/s	5 N	-	-	0.40	-	-	
RF sputtered PTFE		1 cm/s	5 N	1 µm	0.15	0.30	3.1×10^{-6} mm^2/traverse	2.0×10^{-7} mm^2/traverse	-90
Electroless Ni-PTFE	Al_2O_3 pin (9 mm ø)	20 cm/s	10 N	15 µm	-	0.48	-	0.36×10^{-6} mm^3/Nm	
PTFE-Epoxy	carbon steel (4.8 mm ø)	100 cm/s	2 N	200 µm	0.224	0.133	988×10^{-6} mm^3/Nm	4.55×10^{-6} mm^3/Nm	-99.5
Emralon 333	chrome steel (7 mm ø)	2.5 cm/s	0.5 N	25 µm		0.08		22.9×10^{-6} mm^3/Nm	

Comercially available

This investigation presents a facile process to improve the wear resistance of PTFE without sacrificing its low COF. This is achieved by using a biomimetic adhesive, polydopamine (PDA), to adhere the PTFE film to the substrate as well as ceramic and metallic nanoparticle fillers of various sizes to improve the wear resistance of the PTFE film. The results show that using a combination of a PDA primer and Cu nanoparticle fillers in the PTFE film can provide a collective effect that increases the durability or wear life of PTFE films by more than 940 times.

Although the focus of this investigation is on the development of a lubricating thin film, the knowledge gained about the interaction of PTFE and PDA can be used to improve the adhesion of PTFE to various substrates/films, for a wide range of applications. For example, PTFE is currently being investigated as a material for use in integrated circuits due its low dielectric constant. The adhesion of metallic coatings to PTFE in this application has been an issue of

great concern [10]. PTFE is also used as a coating to produce self-cleaning surfaces [11]; wear of such coatings is also a problematic issue. The results from this investigation may help to reduce wear issues in such films.

1.1. Background and Motivation

In mechanical systems, the components that make up mechanical assemblies are typically fabricated from metallic materials [12]. As the surfaces of these metallic components come into contact with each other, the issues of friction and wear come into play. Tabor [13] studied the interaction between metals and found that at relatively large distances between two metallic surfaces there are weak Van der Waals forces at play, but as the distance between these surfaces is reduced to the interatomic level, metallic bonds are formed. These strong bonds allow for material to be transferred from one surface to the other as they slide against each other, producing a very high wear rate. One solution to this problem is to avoid metal to metal contact by incorporating non-metallic components into these mechanical systems [12, 13].

Many materials have been investigated as potential materials to be used in combination with metallic components in mechanical systems to reduce friction and wear. These non-metallic, low friction materials are called tribological materials and exhibit weak adhesion to metallic surfaces and low COF. In order to use mechanical components made from tribological materials, they must meet certain design criteria for physical and mechanical properties such as: strength, stiffness, fatigue life, thermal expansion, and damping [12]. Finding materials with these physical and mechanical properties in addition to excellent tribological properties can be very difficult. As a result, it is more common for engineers and tribologists to use a thin lubricating layer composed of a tribological material.

Traditionally, grease, mineral oils, and synthetic fluid lubricants have been used in the lubrication of mechanical assemblies. However, as new technology emerges which requires lubrication in extreme conditions, much focus has shifted to solid lubricants. At high temperatures most traditional lubricants will become less effective due to oxidation, thermal degradation, or decrease in viscosity. These lubricants are only effective at temperatures below 170 °C [14]. Solid lubricants, on the other hand, can perform at much higher temperatures. Hexagonal boron nitride films, for example, can be used in temperatures up to 1500 °C and exhibit a COF as low as 0.14 [15]. PTFE can be used at temperatures up to 260 °C without significant changes to its lubrication properties [16]. Solid lubricants with low vapor pressure, such as PTFE, are also appealing for space application where lubricants are expected to perform in high vacuum. In these conditions, traditional lubricants would evaporate and outgas, posing a risk to equipment.

1.1.1. Solid Lubricants as Thin Film Coatings

Using recent advances in coating technology such as physical vapor, chemical vapor, and plasma-enhanced chemical vapor depositions, it is now possible to apply solid lubricants as thin film coatings possessing low friction and wear resistant properties. In addition, the development of materials characterization tools such as scanning electron microscopy (SEM), X-ray photoelectron spectroscopy (XPS), scanning Auger microscopy, time-of-flight secondary mass spectroscopy, and focused ion beam (FIB) microscopy has allowed scientists to develop a better understanding of the atomic interaction of these materials and their influence on tribological performance. Solid lubricants can be ferrous metals, ferrous alloys, non-ferrous metals, non-ferrous alloys, ceramics, cermets, inorganic soft metals and polymers [17].

These solid lubricant films are typically very thin, under approximately 25 μm, and have a finite wear life. Because of the difficulty in disassembling mechanical components to reapply lubricating films [18], the material for the films must be carefully selected to last for the life of the system they are a part of. Because of this, much focus has been placed in extending the wear life of various solid lubricant film materials.

The study of the friction and wear of thin films shows that they can behave quite differently to bulk materials. In bulk materials, friction and wear is mainly determined by the properties of both opposing bodies. In thin film coatings on the other hand, friction and wear depend on an adequate combination of the hardness, modulus of elasticity, shear strength, fracture toughness, and thermal expansion of both the substrate and the coated film [19]. Furthermore, the most common causes of failure in thin films are not the conventional wear mechanisms in bulk material. Instead, failure is usually a result of the detachment of the film from the substrate caused by adhesive failure, fracture of the film caused by cohesive failure, or subsurface fracture [19].

Thin films are divided into two categories: soft and hard films. Soft films are defined as those having hardness below 10 GPa and hard films are those with hardness values above 10 GPa [20]. Either type must be selected based on the application conditions. The use of soft films on hard substrates, for example, not only reduces friction but also reduces contact stresses that can potentially produce subsurface cracking. However, soft films are highly susceptible to wear. Hard, brittle films on the other hand, are very resistant to abrasive wear, yet are susceptible to subsurface cracking at high contact pressures [19]. For this reason, it is important to select the type of film needed based on clearly established application conditions.

1.1.2. Hard Coatings

Hard coatings are used in applications where high loads and high temperatures (1000 °C or higher) are seen. Thin hard coatings on softer, tough substrates can provide protection against scratching from a hard counterface or debris [21]. This is especially beneficial for cutting tools. Aluminum oxide, titanium nitride, and titanium carbide are often used as protective coatings to reduce wear at high temperatures. These coatings significantly increase the life of cutting tools (up to ten times) but do not exhibit lower friction, which makes them unsuitable for use in low-friction applications [21]. Recently, coatings have been developed such as diamond like carbon (DLC), which offers a hard scratch resistant surface as well as low friction. These coatings form a low shear strength layer at the surface and form transfer layers on the opposing surface as a result of high pressure rubbing [21]. This produces what is called self-lubrication and provides the surface with an exceptionally low COF. These coatings are used in applications such as magnetic disks in computers and machine components. The thicknesses of these coatings are limited due to high internal stresses which cause spalling, cracking and delamination [22]. Some other causes of failure are: localized overload causing delamination when the substrate/coating bond strength is exceeded [22], third body wear resulting from debris, and high spot temperature which produces thermal degradation of the coating [22]. Hard ceramic coatings such as oxides, carbides, nitrides, borides and silicides are also studied for use as solid lubricants. However, intrinsic residual stresses are a problem for these films, causing coating rupture, loss of adhesion, and substrate cracking [21].

1.1.3. Soft Coatings

As mentioned above, soft coatings are typically used in combination with hard substrates to reduce sliding friction as well as to reduce contact stresses. Soft coatings typically suffer from

high wear rates; therefore, careful consideration must be made to the following parameters: film thickness, surface roughness, sliding speed, load, environment, counterface material, and deposition method. These coatings are divided into three categories: soft metals, lamellar solids, and polymers [21].

Soft metals can make excellent solid lubricant films because of their low shear strength which gives them good frictional properties. Lead, silver, gold and copper are examples of soft metals which are typically used as solid lubricants. The tribological performance of these films depends on the adhesion of the film to the substrate, film thickness, surface roughness, load, and sliding speed. The surface roughness of the counterface and substrate especially, plays a crucial role in the durability of soft metal films. If the film is very thin in comparison to the magnitude of the surface roughness of the substrate and counterface, the asperities on these surfaces will interact, resulting in high wear. On the other hand, if the film is thick, and the surface roughness of the counterface is very large, the film will experience microcutting. These films will perform better when rubbed against smoother surfaces [21].

Lamellar solids can be either hard or soft materials. The layered structure of lamellar solids gives these materials low shear strength as a result of weak interactive forces between plate-like crystallites. These plates can easily slide over each other giving lamellar solids excellent frictional properties. The plate-like crystallites are composed of faces with low surface energy which contributes to the weak adhesion between the plates [21, 23]. Some lamellar solids which are often used for tribological applications are graphite, graphite fluoride, MoS_2, HBN, H_3BO_3, WS_2, GaSe, GaS, SnSe, and $NbSe_2$ [21].

Polymer coatings are attractive because of their low friction, moderate wear resistance, good corrosion resistance, self-lubricating properties, low noise emission, and low production cost

[21]. Soft polymer coatings such as PTFE are applied to surfaces by spraying, dipping, spin coating, vacuum deposition, electrochemical methods, and pressure casting [21, 24, 25]. Typical thicknesses of these films range from a few micrometers to several millimeters [21].

The typical COF exhibited by polymers ranges from 0.15 to 0.6 [17, 21]. The wear rate of polymers is relatively low for moderate loading conditions; however, most polymers are not suitable for high contact pressures, where they exhibit high wear rates. The wear mechanisms typically observed in polymers are classified as cohesive or deformation and interfacial wear [21, 26-28].

For cohesive or deformation wear, polymers dissipate frictional energy through both adhesion between contacting asperities and through subsurface material deformation. Elastomers, ductile polymers, and brittle polymers will suffer different types of deformation, such as elastic or viscoelastic deformation that results in the tearing of material, plastic or viscous flow which results in ductile failure or displacement of material, and finally brittle failure which is characterized by fracture, respectively. Cohesive wear is associated with ploughing and fatigue [21].

In interfacial wear, polymers will dissipate frictional energy through adhesion between asperities, resulting in the formation of a transfer film, as well as through chemical changes such as scission and cross linking of polymer chains. The ultimate strength and modulus of elasticity of polymers are up to ten times lower than that of metals, making most polymers unsuitable as the constituent material of many mechanical components. In addition, the thermal expansion coefficients of polymers are high and their thermal conductivity is low making the dissipation of heat resulting from friction very difficult [21].

In this investigation, PTFE was selected as a solid lubricant coating to take advantage of its low COF, high temperature resistance, and chemical resistance [29, 30]. The application in mind is the coating of metallic surfaces of components that make up mechanical assemblies. The typical failure modes of these metallic components are corrosion, abrasive wear, adhesive wear, fracture and fatigue. Because PTFE is a soft polymer, it has the potential of reducing contact stresses between mating parts, and decreasing the possibility of fracture and fatigue failure in these components. The chemical resistance of PTFE makes it an ideal choice to also reduce corrosion in metallic parts. The issue of using PTFE is the limited wear life of the coating. Wearing away of the PTFE coating leaves the mechanical component vulnerable to abrasive and adhesive wear. This investigation solves the issue of wear in PTFE by increasing the wear resistance through the use of an adhesive primer and wear reducing nanoparticles.

1.1.4. PTFE as a solid lubricant

PTFE is commonly used as a solid lubricant in many mechanical applications due to its self-lubricating properties, low COF, high temperature resistance, and chemical resistance [29, 30]. PTFE is composed of repeating tetrafluoroethylene (TFE), C_2F_4 monomer units. The low COF observed in PTFE is a result of this un-branched, chain-like molecular structure. Aligned PTFE molecules are joined by weak Van der Waals forces [31] which allow the chains to easily slide past each other.

1.1.5. PTFE Synthesis

PTFE can be synthesized by two methods. The first method is through pyrolysis of difluorochloromethane, $CHClF_2$. This method yields TFE as well as hydrogen chloride, HCl, as a byproduct. PTFE is then formed through free radical initiated addition polymerization of TFE gas. Depending on whether or not dispersing units are used in the aqueous medium in which the

polymerization process is carried out, three different PTFE forms can be produced. If no dispersing agents are used, the PTFE will partially coagulate, forming a precipitated resin. This resin is then dried and ground to form a fine PTFE powder. If a dispersing agent is used, the PTFE will not coagulate, allowing small colloidal particles suspended in aqueous medium to be formed. These colloidal particles are typically around 2 μm in diameter. Finally, a fine PTFE powder may also be produced using an initiator and emulsifying agent in the aqueous medium in which the polymerization process occurs [32].

The level of achieved polymerization of TFE can be very high, producing PTFE of very high molecular weight. The molecular weight of PTFE is typically in the order of 10^6 to 10^7 g/mol and can even exceed 10^8 g/mol [32]. The high molecular weight of PTFE gives it a very high melt viscosity, greater than 10^{11} Pa·s, which prevents this polymer from being processed in its molten form. As a result, PTFE must be processed or shaped into mechanical components through powder compaction, sintering and machining [33].

1.1.6. PTFE Structure

The PTFE molecule possesses a helical structure formed of a carbon backbone surrounded by Fluorine atoms, as shown in Figure 1.1. This conformation gives PTFE a cylindrical, rod like structure with a smooth surface. The helical structure undergoes structural transformations at 19, 30, and 150 °C. Below 19 °C, PTFE has a 13_6 helical conformation. This means that it takes 13 $-CF_2-$ units to make up 6 turns of the helix. This phase of PTFE is considered the most stable. At temperatures above 19 °C, the PTFE structure changes to a 15_7 helix and the material becomes less densely packed. Above 30 °C, PTFE will maintain its 15_7 helical structure; however, the longitudinal displacements become more disordered than those observed at lower temperatures. Above 150 °C the PTFE molecule undergoes yet another transition where the

level of disorder in the longitudinal displacement increases even further. These structural changes to the PTFE structure may influence the tribological behavior of PTFE [34].

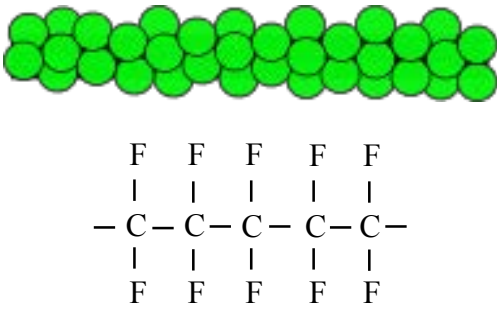

Figure 1.1: PTFE Molecular Structure.

In addition, PTFE is classified as a semicrystalline polymer formed of stacked crystalline and amorphous regions [34]. The size of the crystallites observed in PTFE is another factor that plays a significant role in the friction and wear observed in PTFE. As shown in Figure 1.2 (a), PTFE is essentially formed of a lamellar structure composed of parallel slices called striae (crystallites). These parallel slices form bands which are approximately 100 μm in length and between 0.2 to 1 μm in width. As shown in Figure 1.2 (b), each striae within these bands has a thickness ranging between 20 and 100 nm depending on the conditions used during quenching, and a separation of approximately 30 nm between striations [34]. The slices are highly crystalline regions which will easily slide past each other as an object moves tangential to the surface. Olabisi describes this mechanism as a deck of cards, in which the top card is removed as an object slides against it [32, 35]. This process causes the material to easily shear off so that a transfer film can be formed on the counterface. The formation of a transfer film on the counterface results in PTFE essentially rubbing against itself, enabling the self-lubrication

property of PTFE regardless of counterface material type. This in turn further reduces the friction of the system.

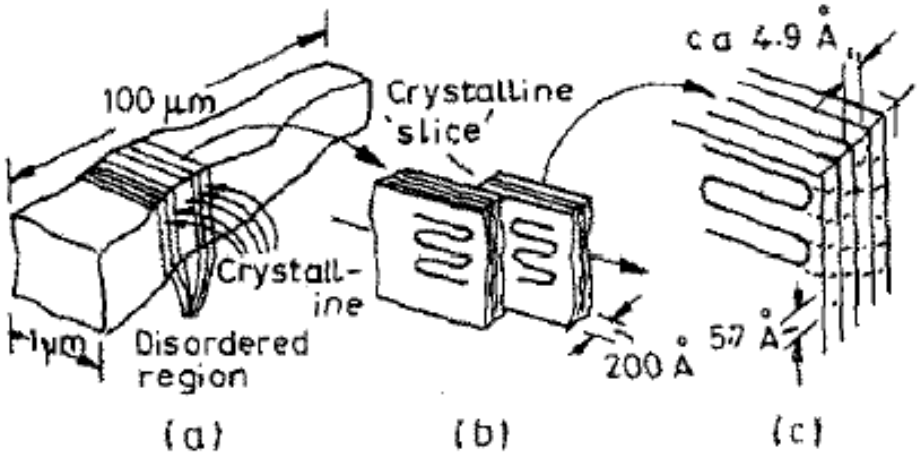

Figure 1.2: Structure of PTFE: (a) semi-crystalline block or "band"; (b) crystalline slices of "striae" after sliding; (c) hexagonal array of chains within slices. The structural arrangement shown in (a) and the sliding of crystalline slices is based on published work. However, the arrangement of chains within individual slices as shown in (b) and (c) is deduced from the friction-film structure. There is yet no direct evidence that the chains are in fact so oriented within the slices [34]. Reprinted from Wear, 158, S.K. Biswas and Kalyani Vijayan, Friction and Wear of PTFE – a Review, 193-211, 1992, with permission from Elsevier, and permission from Macmillan Publishers Ltd: Nature, K. Rachel Makinson, D. Tabor, Friction and Transfer of Polytetrafluoroethylene, 201, copyright 1964.

Unfortunately, the repetitive development and removal of the transfer film causes unfilled PTFE to also have a very high wear rate, close to 10^{-3} $mm^3/(N \cdot m)$ [36, 37], making pure PTFE less desirable as a lubricant. As a result of PTFE's susceptibility to wear, many attempts have been made to combine PTFE with micro and nanoparticle fillers to improve its wear performance. Various micro and nanoparticle fillers have been used, such as glass fiber [38], alumina [39], and graphite [40]. Nanoparticle fillers have shown to affect PTFE in the following ways: increasing the crystallinity, improving the ultimate strength, increasing elongation to

failure, and improving toughness. However, an increase in these properties does not always result in a reduced wear rate [9].

Bahadur concluded that it is the decomposition of the filler, generating reaction products between PTFE and the filler, which can improve the bonding of a transfer film to the counterface, and thus, enhances the wear resistance of PTFE [41]. Furthermore, some studies have shown that although PTFE is chemically inert, metal fluoride compounds have been found at the interface between the transfer film and the metal counterface rubbing against filler reinforced PTFE [31]. This indicates that part of the transfer film may chemically bond to the counterface. The problem with many fillers used in PTFE composites is that they produce an increase in the COF, especially with higher filler concentrations. In the case of alumina reinforced bulk PTFE, for example, the wear rate under a 6.4 MPa contact pressure against a 347 stainless steel counterface was reduced from 7.15×10^{-4} $mm^3/N \cdot m$ to 1.2×10^{-6} $mm^3/N \cdot m$ with 20 wt.% alumina filler concentration in PTFE. However, the COF increased from approximately 0.15 for unfilled PTFE to 0.2 for the composite [42]. Therefore, a great obstacle in the use of micro and nanoparticle PTFE composites has been to provide both wear resistance as well as a low COF.

1.1.7. PTFE Nanoparticle Composites

The incorporation of fillers in polymers can produce a change in the polymer's mechanical properties. Many studies have found that by using various fillers, the elastic modulus of polymers can be increased, thus allowing polymers to support higher loads while undergoing less deformation [43, 44]. In addition to increasing the elastic modulus, studies have shown that as a result of using certain fillers, the tensile strength of the polymer may also be reduced [43, 45]. Lower tensile strengths allow small asperities to shear off more easily, reducing the friction and

preventing large scale removal of material. Chen et al. found that adding SiO_2 micro-particles reduced the tensile strength of PTFE. They attributed the tensile strength reduction to the low adhesion between the filler and PTFE matrix [43], decreasing cohesion within the film.

It has also been determined that certain fillers in polymers will preferentially support applied loads, consequently reducing stress and strain in the polymer. Lancaster et al. studied the influence of carbon fiber reinforcement on the friction and wear of polymers. They found that reduced wear in reinforced polymers was caused by fibers exposed during sliding that preferentially supported part of the applied load [46]. Because the fibers support the majority of the load, the friction and wear of the composite polymer are less affected by changes in speed and temperature which typically have a drastic effect on polymers.

1.2. Proposed Solution

The goal of this study is to develop a low friction, low wear PTFE composite coating. To resolve the issue of PTFE's low wear resistance, SiO_2, Au, and Cu nanoparticles will be used as fillers to reinforce the PTFE film. In addition, to resolve PTFE's delamination issue resulting from poor adhesion of the film to the substrate, PDA will be used as an adhesive primer prior to a PTFE top coat. To be commercially feasible, the fabrication process must be low cost and scalable for mass production. For this reason, a simple dip coating of substrates into aqueous colloidal dispersions was selected as the deposition method for the coating.

1.3. Layout of Dissertation

This dissertation is organized in the following manner. Chapter 2 presents a literature review of PTFE composite films that have been studied for use in tribological applications. This chapter also introduces PDA as a solution to PTFE adhesion and gives a background of the development and uses of PDA. The different materials studied as nanoparticle fillers in this investigation are

also introduced. Chapter 3 discusses the theory involved in the analysis of contact mechanics, friction and wear. This chapter also presents the characterization tools utilized in this investigation and gives a brief summary of the functionality of these tools. Chapter 4 describes the design of experiments, and outlines each study within this investigation. Chapter 5 introduces a study on the effect of dip-coating withdrawal speeds on the coating thickness of colloidal PTFE films. Chapters 6 and 7 present studies on the influence of SiO_2 and Au nanoparticles on the tribological performance of PTFE films. Chapter 8 presents a study on the use of a PDA adhesive layer to improve the tribological performance of PTFE films. Chapter 9 describes the examination of the combined effects of PDA and Cu nanoparticle fillers on the tribological properties of PTFE. Finally, Chapter 10 presents the conclusions drawn from this investigation and discusses potential future directions for the further development of the low friction, wear resistant PTFE composite film.

Chapter 2

Literature Review

PTFE composites with various micro and nanoparticle fillers such as glass fiber [38], alumina [39], and graphite [40] have been studied. These investigations have been carried out on bulk PTFE. Although there has been much progress made in the tribological study of bulk PTFE, there has been very little focus placed on the tribological performance of PTFE thin films [21].

2.1. Investigations on the tribological performance of PTFE composite films

PTFE/nanodiamond [47] , Al_2O_3-Ti/PTFE [5], RF sputtered PTFE [6], Electroless Ni-PTFE [7], PTFE/Epoxy [8], PTFE/carbon nano-particles [48], and PTFE/Al_2O_3 micro-assembling film [49] are a few examples of investigations performed on PTFE nanocomposite films. Each of these films has shown different levels of wear resistance and frictional behavior.

2.1.1. Tribological properties of PTFE and nanodiamond films

One of the few studies carried out on PTFE composite films is that of Lee et al. [47]. Lee studied the use of nanodiamond particles (5-10 nm) as a filler in PTFE films. The nanodiamond particles used in his study were fabricated through the detonation method and were added to the PTFE matrix up to a concentration of 4 wt.%. The PTFE/nanodiamond composite was sprayed onto an aluminum substrate. After spraying, the films were dried at 100 °C for 15 min and then heated at 400 °C for 15 min which resulted in a final film thickness of 30 μm [47].

A ball-on-plate testing method was used for the tribological analysis. The counterface selected for the friction tests of the samples was a silicon nitride ball of 5.6 mm diameter. The results showed that the filler concentration that exhibited an optimal friction and wear performance was 2 wt.% of nanodiamond. At 2 wt.%, the nanodiamond filler reduced the COF of the PTFE film from 0.21 to 0.16 and the wear track width from approximately 0.85 to 0.44

mm at room temperature. The improved performance of this coating was attributed to the lubricating properties of the nanodiamond particles at the surface, the hardening effect these particles had on the PTFE matrix, and the transfer film formed by the PTFE which produced a self-lubricating effect. The tribological properties of the film were observed to deteriorate at nanodiamond concentration above 2 wt.%. This deterioration in performance was attributed to agglomeration of nanodiamond particles [47].

2.1.2. Ceramic/fluoropolymer composite coating by thermal spraying

A study, carried out by Mateus et al. [5], looked at the effect of hydrogen percentage and spraying distance in the tribological properties of plasma sprayed Al_2O_3-Ti/PTFE composites. The method of deposition used, produced relatively thick films of over 50 μm thick. Four different plasma sprayed Al_2O_3-Ti composites were evaluated:

1. A commercially available Al_2O_3–TiO_2/PTFE composite powder (70 wt.% Al_2O_3-TiO_2 and 30% Al_2O_3 and TiO_2 coated PTFE particles)
2. Al_2O_3– TiO_2 + 8 vol.% PTFE
3. Al_2O_3–TiO_2 + 8 vol.% PFA
4. Co-injected Al_2O_3–TiO_2 + 8 vol.% PFA

After the coating was deposited, the samples were heated to a temperature of 350 °C for 15 min and cooled at room temperature.

The tribological tests were carried out using a ball-on-disk configuration. The ceramic/polymer composites were spray coated onto aluminum disks. The disks were then slid against a 6 mm-diameter 100C6 steel ball counterface using a CSEM tribometer. The tribological tests were carried out under a normal load of 5 N and a sliding speed of 50 cm/s.

The results showed that all but one of the composite films had a COF ranging between 0.40 and 0.44 after a sliding distance of 500 m. The co-injected Al_2O_3–TiO_2 + 8 vol.% PFA exhibited a COF that steadily increased from approximately 0.15 to 0.30 after a sliding distance of 500 m. In all four samples types, the counterface experienced wear during the sliding process. Steel from the counterface was transferred to the coated surface. Of the four samples, co-injected Al_2O_3–TiO_2 + 8 vol.% PFA also showed the least amount of wear in the counterface. The better performance of the co-injected sample was attributed to a larger amount of polymer present at the interface between the coating surface and the steel counterface [5].

2.1.3. Friction and wear of sputtered PTFE films

Nishimura et al. [6] are some of the few investigators who have studied the tribological properties of PTFE films produced by radio frequency (RF) sputtering [6, 50]. The objective of their investigation was to study the lubricating effect of sputtered PTFE films at elevated temperatures in air and in vacuum. Nishimura's investigation used a diode type sputtering apparatus with a maximum RF power supply of 1kW. The PTFE films were sputtered onto both SUJ 2 and SUS 440C disks. The resulting coating thickness of the films were approximately 1 μm.

A pin on disk configuration was used for the friction tests, utilizing an ASEM built-in friction tester which allowed in-situ observation of the worn surface. The tests were carried out in a linear reciprocating manner and performed in oxygen, air, nitrogen, and vacuum using a normal load of 5 N and a sliding speed of 10 mm/s.

They found that the COF of sputtered PTFE films is higher than what is typically seen for bulk PTFE. The COF of the sputtered films was observed to range between 0.30 and 0.35 for the first 20 to 50 sliding cycles. The COF was then seen to rise to and exceed a value of 0.40

before dropping down again and finally increasing past a value of 0.50. They determined that the initial rise to 0.40 was a result of metal to metal contact between the samples substrate and the counterface. They determined this by measuring the electric contact resistance which drops at this point of high friction. The investigators concluded that the friction performance of the sputtered PTFE films can be divided into two stages. During the first stage, there is sufficient film thickness to separate the substrate and counterface. During the second stage, there is metallic contact between the opposing surfaces. The first stage is relatively short and the second is much longer. This speaks to the replenishing ability of the sputtered PTFE films. When these films were compared to the performance of a PTFE plate tested using the same condition, it was observed that on average the COF value of the sputtered films was twice that of the PTFE plate.

Using SEM the investigators observed that the PTFE plate wore in soft, long films. The sputtered films, on the other hand, produced small brittle particles as a result of the wear process. It was concluded that sputtered PTFE films are harder than bulk PTFE. It was also determined that sputtered PTFE films have wear rates up to 10 times lower than those seen for bulk PTFE [6, 21].

2.1.4. Development of electroless NiP-PTFE-SiC composite coatings

The goal of this study was to produce high hardness, low friction, and low surface energy films by electroless plating of Ni-PTFE-SiC. Four different coatings were evaluated: electroless Ni, electroless Ni-PTFE, electroless Ni-SiC, and electroless Ni-PTFE-SiC coated mild steel. The electroless Ni composition and plating conditions were maintained constant for each of the four coatings. The coatings were finally annealed at a temperature of 400 °C producing a resulting film thickness for each of the coatings of approximately 15 μm [7].

The hardness of the films was measured using micro hardness indentation. The tribological properties were determined using a pin-on-disk tribometer with a 9 mm diameter alumina pin as the counterface. The friction tests were carried out at a sliding speed of 20 cm/s and under a normal load of 10 N. The tests were run for a distance of 4000 m. A Talysurf profilometer was then used to determine the cross-sectional profile of the wear track which enabled the cross-sectional area to be used to calculate the wear loss and normalized wear rate [7].

The results show that the electroless Ni-PTFE had the lowest COF with a value of approximately 0.48 but lowest hardness with a value of 421HV50 after annealing. It also had one of the lowest wear rates at 0.36×10^{-6} mm^3/Nm. It was determined that the formation of a PTFE transfer film on the alumina pin counterface allowed for PTFE against PTFE sliding which resulted in a lower COF and wear rate. The electroless Ni-SiC coating showed better load bearing ability because of its higher hardness (1365HV50); however, this did not translate into a lower wear rate. Electroless Ni-SiC had a wear rate of 0.45×10^{-6} mm^3/Nm [7].

2.1.5. Wear resistant solid lubricant made from PTFE and epoxy

McCook et al. [8] studied the tribological performance of composite coatings consisting of PTFE and epoxy. The investigation claims to use expanded PTFE as a scaffolding and epoxy as reinforcement. Four different films were evaluated in this investigation: skived PTFE, low density PTFE, high density PTFE, and epoxy. In contrast to the expanded PTFE, the skived PTFE consists of full density PTFE. Expanded PTFE on the other hand, is porous and consists of discrete nodes of dense PTFE which are interconnected by PTFE fibrils. In this study, the low density PTFE sample was composed of PTFE (50 wt.%) and epoxy. The high density samples were composed of PTFE (70 wt.%) and epoxy. These films, with thicknesses of approximately 200 μm, were then cured onto carbon steel circular disks. The resulting thickness for the high

density PTFE composite film was 150 μm, and the resulting thickness for the low density PTFE composite film was 100 μm.

Tribological tests were carried out on an open rotating pin-on-disk tribometer. Tests were carried out at speeds ranging from 0.25 to 2.5 m/s and normal loads between 1 and 3 N. The centerpoint of 1 m/s and 2 N was repeated 5 times to give a statistically significant representation of the friction and wear performance under those testing conditions. A 4.8 mm diameter low carbon steel sphere was used as the counterface.

The results show that the lowest wear rate and COF for the centerpoint testing condition corresponds to the low density PTFE composite. For this coating, the average COF was 0.133 and the average wear rate was 4.55×10^{-6} mm^3/Nm. Skived PTFE, on the other hand, exhibited a COF of 0.224 and wear rate of 988×10^{-6} mm^3/Nm. From these results, the authors determined that the composite coating of expanded PTFE and epoxy has a wear rate that is 100x lower than that of pure PTFE in addition to a significantly lower COF. The results also show that the addition of epoxy increases the elastic modulus and hardness of the film within these areas which may reduce the contact area between opposing surfaces. The authors determined that the improved tribological performance of the composite film is a result of PTFE being drawn out from the nodes and creating a film over the epoxy regions, essentially producing a surface layer composed entirely of PTFE [8].

2.1.6. Tribological behavior of PTFE nanocomposite films reinforced with carbon nanoparticles

Lee et al. [48] studied carbon-based nanoparticles/PTFE composites. The carbon nanoparticles were synthesized by heat treating nanodiamond between 1000 and 1900 °C. The carbon particles were then milled using micron sized beads in chemically treated water which

yielded the nanometer sized carbon particles. These particles were subsequently mixed with PTFE and finally coated on an aluminum substrate, producing 10 μm thick films.

The tribological properties of the film were tested using a ball-on-plate configuration. The counterface used was a steel ball with 12.7 mm diameter. The sliding speed and normal load used in this study were 4 cm/s and 33.3 N respectively. All the tests performed were carried out at room temperature and under dry conditions.

The optimal concentration of carbon nanoparticles in PTFE was shown to be 2 wt.%. The results for the friction test showed that the COF remained at 0.1, similar to that of the pure PTFE coating. The wear rate, on the other hand, was reduced from 16.2×10^{-6} to 3.5×10^{-6} $mm^3/N{\cdot}m$ compared to pure PTFE. The improved performance was attributed to the low COF of the carbon nanoparticles. It was also observed that carbon nanoparticles heat treated at 1000 °C provided the best tribological results. Higher heat treating conditions of the carbon nanoparticles caused a higher extent of aggregation and, as a result, larger particle sizes which increased the wear rate of the film [48].

2.1.7. Structure & micro-tribological properties of PTFE/Al_2O_3 micro-assembling film

Tang et al. [49] studied RF mangnetron sputtered micro-assembling PTFE and Al_2O_3 multilayer films. The objective of their investigation was to reduce the wear in elastic metallic-plastic thrust bearing pads by incorporating this film as a coating. PTFE and Al_2O_3 were alternatively sputtered on an elastic metallic-plastic pad with N+ implantation used in between layers to improve adhesion between them.

The tribological tests were performed using an atomic force and friction force microscope. The results showed that the COF of PTFE/Al_2O_3 multilayer was 0.108, which was greater than

the COF of 0.057 observed for pure PTFE, whereas the worn depth was 1/10 that of pure PTFE [49].

2.1.8. Summary of PTFE composite films

Each of the investigations discussed above show much insight into the tribological properties of PTFE films and the effect of incorporating other materials to produce more wear resistant PTFE composites. Of the seven films, there are three that stand out.

First, PTFE and nanodiamond exhibits a significant reduction in both the COF and wear rate compared to pure PTFE. The incorporation of nanodiamonds at a concentration of 2 wt.% reduced the COF of PTFE by 24% and the wear track width by 48%. This coating shows much promise; however, there are a few key areas that may need further evaluation. First, the friction tests were performed for a very short time (6 min). Although the initial wear rate may be much lower for the composite film, this does not automatically translate to a longer wear life. The initial wear at the surface is dominated by adhesive and abrasive wear between asperities of opposing surfaces; however, after prolonged repetitive sliding it is possible that the film can suffer from drastic wear as a result of delamination or flaking resulting from crack formation. Second, the wear of the film is only determined in terms of wear track width. To accurately measure the wear of the film, it would be necessary to determine the cross-sectional area of the wear track.

The second film that stands out is electroless Ni-PTFE. This type of coating is currently used commercially because of its low wear rate. However, the applications of this film are limited because the film exhibits a significantly higher COF than pure PTFE. Electroless Ni-PTFE is commonly used in the prevention of galling in screws, splines and clutches.

Finally, PTFE and epoxy is likely the most promising film of the seven mentioned above. This film had a COF that was 40% lower than that of pure PTFE and a wear rate that was over 100 times lower than pure PTFE. An interesting observation is that the tribological tests were carried out at very high sliding speeds at which PTFE typically shows significantly higher COF and wear rates. One drawback of this film is that the fabrication process seems to limit the thickness of the films to much higher thicknesses than are typically used in these types of low friction coatings.

There is still much room for improvement and more research needed to produce low friction PTFE composites with high wear resistance. The wear of PTFE films is not only due to the localized wear of PTFE at the film surface, but also due to the delamination of the film resulting from weak adhesion of the film to the substrate. To increase the adhesion, investigators have typically used surface roughening techniques as well as primer coats to allow PTFE to physically lock and chemically bind to the surface. Primers such as polyamide acid [51] and fluorinated ethylene propylene/PTFE blends [52] have commonly been used for this purpose. To ensure durability, these films typically have thicknesses above 20 μm [51, 52]. The large thickness of these films, as well as the need for large peak-to-valley roughness on the substrate surface, limits their use in many applications where thin films are required. The investigation presented in this dissertation studies the effect of using PDA as an adhesive to improve the wear resistance of PTFE thin films.

2.2. Polydopamine as a Solution to PTFE Film Adhesion

Adhesive failure is a particular issue for PTFE thin films which have very low surface energy and have a hard time adhering to any substrate. However, there is one organism that is able to attach itself to PTFE. Mussels found in marine environments secrete proteins which allow them

to attach to both organic and inorganic surfaces under water and in tidal conditions [53-55]. Figure 2.1 shows a mussel attached to a glass surface [56].

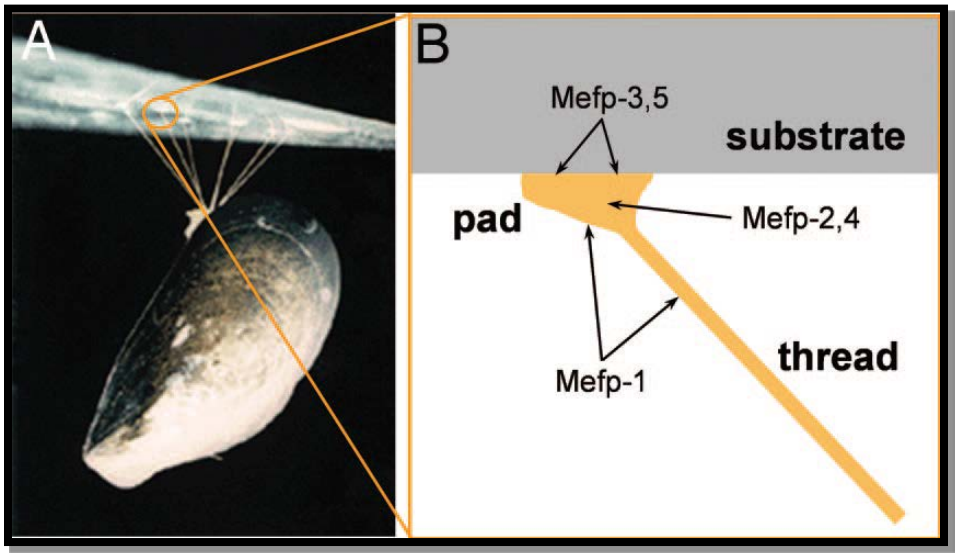

Figure 2.1: Biodistribution and amino acid composition of mussel adhesive proteins of *M. edulis*. (*A*) Photograph of a mussel attached to a glass surface, showing the byssal threads and adhesive pads. (*B*) The biodistribution of Mefps. Mefp-3 and Mefp-5 are found at the pad–substrate interface [56]. Reprinted from PNAS, 103/35, Haeshin Lee, Norbert F. Scherer and Phillip B. Messersmith, Single-molecule Mechanics of Mussel Adhesion, 12999-13003, 2006 with permission from Proceedings of the National Academy of Science of the United States, Copyright (2006) National Academy of Sciences, U.S.A.

Lee et al. [56] determined that out of the 5 Mytilus edulis foot proteins (Mefp) found in the byssal threads secreted by mussels, it is Mefp-3 and Mefp-5 that are found at the interface between the threads and the surface they attach to. Mefp-3 and Mefp-5 contain 3,4-dihydroxy-L-phenylalanine (DOPA) and lysine peptides, which are believed to play an important role in the adhesion process [53, 57-61]. Although the exact mechanism behind the adhesive property of these proteins is not known, it is believed that the catechol functional groups in DOPA and amine in Lysine play a significant role. Lee et al. [53] found that by polymerizing dopamine, the

commonly known neurotransmitter containing the same functional groups as DOPA and Lysine, the adhesive properties of mussels can be replicated. PDA is synthesized through pH induced oxidation of dopamine hydrochloride in a basic solution. It has shown to adhere to many materials, including PTFE. However, the adhesive strength or type of bond formed on PTFE is unknown [53].

The formation of PDA is similar to the biosynthesis of melanin in that it undergoes an oxidative reaction to form dopamine into 5,6-dihydroxyindole (DHI), which covalently bonds to produce the polymer chains [62]. However, some authors suggest that a significant amount of dopamine remains unpolymerized and instead physically self assembles with DHI forming trimers as seen in Figure 2.2 [63].

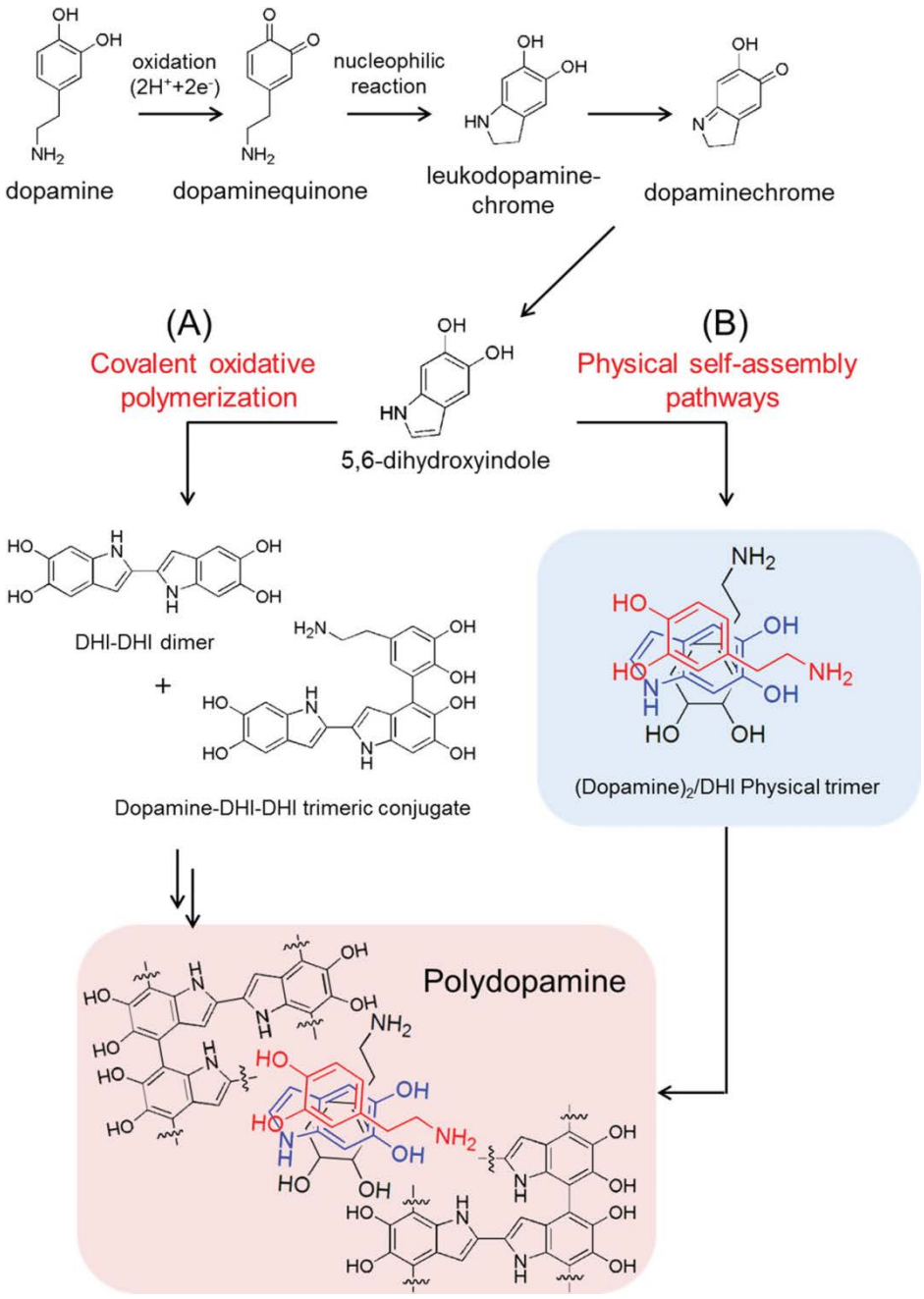

Figure 2.2: Polydopamine synthesis occurs via two pathways: A) a pathway of covalent bond-forming oxidative polymerization and B) a newly proposed pathway of physical self-assembly of dopamine and DHI [63]. Reprinted with permission from John Wiley and Sons, copyright 2012 WILEY-VCH Verlag GmbH & Co. KGaA, Weinheim.

2.2.1. Polydopamine/Steel and Polydopamine/PTFE interaction

In this investigation PDA is used as a binder to adhere a PTFE top coat to a stainless steel substrate. At the PDA/steel interface, it is expected that PDA will undergo two electron oxidations to produce its quinone form, binding to the stainless steel substrate through its oxygen groups [64]. The interaction between PDA and PTFE, on the other hand, is not well understood. A similar process, however, is that of bio-adhesion on PTFE dental implants. Muller et al. [65] showed that bovine serum albumin (BSA) formed a very strong bond on dental implants made of PTFE. He concluded that the hydrophobic surface of PTFE had a preferential adsorption of hydroxide ions when submerged in water and that the BSA protein formed hydrogen bonds with the adsorbed hydroxide ions [65]. Because BSA has similar functional groups to PDA, it is believed that he same binding process may be occurring here. Figure 2.3 shows the interaction between stainless steel, PDA and PTFE. To prove the strength of the PTFE – PDA bond, a thin sheet of PTFE was immersed into a PDA solution for 24 hours. After this sheet was removed from the PDA solution, it was sonicated in DI water for 20 minutes. The purpose of this experiment was to observe if the film would remain on the PTFE sheet or be removed as a result of the sonication process. The dark PDA film on the surface of the sheet was not removed and the color of the water did not change. This indicates that the PDA film forms a relatively strong bond with PTFE.

2.3 Nanoparticle fillers used to improve the wear resistance of the PTFE top coat.

Many nanoparticle fillers that have been used in bulk PTFE as a wear reducing agent may also provide the same benefits in PTFE films. The following nanoparticles were used in this investigation to improve the wear resistance of PTFE films.

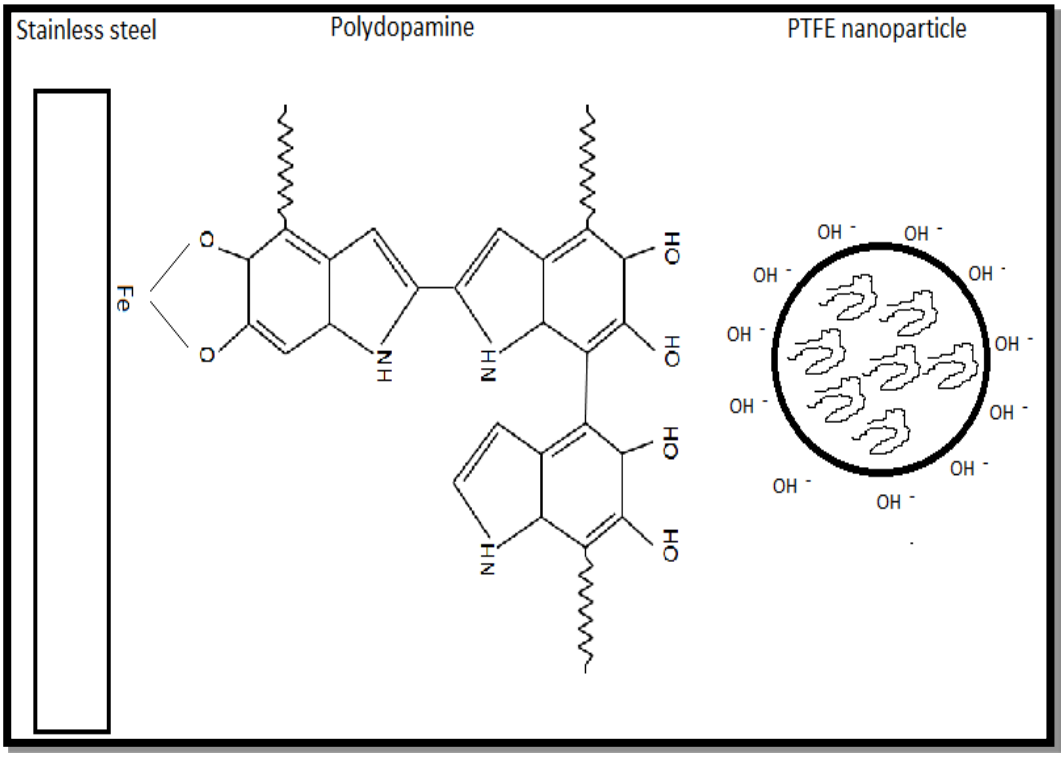

Figure 2.3: Stainless Steel – polydopamine – PTFE interaction.

2.3.1. SiO_2 nanoparticle filler

The benefit of SiO_2 nanoparticles can be attributed to their hardness. As such, SiO_2 nanoparticles have been used as a filler to improve the wear resistance of polymers such as polyetherketone [66]. These nanoparticles have proven to have the ability to increase the development of a transfer film on the counterface [66] and to increase the tensile strength, tensile modulus, and impact strength of polymer resins [67], consequently increasing the wear resistance of the films. However, it was also determined that for SiO_2 concentrations above 7.5 wt.% the wear rate of the polymer increased. It is believed that, at higher concentration, the SiO_2 nanoparticles agglomerate [67] and may cause third body wear (nanoparticles acting as abrasive bodies which plough through the polymer).

2.3.2. Au nanoparticle filler

Au is an attractive tribological material because of its low shear strength. Although most metal on metal contact is problematic due to cold welding, this issue is not as challenging for low shear strength metals such as Au. The low shear strength allows Au to act as a solid phase lubricant. The use of Au is also advantageous because it is highly inert, which allows it to be stored in atmospheric conditions for a long period of time before it is used [68]. Many studies have been performed on the tribological properties of Au.

For example, Olea-Mejia et al. studied the tribological properties of polymer nanohybrids containing Au nanoparticles obtained by laser ablation. In their investigation, polystyrene and Au were combined to produce compression molded specimens. They found that by incorporating a 0.3 wt.% concentration of Au, the COF and wear of polystyrene decreased. The decrease in friction was attributed to Au nanoparticle being trapped between the two opposing surfaces and creating a lubricious layer at the interface [69].

Amorphous hydrogenated carbon films containing Au nanoparticles were studied by Yan et al. They found that Au concentrations of 2 wt.% and 4 wt.% significantly reduced the friction and wear of the film. The optimal concentration of Au proved to be 2 wt.%, which showed a COF of approximately 0.14 and lasted for 10,000 sliding cycles. The improved tribological performance is a result of gold particles shearing off from the film and depositing on the counterface producing a tribofilm [70].

Puniredd et al. studied the use of Au nanoparticles within immobilized fluorinated dendrimers. They found that, by adding the Au particles after the fluorination step, they were able to reduce the particle sizes and further reduce the COF of the film. This processing sequence resulted in films with a COF of 0.24 [71].

2.3.3. Cu nanoparticle filler

Copper is a material with high ductility, high thermal conductivity and low hardness, which allows it to be used in high temperature tribological applications. Copper has also been known to produce copper oxide at the friction interface, enabling it to maintain a stable coefficient of friction at a wide range of temperatures [72]. The addition of copper nanoparticles in lubricating oils has shown to decrease friction, reduce wear, and provide self-repairing properties to sliding surfaces [73, 74].

The use of Cu nanoparticles in bulk PTFE has also been well investigated. Jia et al. added Cu nanoparticles to PTFE/serpentine composites and found that the Cu nanoparticles significantly reduced the friction and wear of the composite [75]. Yan et al. added Cu nanoparticle to PTFE/nano-expanded-graphite and found that Cu increased the hardness, modulus of elasticity, yield strength, and tensile strength of the composite [76]. An increase in these mechanical properties has shown to improve the tribological properties of PTFE.

Chapter 3

Theoretical Background

Tribology is the field of science and engineering that studies the interaction between contacting surfaces in relative motion. This field studies the influence of contact conditions, material chemistry, surface micro- and nano-scale topography, environmental conditions, material mechanical properties, and energy inputs like, speed and load, on the friction and wear of contacting surfaces in relative motion.

3.1. Contact between solid surfaces

When two surfaces come into contact, the real contact area is defined by discrete contact points between asperities on the surfaces. This real contact area is typically only a small fraction of the apparent contact area. As the normal load forcing the surfaces into contact is increased, these asperities will deform allowing lower asperities to also come into contact and increasing the contact area. Depending on the material, the deformation can be elastic, plastic, viscoelastic or viscoplastic [77].

Although a large number of asperities come into contact when two surfaces come into proximity with each other, analysis is typically simplified by observing the contact between single asperities. This reduces the analysis to that of two curved bodies undergoing deformation. These bodies will undergo either elastic deformation or plastic deformation, or a combination of the two [77].

3.1.1 Elastic Contact

The first analysis method is concerned with elastic deformation and was developed by Heinrich Hertz in 1882 [77, 78]. Hertz's description of elastic contact between bodies is known as Hertzian contact. This contact model holds the following assumptions: the surfaces are

continuous, smooth and non-conforming, the strains are small, each solid can be considered as an elastic half-space in the proximity of the contact region, and the surfaces are frictionless [77]. Figure 3.1 shows the contact between two opposing bodies. The point of contact between the bodies is located at the x-y plane. The direction of the loading between the two surfaces is oriented along the z axis. As the bodies are compressed under a normal load they undergo elastic deformation causing points T_1 and T_2 to move towards point O in the z direction. The amount of deformation is characterized by δ_1 and δ_2 for each respective body. The extent of this deformation occurs in the z direction. The dashed lines in the figure represent the location of the surface of the bodies if they did not undergo deformation but rather overlapped each other. This serves to show the extent of the deformation. The diameter of the contact area, $2a$, increases as a function of δ_1 and δ_2.

If the two opposing bodies are spheres of radius R_1 and R_2, the contact area is circular with a diameter of $2a$. The value for a is given by the equation:

$$a = \frac{\pi p_0 R}{2E^*} = \left(\frac{3WR}{4E^*}\right)^{1/3} \tag{3.1}$$

where E^* is the effective modulus, p_0 is the maximum contact pressure, r is the effective curvature and W is the applied normal load. The total deformation $\delta = \delta_1+\delta_2$ can be represented by the following equation:

$$\delta = \frac{a^2}{R} = \left(\frac{\pi p_0}{2E^*}\right)^2 R = \left(\frac{9W^2}{16RE^{*2}}\right)^{1/3} \tag{3.2}$$

The pressure distribution resulting from contact between two spheres is given by the following equation:

$$p = p_0[1 - (r/a)^2]^{1/2} \tag{3.3}$$

Where the maximum contact pressure, p_0 is 3/2 the mean contact pressure p_m and can be expressed by the following equation:

$$p_0 = \frac{3}{2}p_m = \frac{3W}{2\pi a^2} = \left(\frac{6WE^{*2}}{\pi^3 R^2}\right)^{1/3} \tag{3.4}$$

The effective modulus can be calculated using Young's modulus E and Poisson's ratio v for each of the materials composing each of the spheres:

$$\frac{1}{E^*} = \frac{1 - {\nu_1}^2}{E_1} + \frac{1 - {\nu_2}^2}{E_2} \tag{3.5}$$

The effective curvature is calculated based on the radius of each sphere [77, 78]:

$$\frac{1}{R} = \frac{1}{R_1} + \frac{1}{R_2} \tag{3.6}$$

Because of the low thickness of the films studied in this investigation, steel on steel contact was assumed and the Hertzian model was used to determine the contact

pressure between opposing bodies.

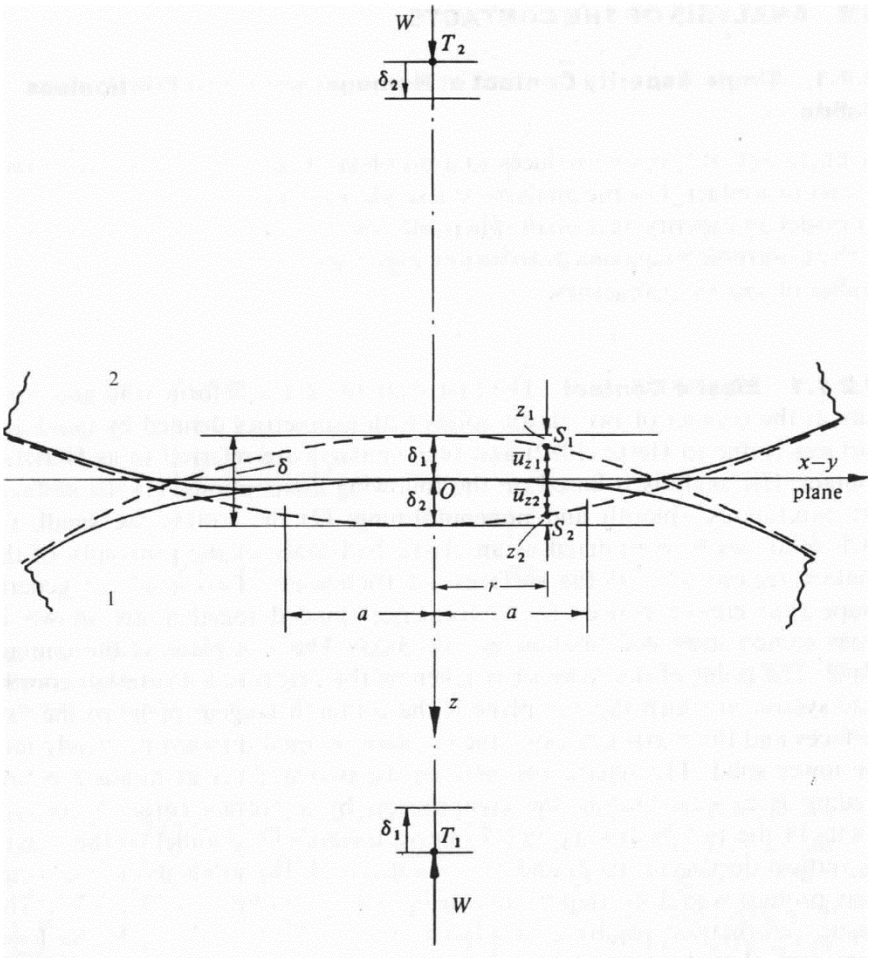

Figure 3.1: Schematic of Elastic contact - Hertzian model [77, 78]. Reprinted with permission from John Wiley and Sons, copyright 2002 by John Wiley and Sons, New York. All rights reserved.

3.1.2 Elastic-Plastic Contact

At small loads between two opposing bodies, the surfaces are deformed elastically, with the maximum shear stress, τ_{max}, occurring below the surface. As the load is increased and τ_{max} exceeds a critical shear stress for the material, the body will experience plastic flow. As the load

is increased, the area that has experienced plastic flow expands until it reaches the surface. Once the plastic zone reaches the surface, the deformation becomes fully plastic [77].

3.2. Surface topography

Finished products have surface properties that are different from the bulk material. The machining process which produces the desired surface finish results in deformation, strain hardening, recrystallization, and texturing. These surfaces can be divided into six layers: the deformed layer, Beilby layer, chemically reacted layer, chemisorbed layer, and physisorbed layer [21]. The deformed layer resulting from the applied stresses during surface finishing is typically 10-100 μm. In metal and alloy surfaces, this layer is followed by the Beilby layer, which is the result of melting and surface flow produced during machining. This layer is typically 1 - 100 nm thick and has an amorphous or microcrystalline structure. On top of the Beilby layer, is the chemically reacted layer. Metals and alloys, for example, will form an oxide layer, such as Fe_2O_3, Fe_3O_4, or FeO in iron. Polymers, on the other hand, do not typically form an oxide layer, but the polymer chains may break and cross link as a result of the machining process producing a different chemical composition at this layer. This layer is followed by a chemisorbed and physisorbed layer which is usually less than 1 nm thick and is composed of adsorbed molecules of water vapor, oxygen or hydrocarbons [21].

The machining process will also produce a topography of peaks and valleys on the surface which can be characterized by surface roughness. The surface roughness parameter that is most commonly used is the average surface roughness Ra, which measures the arithmetic average deviation of the surface profile from the mean [21]. The root mean squared or RMS roughness Rq, is also commonly used to characterize the surface topography. The surface roughness plays a very important role in the friction and wear of surfaces [21].

3.3. Friction

Friction can be defined as "the resistance to motion during sliding or rolling that is experienced when one body moves tangentially over another with which it is in contact" [77]. The tangential force required to initiate movement of one body over the other is called the static friction, and the force required to maintain this motion is called the dynamic friction [77]. Bowden and Tabor proposed that sliding friction is dominated by both adhesion and deformation mechanisms acting between the contacting asperities of two mating surfaces.

The adhesion of asperities is caused by physical or chemical interactions at the interface between two surfaces. Physical interactions include hydrogen and van der Waals bonds, while the chemical interactions are covalent, ionic or electrostatic, and metallic bonds [77, 79]. Needless to say, chemical bonds produce a much higher adhesive force and, therefore, a higher frictional force than physical bonds. For this reason, lubricants with low surface energies are sought out.

The deformation mechanism, on the other hand, occurs as the opposing asperities of each surface mechanically interlock and act as a barrier to the moving body, and also vertically as the two surfaces are pressed together. The frictional force resulting from this mechanism is determined by the energy required for micro-scale deformation of the asperities. As the opposing surfaces slide over each other, the asperities experience both elastic and plastic deformation. If one surface is much harder than the other, the system will experience macro scale deformation where the harder surface ploughs/cuts through the softer surface producing grooves orders of magnitude larger than that of the asperities [77].

Friction produced during sliding contact is not constant, but experiences changes as the sliding process progresses. Frictional development can be classified into three stages, the

running-in period, steady-state, and finally the breakdown or destruction period. During the running-in period, the friction is a result of ploughing of the surface by the asperities on the counter face. As the surface is polished and contaminants are removed from the surface, the frictional force will settle to a more constant value which characterizes the steady-state period. As a result of the surface polishing and removal of asperities, the adhesion component of the friction typically increases for the steady-state period. Depending on the combination of hard and soft surfaces, the wear debris formed during sliding can either become trapped between the two surfaces and cause more ploughing, or fill in the valleys of the counterfaces producing a smoother contact between both surfaces [77]. Finally, as the lubrication film or coating is removed, and the substrate of the specimen is exposed to the counterface materials, the friction will increase drastically as the two unlubricated surfaces plough into each other.

3.4. Wear

Wear is a process that occurs during sliding, rolling, or impact motion of two opposing surfaces. Although many define wear as the removal of material from a surface, wear constitutes any damage to the surface, whether material is removed or not. There are six main wear mechanisms: (1) adhesive, (2) abrasive, (3) fatigue, (4) impact by erosion and percussion, (5) chemical (or corrosive), and (6) electrical-arc induced wear. However, the wear mechanism of a system is not limited to only one of these but can include any combination of the six [77]. To reduce wear, the materials of opposing bodies in a mechanical system must be carefully selected based on their mechanical properties such as hardness, fracture toughness, modulus of elasticity and shear strength.

Adhesive wear is a result of asperities of opposing surfaces coming into contact with each other and forming physical and/or chemical bonds. The relative motion between these surfaces

then causes the asperities of the softer material to deform and fracture, producing debris and transferring material to the counterface [21]. The influence of this adhesive force on friction was first described by Bowden and Tabor [80] and is now recognized as critical factor in friction and wear of surfaces [21].

Abrasive wear and asperity deformation are usually classified together. Abrasive wear occurs when a harder surface is rubbed against a softer surface and the asperities of the harder surface plough into the softer material. Abrasive wear can also occur as a result of a hard particle being introduced between the two sliding surfaces; this is called third body wear. These particles can be debris resulting from the sliding process or external contaminants that are trapped between both surfaces [21].

Fatigue and delamination wear are also classified together. Fatigue wear is a result of the formation of cracks resulting from loading and unloading of a surface. At a certain stress level, this repetitive loading and unloading will cause the formation and growth of cracks within the material which produce large scale removal of material. This wear mode is typical of rolling contact. The stress field produced by this contact shows a maximum stress point below the surface of the specimen. The maximum stress is typically located approximately one third of the contact length below the surface. This repetitive stress will form cracks which form at material voids or dislocation pile-ups. These cracks will then propagate and join with other cracks to release material. Delamination wear is a type of fatigue wear that occurs in sliding contacts. In this case, the cracks will form below the surface and propagate parallel to the surface producing delamination of long sheets of material [21, 81].

Finally, chemical wear is a wear process that is characterized by chemical changes to the material resulting from the relative motion between surfaces. As one surface rubs against the

other, the pressure, heat and frictional force involved in the process will result in chemical changes to the material, such as the breaking of bonds and formation of new bonds amongst molecules as well as bonds with other molecules present in the environment such as oxygen, water vapor, and hydrocarbon contaminants. These chemical changes will result in changes to the mechanical properties of the material which will influence wear [21].

In order to understand the triblogy of a contact between two surfaces in relative motion, it is necessary to determine the input and output parameters in the system. The input parameters include data such as the macro- and micro-scale geometry of the surfaces, the chemical composition of the materials, topography, environmental conditions (temperature, humidity), shear strength, elasticity, and viscosity. The energy input to the system must also be considered, such as the applied load and velocity. Once the tribological process is initiated, there are many output factors that will produce secondary effects in the system, such as chemical reactions, debris formation and material deformation. In addition, as the process unfolds, there will be changes to the initial geometry and chemical composition that will affect the friction and wear output of the process [77] .

3.5. Dip Coating

The Landau-Levich model is commonly used to determine film thickness of dip-coated films. This model specifically describes the behavior of Newtonian and non-evaporating fluids. The model balances two opposite forces, the adhesion of the fluid to the dip-coated surface and gravity induced viscous drag. The coating thickness, h, is thus determined by the solution density ρ, surface tension γ, viscosity η, gravity g, and dip-coating withdrawal speed u [82].

$$h = \frac{0.94\eta^{\frac{2}{3}}}{\gamma^{\frac{1}{6}}(\rho g)^{\frac{1}{2}}} u^{\frac{2}{3}} \qquad 3.7$$

However, most dip-coating applications use non-Newtonian fluids. Sol-gels and colloidal dispersion are typically used to deposit films on substrates. The resulting film thickness of these dispersions is affected by constant evaporation of the solvent which causes the viscosity, density and surface tension to be always changing. Thus, the thickness can be manipulated by varying the solids concentration as well as the withdrawal speed. A study by Faustini et al. [82] determined that the deposition of these films is governed by two regimes. They found that the first regime occurs at withdrawal speed above 60 mm/min. This regime is dominated by gravity induced viscous drag and is defined by the Landau-Levich model; in this regime the film thickness increases proportionally to the withdrawal speed. The second regime in this model occurs at withdrawal speeds below 12 mm/min. At these low speeds, the progression of the drying line of the coating is so slow that the solvent evaporation rate becomes a dominant factor in the film thickness. The meniscus is continuously fed by a capillary rise and the solvent evaporates before the gravity induced viscous drag pulls down the solids. In this regime the film thickness is inversely proportional to the withdrawal speed. Between 12 and 60 mm/min, the two regimes offset each other producing a film of minimum thickness [82].

Chapter 4

Experimental Design and Characterization Tools

The goal of this investigation was to develop a low friction, low wear PTFE composite coating. In order to meet this goal, experiments were designed that incorporated fabrication/processing parameter and testing conditions as variables, and friction, wear, surface chemistry and surface topography as quantifiable outcomes. This chapter presents the design of experiments (DOE) and also describes the science behind the equipment and measurement techniques used in each experiment.

4.1. Experimental Design

The investigation was divided into five sections: (1) influence of dip coating withdrawal speed on film thickness of colloidal PTFE; (2) wear resistant PTFE/SiO_2 nanoparticle composite film; (3) use of Au Nanoparticle filled PTFE films to produce low friction and low wear surface coatings; (4) wear resistant PTFE thin film enabled by a PDA adhesive layer; and, (5) combined effect of incorporating PDA as an adhesive layer and copper nanoparticle fillers in PTFE. The investigation was divided as such to evaluate the effect of hard nanoparticle fillers, soft nanoparticle fillers, priming with an adhesive layer, and finally combining the adhesive layer with nanoparticle fillers. Each of the five sections of this investigation had its individual objectives:

1. Influence of dip coating withdrawal speed on film thickness of colloidal PTFE

Objectives:

a) Determine whether the film thickness of dip coated colloidal PTFE fits the Landau-Levich model or the two regime model presented by Faustini.

b) Optimize the dip coating withdrawal speed and insertion orientation of the substrate to reduce variation in film quality.

2. Wear resistant PTFE/SiO_2 nanoparticle composite film

a) Objectives: Determine the effect of SiO_2 nanoparticle concentration on the friction and wear of PTFE films.

3. Use of Au Nanoparticle filled PTFE films to produce low friction and low wear surface coatings

Objectives:

a) Determine the effect of Au nanoparticle fillers on the friction and wear of PTFE films
b) Examine the dominant wear mechanism in PTFE thin films and PTFE + Au nanoparticle composite thin films.

4. Wear resistant PTFE thin film enabled by a PDA adhesive layer

Objectives:

a) Determine the effect of a PDA adhesive layer on the tribological performance of a PTFE film.
b) Examine the chemical changes in PTFE and PDA/PTFE as a result of sliding friction tests.

5. Combined effect of incorporating PDA as an adhesive layer and Cu nanoparticle fillers in PTFE

Objective:

a) To evaluate and understand the combined tribological effect of using a PDA adhesive primer and Cu nanoparticles as fillers in a PTFE top coat.

b) Evaluate the relationship between normal load and friction and wear of PDA/PTFE composite films.

4.1.1. Determine the effect of dip coating withdrawal speed on the film thickness

Faustini et al. describe the limitations of using the Landau-Levich model to determine the film thickness of dip coated colloidal and sol-gel solutions. They propose a two regime model in which the film thickness is inversely proportional to the dip coating withdrawal speed at speeds below 12 mm/min and proportional to the dip coating withdrawal speed at speeds above 60 mm/min [82]. This study evaluated whether a colloidal PTFE nanoparticle dispersion would follow Faustini's model or the traditional Landau-Levich model introduced in section 3.5. In order to do this, stainless steel samples were dip coated using withdrawal speeds within each regime as shown in Table 4.1. These results helped determine what dip coating conditions would provide the most predictable and repeatable coating thicknesses. In addition, the surface roughness of the samples prepared using each of the withdrawal speeds was also measured.

Table 4.1: DOE for study of the effect of dip coating withdrawal speed on the film thickness and roughness of colloidal PTFE nanoparticle dispersions.

Sample	Withdrawal	Substrate dipping orientation	Experiment
1, 11,	1 mm/min	perpendicular to polishing lines	Film thickness, roughness
2, 12,	5 mm/min	perpendicular to polishing lines	Film thickness, roughness
3, 13,	10 mm/min	perpendicular to polishing lines	Film thickness, roughness
4, 14,	60 mm/min	perpendicular to polishing lines	Film thickness, roughness
5, 15,	100 mm/min	perpendicular to polishing lines	Film thickness, roughness
6, 16,	1 mm/min	parallel to polishing lines	Film thickness, roughness
7, 17,	5 mm/min	parallel to polishing lines	Film thickness, roughness
8, 18,	10 mm/min	parallel to polishing lines	Film thickness, roughness
9, 19,	60 mm/min	parallel to polishing lines	Film thickness, roughness
10, 20,	100 mm/min	parallel to polishing lines	Film thickness, roughness

To determine the variation in film thickness at different locations within each sample, the experiments listed in Table 4.2 were carried out. This study helped determine what dipping withdrawal speed would be better suited to produce samples with even films that would allow for repeatable friction tests. The values for withdrawal speed in Table 4.2 are listed in mm/min to reflect the actual parameters that were input into the dip coater software.

Table 4.2: DOE for study of the effect of dip coating withdrawal speed on the film thickness variation within each sample.

Sample	Withdrawal speed	Experiment
31	10 mm/min	Analysis of film thickness variation
32	40 mm/min	Analysis of film thickness variation
33	70 mm/min	Analysis of film thickness variation
34	100 mm/min	Analysis of film thickness variation

4.1.2. Determine the effect of SiO_2 nanoparticle concentration on the friction and wear of PTFE films.

Many investigations have found that the optimal concentration of nanoparticle fillers in polymers can vary with the type of material used. Zheng et al. [67] found that for SiO_2 nanoparticles of 15 nm diameter in an epoxy resin matrix, the wear resistance decreases at concentrations above 7.5 wt.%. Hence, this experiment was designed to evaluate the tribological performance of PTFE films filled with 0-10 SiO_2 wt.%. As shown in Table 4.3, the study was carried out for SiO_2 dip coating dispersion concentrations of 0, 1, 5 and 10 wt.%. The experiment was repeated for three different samples at each concentration to obtain the effect of filler concentration on the tribological performance of the films. The friction tests were carried out for 1000 cycles using an applied normal load of 20 g, and then repeated using a normal load of 50 g. To observe the tribological behavior under lower loads and longer testing durations, the top performing sample with the highest concentration of SiO_2 and the top performing sample

with pure PTFE were also tested under an applied load of 10 g for a total of 6000 cycles. Finally, wear and chemical analyses were also performed on pure PTFE, PTFE + 5 wt.% SiO_2, and PTFE + 10 wt.% SiO_2 samples which showed the best performance in the 50 g friction tests.

Table 4.3: Study on the effect of SiO_2 concentration on the tribological performance of PTFE.

Sample	SiO_2 (wt.%)	Experiments
35	0 (control)	10 g, 20 g and 50 g friction test, wear analysis, chemical
36	1	20 g and 50 g friction test
37	5	20 g and 50 g friction test
38	10	20 g and 50 g friction test
39	0 (control)	20 g and 50 g friction test
40	1	20 g and 50 g friction test
41	5	20 g and 50 g friction test, wear analysis, chemical analysis
42	10	20 g and 50 g friction test
43	0 (control)	20 g and 50 g friction test
44	1	20 g and 50 g friction test
45	5	20 g and 50 g friction test
46	10	10 g, 20 g and 50 g friction test, wear analysis, chemical

4.1.3. Determine the effect of Au nanoparticle fillers on the friction and wear of PTFE films

Au nanoparticles are used as fillers in solid lubricants because of their low shear strength. Investigators have found that at a concentrations as low as 0.15 wt.%, Au can be effective in reducing the wear rate of certain polymers such as polystyrene [69]. Because of processing limitations and the cost of Au, the use of Au nanoparticles was limited to a concentration of 0.07 wt.%. This was the highest concentration available to the investigator. To study the effect of a 0.07 wt.% Au nanoparticle filler on the tribological performance of PTFE films, the experiments listed in Table 4.4 were carried out. A 20 g friction test was performed on three samples of PTFE and three samples of PTFE + Au. This experiment was repeated for a 50 g normal load. In addition, to examine the dominant wear mechanism in PTFE and PTFE + Au, and to study the

wear progression at various stages of the friction test, friction tests of 30 and 60 cycle duration were performed to allow the characterization of the wear tracks at these stages.

Table 4.4: Study on the effect of Au nanoparticles fillers on the tribological performance of PTFE films.

Sample	Au nanoparticle filler	Experiments
47	No	20 g and 50 g friction test, wear analysis
48	Yes	20 g and 50 g friction test, wear analysis
49	No	20 g and 50 g friction test, wear analysis
50	Yes	20 g and 50 g friction test, wear analysis
51	No	20 g and 50 g friction test, wear analysis
52	Yes	20 g and 50 g friction test, wear analysis
53	No	30 and 60 cycle 50 g friction test
54	Yes	30 and 60 cycle 50 g friction test

4.1.4. Determine the effect of using a PDA adhesive layer on the tribological performance of a PTFE film.

The study shown in Table 4.5 was designed to determine the effect of a PDA adhesive layer on the friction and wear of PTFE. The experiments carried out elucidated the dominant wear mechanism in each sample and provided insight into the role of the PDA adhesive layer. The experiments were repeated on three samples of PTFE and three samples of PDA/PTFE to obtain the effect of the PDA adhesive layer on the friction and wear of the film.

Table 4.5: Study on the effect of using a PDA adhesive layer on the tribological performance of PTFE films.

Sample	PDA adhesive layer	Experiments
55	No	50 g friction test, wear analysis
56	Yes	50 g friction test, wear analysis
57	No	50 g friction test, wear analysis
58	Yes	50 g friction test, wear analysis
59	No	50 g friction test, wear analysis
60	Yes	50 g friction test, wear analysis

To study the wear progression at various stages of the friction test, a study was designed to characterize the wear track after 1, 10, 60, and 1000 friction test cycles. The study was performed on one sample of PTFE and one sample of PDA/PTFE as shown in Table 4.6.

Table 4.6: Study on the effect of using a PDA adhesive layer on the tribological performance of PTFE films.

Sample	PDA adhesive layer	Experiments
61	No	1, 10, 60, and 1000 cycle 50 g friction test, wear
62	Yes	1, 10, 60, and 1000 cycle 50 g friction test, wear

To determine the effect of heat treatment on the surface chemical composition of PDA, the surface chemistry of two stainless steel substrates coated with PDA (one with no heat treatment and one heat treated to 250 °C) were analyzed. This study was also used to evaluate the change in surface chemistry in PTFE and PDA/PTFE after a 50 g friction test. Sample 55 and 58, the two samples which showed the best tribological performance in the 50 g friction test, were selected for this study. The surface chemical composition was analyzed on the intact coating and also inside the wear track produced during the friction test.

Table 4.7: Study on the effect heat treatment on PDA adhesive layer and effect of friction tests on the chemistry of the film.

Sample	Film	Heat treatment	Experiments
55	PTFE	250 °C	Surface chemistry analysis
58	PDA/PTFE	250 °C	Surface chemistry analysis
63	PDA	0 °C	Surface chemistry analysis
64	PDA	250 °C	Surface chemistry analysis

4.1.5. Evaluate and understand the combined tribological effect of using a polydopamine adhesive primer and Cu nanoparticles as fillers in a PTFE top coat.

This study had the purpose of optimizing the heat treatment process and evaluating the combined effect of using a PDA adhesive layer and a Cu nanoparticle filler in PTFE films. The heat treatment optimization experiment consisted of heat treating the samples using an established sequence of 120 °C, 300 °C, and 372 °C. The durations for the last two heating steps of the sequence were optimized to prevent degradation while also effectively fusing the film to the substrate. During the study of PTFE + SiO_2, it was observed that the best tribological performances occurred for samples heated long enough to produce a nearly transparent coating. As a result of this observation, the experiment shown in Table 4.8 was designed to determine the shortest possible durations for heat treatment that could be used to produce a transparent film. A minimal duration was desirable to prevent degradation of the film.

Table 4.8: Optimization of heat treatment PDA/PTFE nanoparticle composite films.

Sample	Film	Heat 1 300 °C	Heat 2 372 °C	Experiments
65	PDA/PTFE	1 min	1 min	Optical observation
66	PDA/PTFE	3 min	3 min	Optical observation
67	PDA/PTFE	4 min	4 min	Optical observation
68	PDA/PTFE	5 min	10 min	Optical observation

The next experiment, shown in Table 4.9, was designed to study the influence of Cu nanoparticles on the friction and durability of PDA/PTFE films.

Table 4.9: DOE of combined effect of PDA and Cu nanoparticle filler in PTFE.

Sample	PDA	PTFE	Cu	Experiments
69	Yes	Yes	No	50 g friction test, wear analysis
70	Yes	Yes	Yes	50 g friction test, wear analysis
71	Yes	Yes	No	50 g friction test, wear analysis
72	Yes	Yes	Yes	50 g friction test, wear analysis
73	Yes	Yes	No	50 g friction test, wear analysis
74	Yes	Yes	Yes	50 g friction test, wear analysis

A wear progression experiment, as shown in Table 4.10, was designed to observe the wear at various stages during the friction tests of PDA/PTFE and PDA/PTFE + Cu nanoparticle films.

Table 4.10: DOE of wear progression study on PDA/PTFE and PDA/PTFE + Cu.

Sample	PDA	PTFE	Cu	Experiments
75	Yes	Yes	No	1, 10, 60, and 1000 cycle 50 g friction test, wear
76	Yes	Yes	Yes	1, 10, 60, and 1000 cycle 50 g friction test, wear

Finally, a linearly increasing load scratch test experiment was designed to determine the load at which failure occurs in PDA/PTFE and PDA/PTFE + Cu nanoparticle films. The experiment design is shown in Table 4.11.

Table 4.11: DOE of linearly increasing load scratch test on PDA/PTFE and PDA/PTFE + Cu.

Sample	PDA	PTFE	Cu	Experiments
79	Yes	Yes	No	linearly increasing load scratch test
80	Yes	Yes	Yes	linearly increasing load scratch test
81	Yes	Yes	No	linearly increasing load scratch test
82	Yes	Yes	Yes	linearly increasing load scratch test
83	Yes	Yes	No	linearly increasing load scratch test
84	Yes	Yes	Yes	linearly increasing load scratch test

4.2. Characterization Tools

4.2.1. Tribometry

In order to measure the frictional force on samples and produce wear tracks which could later be analyzed to reveal wear progression, two types of tribometers were used. The first tribometer used is an automatic friction abrasion analyzer (TS501, Kyowa Interface Science Co., Ltd.). The TS501 tribometer functions in a linear reciprocating manner. An image of the equipment and a diagram of the experiment setup are shown in Figure 4.1. As the stage is moved under an

applied normal load, a frictional force is generated which is measured by a load cell. The type of counterface used in the friction tests was a chrome steel counterface of 7 mm diameter.

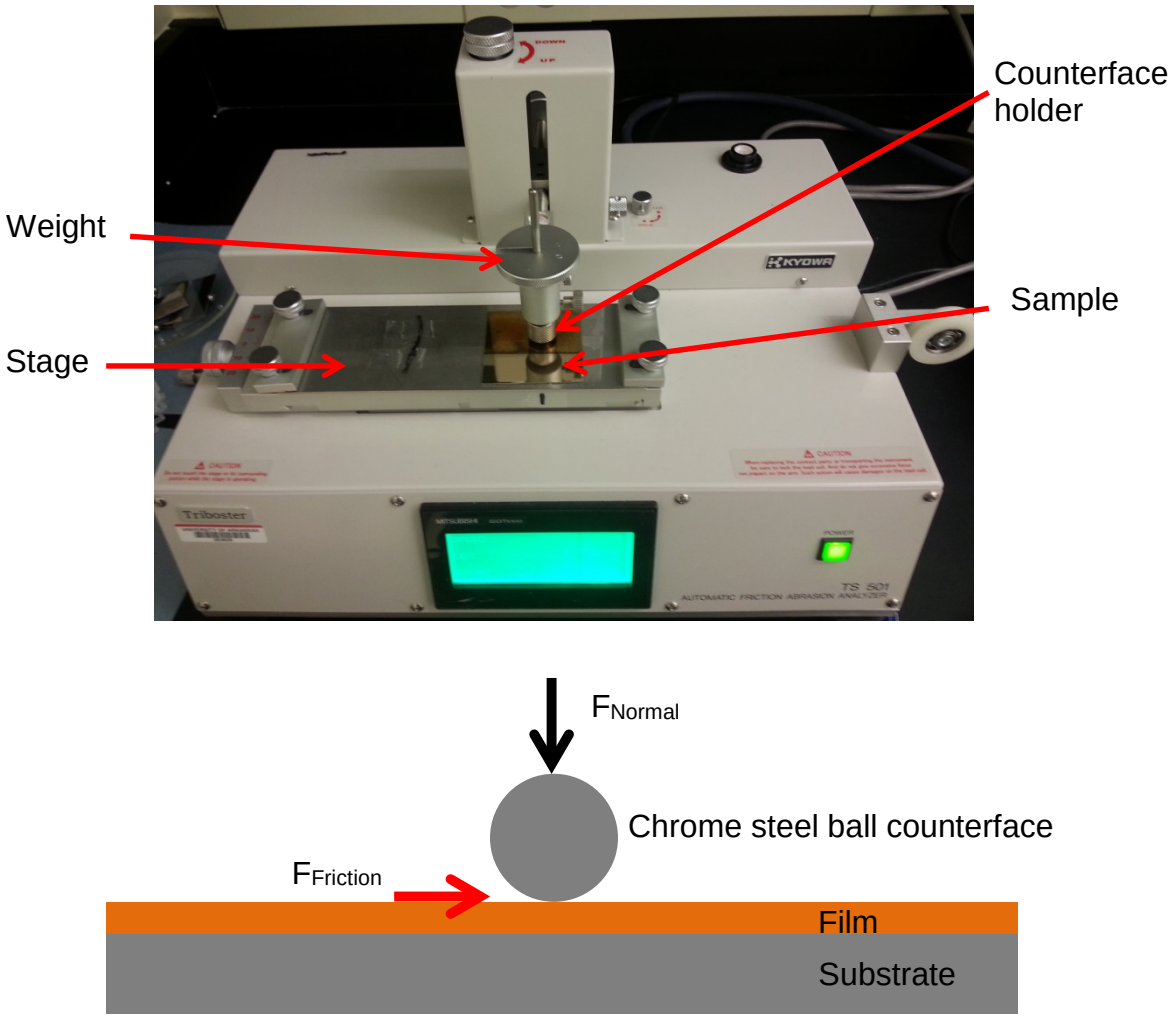

Figure 4.1: Tribological testing setup – Kyowa TS501.

The load cell only measures the frictional force as the stage slides to the right and not as it returns to the start position. The TS501 has a sampling rate of 200 Hz or one data point every 5 ms. This data is then used to determine the static COF (μ_s), dynamic COF (μ_k), maximum dynamic COF (μ_{kmax}), minimum dynamic COF (μ_{kmin}), and the difference between the max and min dynamic COF ($\mu_{kw} = \mu_{kmax} - \mu_{kmin}$). Point A in Figure 4.2 represents the point at which the

COF rises above 0.02. Point B represents 0.5 seconds of elapsed time after Point A. Point C is the point where 95% of the total cycle duration has elapsed. Point D represents the point at which there is 0.6 seconds left before point E, where the COF drops below 0.02 again as the stage comes to a stop. The static COF μ_s for each cycle is obtained from the maximum value between A and B. The dynamic COF is determined by taking the average value between B and C [83].

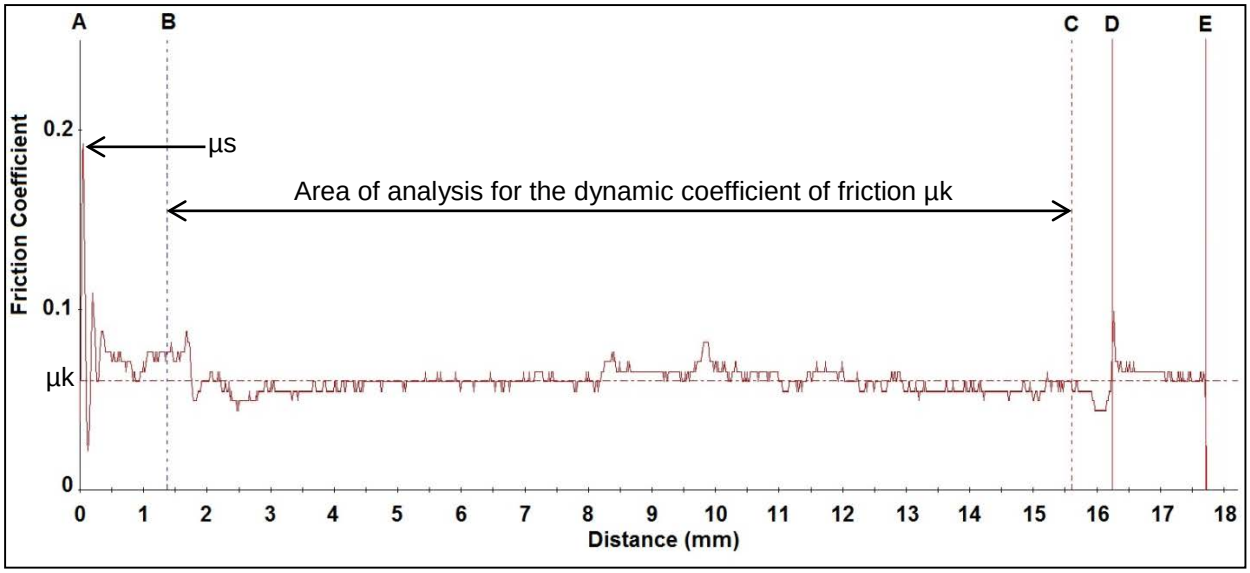

Figure 4.2: Kyowa tribometer area of analysis.

A Nano + Micro Tribometer (UMT-2, Bruker, Santa Barbara, CA) was used to perform linear reciprocating and load dependent scratch tests. The UMT-2 is a fully computerized tribometer that allows high resolution friction measurements [84]. The system is shown in Figure 4.3. The load sensor used for the experiments in this investigation is the FL model, which can measure Fx and Fz loads up to 500 mN with a resolution of 50 μN. The software for the UMT-2 system does not automatically calculate the static and dynamic portions of the COF, so

these values were calculated by exporting the data captured to excel and using a similar method as the TS501 to calculate these values.

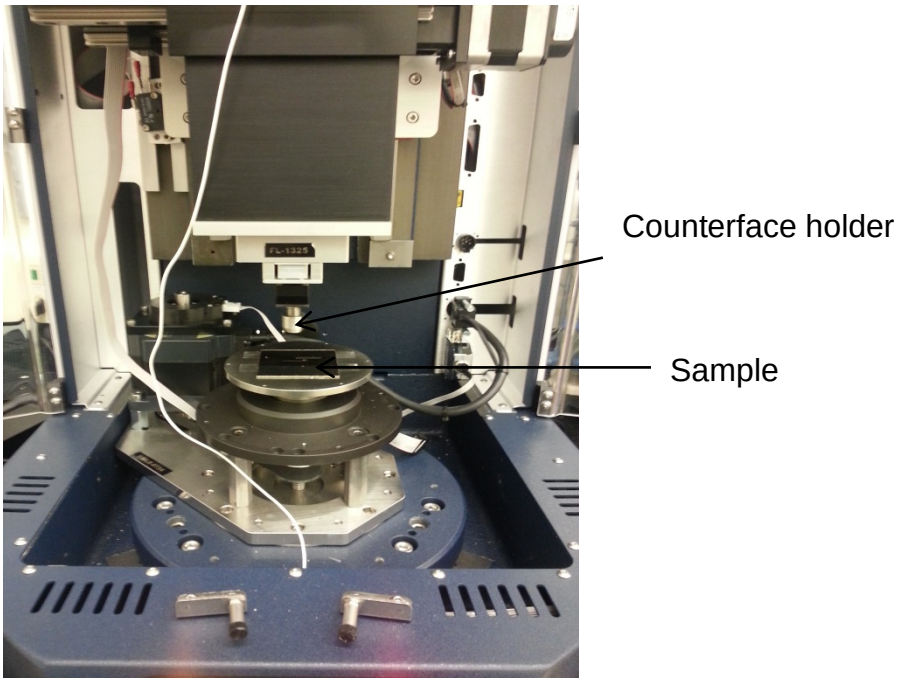

Figure 4.3: UMT tribometer.

To ensure accurate friction measurements, both tribometers were carefully calibrated prior to the beginning of the tests. In addition, all counterfaces used were cleaned using a strict cleaning process identical to the sample cleaning process used in each study. The cleaning procedure is described in detail in section 5.2.1.

4.2.2. Surface Topography Characterization

An atomic force microscope (AFM; Dimension Icon, Bruker, Santa Barbara, CA) was used to characterize the surface topography. Two imaging techniques were utilized in this investigation. The first is Bruker's ScanAsyst mode which uses algorithms to continuously

monitor and change imaging parameters such as setpoints, feedback gains, and scan rates to produce high quality images. This technique was used to characterize micro and nanoscale features on the sample surface. The second technique used was that of Peak force QNM (Quantitative Nanomechanical Property Mapping). This technique was used to map the adhesion force on the sample surface. Finally, single ramp force curves were also captured on the sample surface using the Contact Mode technique. This final technique was used to quantify the adhesion force between a C_4F_8 coated AFM probe and the sample surface.

Figure 4.4 shows a typical AFM cantilever. The distance G is the tip-sample gap. This distance is the difference between the initial tip-sample spacing Z and the cantilever deflection caused by tip-sample interactions D. The distance G is directly proportional to the force applied on the cantilever. The deflection of the tip is measured through a laser which is reflected from the cantilever top surface onto a split photodetector. Thus, the lever deflection is proportional to the position of the reflected laser beam on the photodetector [85].

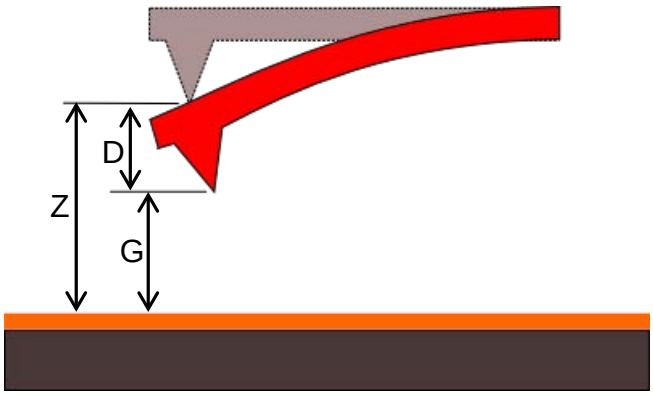

Figure 4.4: Schematic of AFM tip

Figure 4.5 shows the loading curve and cantilever position associated with typical AFM operation. The cantilever approaches the sample surface within the piezo Z range until the tip contacts the sample surface. Subsequent movement of the piezo results in deflection of the

cantilever. Section 1-2 of the curve shows the approach of the tip. As the tip gets closer to the sample surface, tip-sample interaction causes the cantilever to deflect downward and contact the sample surface. This deflection can be seen in section 2-3 of the curve. As the piezo continues to move toward the sample surface, the cantilever is deflected in an upward direction as shown in section 3-4 of the loading curve. Point 4 is the maximum deflection point. At this point, the piezo begins to retract until it reaches point 5 where the retracting force is higher than the tip-sample interactive forces. At point 5, the tip detaches from the sample surface and returns to zero deflection shown as point 6. In contact mode, the cantilever is maintained at point 4 by specifying a deflection setpoint. The tip is then raster scanned along the sample surface and the piezo Z position continuously changes to maintain the specified deflection setpoint. The piezo Z position is then plotted as a function of the x and y position to reveal the surface topography [85, 86].

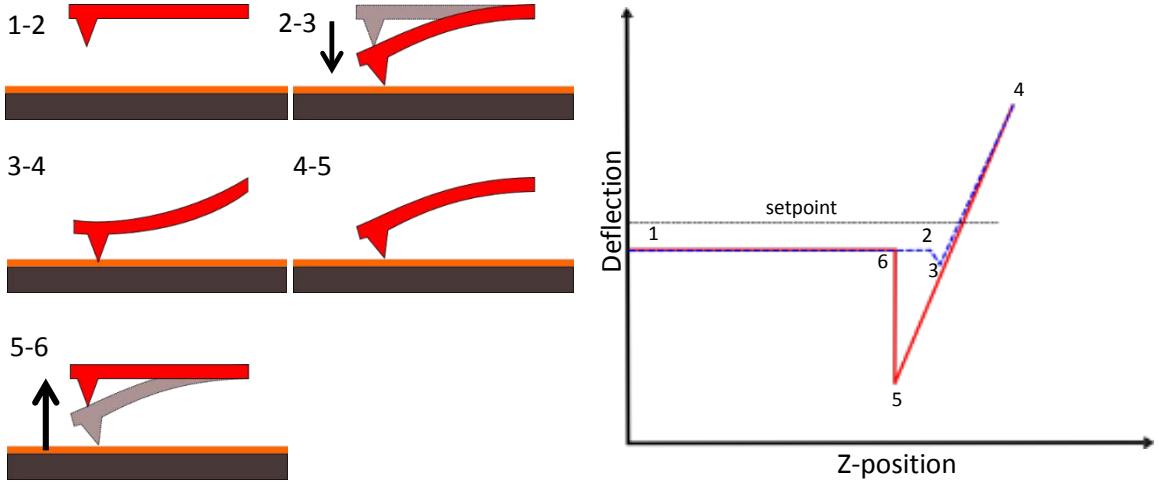

Figure 4.5: Schematic of AFM loading curve and tip position.

Conventional tapping mode is typically used to avoid lateral forces and drag across the surface while maintaining high lateral resolution. In tapping mode, the cantilever is oscillated

near or at its resonant frequency in a direction normal to the sample surface. The cantilever is oscillated by applying an AC signal to the probe holder piezoelectric stack. The drive frequency is maintained constant and the tip-sample spacing is changed to maintain a constant cantilever amplitude without changing the drive frequency. Like in contact mode, the piezo Z position is plotted as a function of the x and y position to reveal the surface topography [85, 86].

The resonance curve of a cantilever in tapping mode is shown in Figure 4.6 (a). The curve, shown in red, represents a cantilever oscillating at or near its resonant frequency. Once the tip comes close to the sample surface, the resonant frequency of the cantilever will shift to a higher value, as shown in the green line in Figure 4.6 (b). The change in resonant frequency is a result of tip-sample interactions which initially repel the tip as it approaches the surface, essentially increasing the spring constant of the cantilever and thus increasing the resonant frequency. Because the cantilever is still driven at the initial frequency f_0, shown in green, the amplitude of the oscillating cantilever drops to a lower value [85-87].

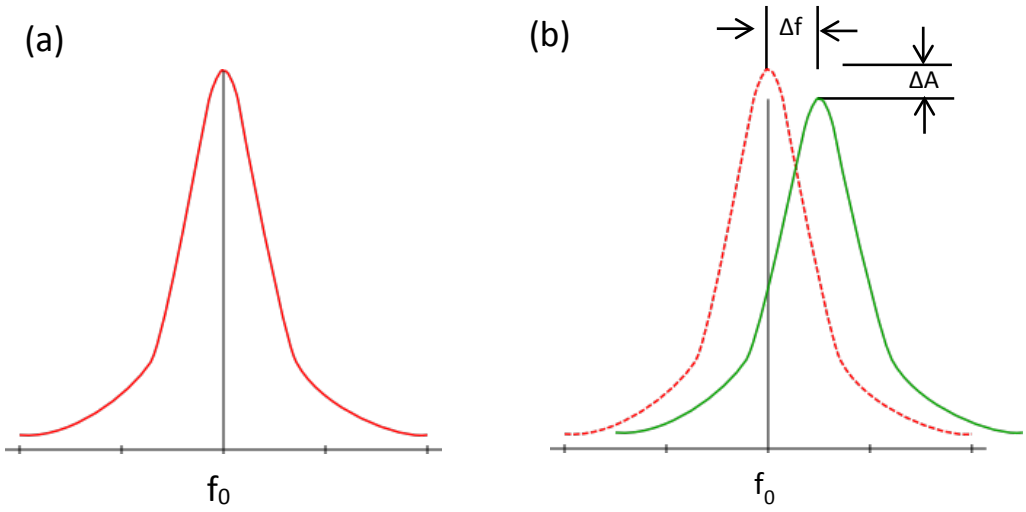

Figure 4.6: Resonance curve of an AFM cantilever in tapping mode (a) away from sample surface (b) close to sample surface.

Bruker's ScanAsyst mode uses Peak Force Tapping as its underlying operation mode. Peak Force Tapping is similar to conventional tapping mode with the difference that the tip oscillations are maintained well below the resonant frequency of the tip cantilever. By oscillating below the resonant frequency, filtering effects and dynamics of resonating systems are avoided. This allows force curves to be continuously captured at frequencies between 1 and 10 kHz. The peak force in each of these curves is then used as trigger values to control the piezo Z position. A feedback algorithm can recognize the individual peak force even though it may be below the setpoint. This allows the user to image a sample surface at much lower forces which is helpful when imaging soft surfaces. Peak force tapping decouples cantilever response from resonance dynamics. This allows ScanAsyst to use the cantilever response values to automatically adjust important imaging parameters such as the setpoints, feedback gains, and scan rates to produce high resolution images without the need for user adjustment [85-87].

A Stylus Surface Profiler (Dektak 150, Veeco Instruments, Inc., Plainview, NY) was used to determine the coating thickness and wear track cross-sectional profile on each sample. This device uses a stylus to physically contact and scan over a surface, revealing a profile of the surface topography. The low inertia sensor which measures the position of the stylus allows the measurement of step heights down to 10 angstroms. The Dektak 150 is equipped with an X-Y automated stage which allows the user to program measurements over 200 different locations as well as producing surface maps from multiple scans. The coating thickness and cross-sectional profiles were measured using a 12.5 μm radius stylus, 3 mg contact force, and scanning speeds no greater than 40 μm/sec to maintain an adequate level of stylus sensitivity. The wear track profile was established by running the stylus along the width of each wear track. The samples were only partially coated with the film, leaving a small area of uncoated stainless steel on each

sample. The coating thickness was determined by running the stylus across the coating edge, measuring the height difference between the uncoated stainless steel and coated film. The average coating thickness for each sample was determined by taking an average of 3 measurements taken at different locations along the coating edge.

4.2.3. Surface Chemistry Characterization

X-ray Photoelectron Spectroscopy (XPS) and Energy-dispersive X-ray spectroscopy (EDS) were used to respectively characterize the surface chemistry and surface elemental composition of all samples, including substrate, coatings, and wear tracks. This characterization was carried out to reveal the chemical composition of the various coatings as well as to observe the chemical changes that resulted from the tribological testing.

The majority of chemical characterization was carried out using X-ray photoelectron spectroscopy (XPS; PHI 5000 VersaProbe, ULVAC-PHI, Kanagawa, Japan). The XPS spectra were obtained using a monochromatic Al K_α (1486.6 eV) source with a 100 μm spot size. Both XPS survey spectrum and high-energy resolution (Hi-Res) scans were acquired. Because PTFE is an insulator, dual-beam neutralization was used to avoid charge build up on the samples. Additionally, all spectra were shifted based on adventitious carbon at a binding energy of 284.8 eV to allow for comparison between spectra.

XPS is a technique that is commonly used for surface chemical characterization. The system functions in ultrahigh vacuum ($<10^{-7}$ Pa) and the sample surface is irradiated with mono-energetic x-rays which causes photoelectrons to be emitted from the sample surface. The kinetic energy of the emitted photoelectrons is then measured by an electron energy analyzer. Using the known energy of the X-ray photons of specific wave length that are irradiating the surface, and

the kinetic energy measured by the electron energy analyzer, the binding energy of the photoelectron can be calculated using Einstein's equation:

$$E_B = h \cdot v - E_K - \phi \qquad 4.1$$

where E_B is the binding energy of the emitted electrons, $h{\cdot}v$ is the energy of the irradiating photons, E_K is the kinetic energy of the emitted electrons, and ϕ is the work function of the spectrometer. The work function of the spectrometer can be calculated based on the Fermi level E_F and the vacuum level E_V [88, 89].

Figure 4.7 depicts the process of irradiating a sample to emit photoelectrons from the surface. X-rays are emitted from an aluminum anode producing Al-K_α photons which have a line energy of 1486.6 eV and a line width of 0.85 eV. The line width is reduced to 0.4 eV through the use of a monochromator. The benefit of using a monochromator is the elimination of effects caused by weaker Al-K_α satellite lines as well as the reduction of the effect of the Bremsstrahlung continuum from the X-ray spectrum of the anode. Figure 4.7 shows an Al-K_α photon being absorbed by a core level electron. Photoemission will only occur from levels where $E_B + \phi$ is less than the X-ray energy $h{\cdot}v$ [88, 89].

In addition to photoemission resulting from emitted core level electrons, Auger electrons are also ejected. This process results when an ionized atom returns to its ground state, and as a result, emits an Auger electron. Both core level peaks and Auger peaks contribute to the final XPS spectrum [89].

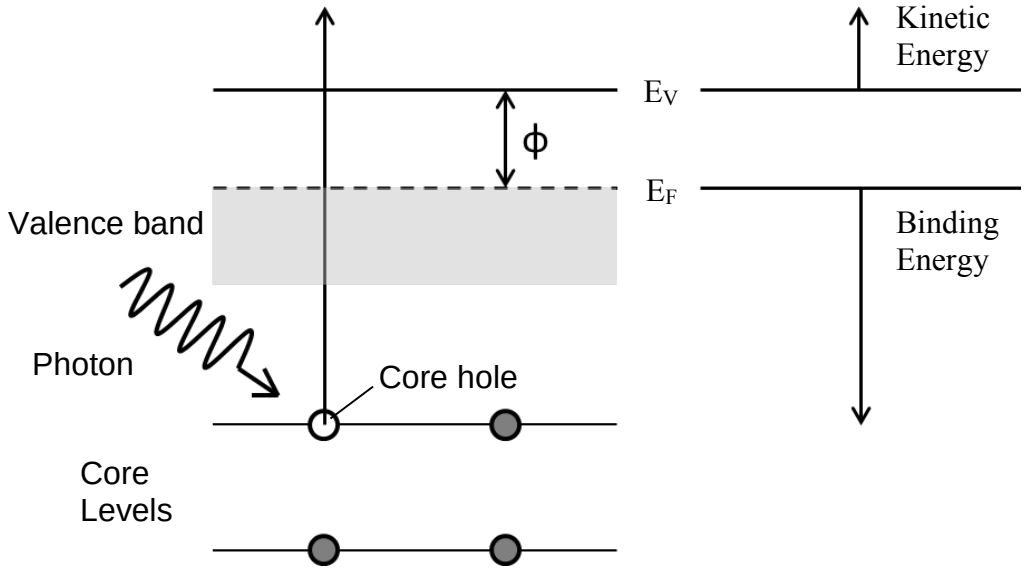

Figure 4.7: XPS surface irradiation and photoelectron emission process.

Energy-dispersive X-ray spectroscopy (EDS) was carried out using a scanning electron microscope (SEM, Phillips/FEI Model XL-30). In contrast to XPS, EDS uses a focused beam of electrons to bombard the sample surface, emitting an X-ray spectrum (lower sensitivity than XPS). The beam is raster scanned over the surface allowing elemental analysis of a relatively large area. The EDS method typically has an overall accuracy of approximately 2% and a sensitivity of 1000 ppm when using routine procedures. The spatial resolution depends on the vertical penetration and horizontal spread of the electron beam; these are a function of density and differ for the type of material being analyzed [90].

4.2.4. Surface Imaging

An optical microscope (model XJP-H100, American Scope, Irvine, CA) was used to characterize each sample and counterface. The optical images were captured to qualitatively compare the wear tracks and to identify film transferred to the counterface after the friction tests.

Additionally, Scanning electron microscopy (SEM, Phillips/FEI Model XL-30) was used to produce SEM micrographs of different magnifications. These micrographs were captured to examine the micro/nano-scale topography of each sample. To better show the surface topography, 45 degree oblique angle views were used for all measurements.

The Phillips/FEI XL30 is an environmental scanning electron microscope that employs a field-emission electron source and has a resolution between 1 and 10 nm. The field emission electron source functions by subjecting a tungsten cathode tip to a strong electric field, allowing electrons to escape by quantum-mechanical tunneling. Because the work function for tungsten is very high (φ=4.5 eV), the electric field needed to allow electrons at the Fermi level to escape is also very high, of the order of 10^{10} V/m. The emitted electrons have a wave length of 0.5 nm and an energy distribution of ΔE=0.3 eV, which allows for high spatial resolution [91].

Chapter 5

Influence of dip coating withdrawal speed on film thickness of colloidal PTFE

5.1. Overview

Section 3.5 presented two models that describe the relationship between dip coating parameters and the resulting coating thickness of a film. The first is the Landau-Levich model and the second is a two regime model presented by Faustini et al. [82]. To see how closely the PTFE aqueous dispersion in this investigation follows these models and to optimize the dip coating parameters to enhance tribological performance, stainless steel samples were dip coated in a PTFE colloidal dispersion at five different withdrawal speeds belonging to each regime described by the models as shown in Table 4.1. The final coating thickness of the film was measured after sintering the film at 337 °C.

5.2. Experimental Methods

5.2.1. Sample Preparation

Pre-cleaned 0.76 mm-thick stainless steel type 316 (McMaster-CARR/9759k31) were first cut into 2.5 cm by 2.5 cm square samples and ultrasonicated in acetone for 20 minutes to removes oils and organic contaminants. They were then immersed in isopropyl alcohol (IPA) and ultrasonicated for 5 minutes. Next the samples were submerged in deionized water to rinse of residues. To conclude the cleaning process, the samples were blown dry using nitrogen gas.

PTFE aqueous dispersion (TE-3859 from DuPont) of 60 wt.% concentration was used as the dipping solution. A dip coater (KSV DC from KSV Instruments Ltd.) was used to deposit the PTFE thin films on the sample surfaces. A total of 30 samples were dip coated at 1, 5, 10, 60, and 100 mm/min (Table 4.1). Six samples were coated at each withdrawal speed. Of these,

three were coated by immersing in a direction parallel to the polishing lines and three were coated perpendicular to the polishing lines.

After dip coating, the samples were dried at 120 °C (as suggested in DuPont's product information) [16] for 2 minutes using a hot plate in order to remove water. Next, the samples were baked in a furnace at 300 °C for 5 min, and finally, samples were annealed at 337 °C for 10 min.

5.2.2. Sample Characterization

A stylus surface profiler (Dektak 150, Veeco Instruments, Inc.) was used to measure the coating thickness and surface roughness of the samples. The measurements were taken using a 12.5 μm radius stylus, 9.8 μN contact forces, and 100 μm/s scan speed for a scan length of 4 mm. The coating thickness was determined using two different methods. First, the thickness was determined by running the stylus across the coating edge, measuring the height difference between the uncoated stainless steel and coated film. Second, the thickness was determined by scratching the surface of the film in five different locations and running the stylus over each scratch to produce a cross-sectional profile. The measurements were taken at different locations on each sample to produce results representative of the overall coating surface.

5.3. Results

Figure 5.1 shows the results for the samples coated perpendicular to the polishing lines. The thickness of the film increased with increasing withdrawal speed and did not follow the 2 regime model described by Faustini et al. [82]. Below the critical withdrawal speed of 12 mm/min the coating thickness increased almost linearly and leveled off at a maximum of approximately 2700 nm between 10 mm/min and 60 mm/min. A decrease in coating thickness between withdrawal speed of 1 and 10 mm/min, as would be expected from the two regime model, was not observed.

Rather, the coating thickness closely followed the Landau-Levich model for Newtonian fluids up to a dipping speed of 10 mm/min, after which the coating thickness saturated at approximately 2700 nm.

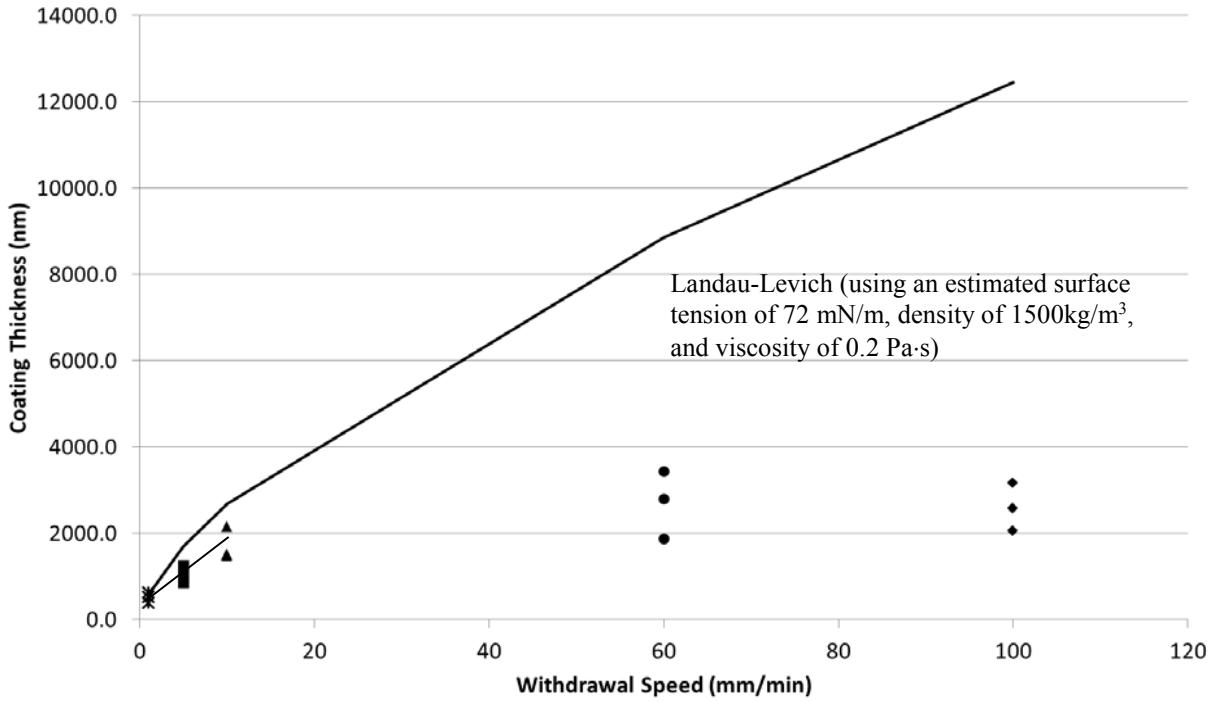

Figure 5.1: Coating thickness vs. withdrawal speed for samples dip coated in a direction perpendicular to the polishing lines of the stainless steel substrate.

Figure 5.2 shows the coating thickness for samples coated in a direction parallel to the substrate polishing lines. Again, the same linearly increasing trend was observed between withdrawal speed of 1 and 10 mm/min as was observed in Figure 5.1, and the coating thickness saturated at approximately 3000 nm. At a speed of 100 mm/min the coating thickness appeared to slightly decrease. However, because of the large error present in thickness measurements for withdrawal speed at or above 60 mm/min, it is not definitive that there is in fact a drop in coating thickness. One observation that can be made is that faster withdrawal speeds have a wider

variation in film thickness. It can be concluded that slower speeds are better if a precise coating thickness is desired.

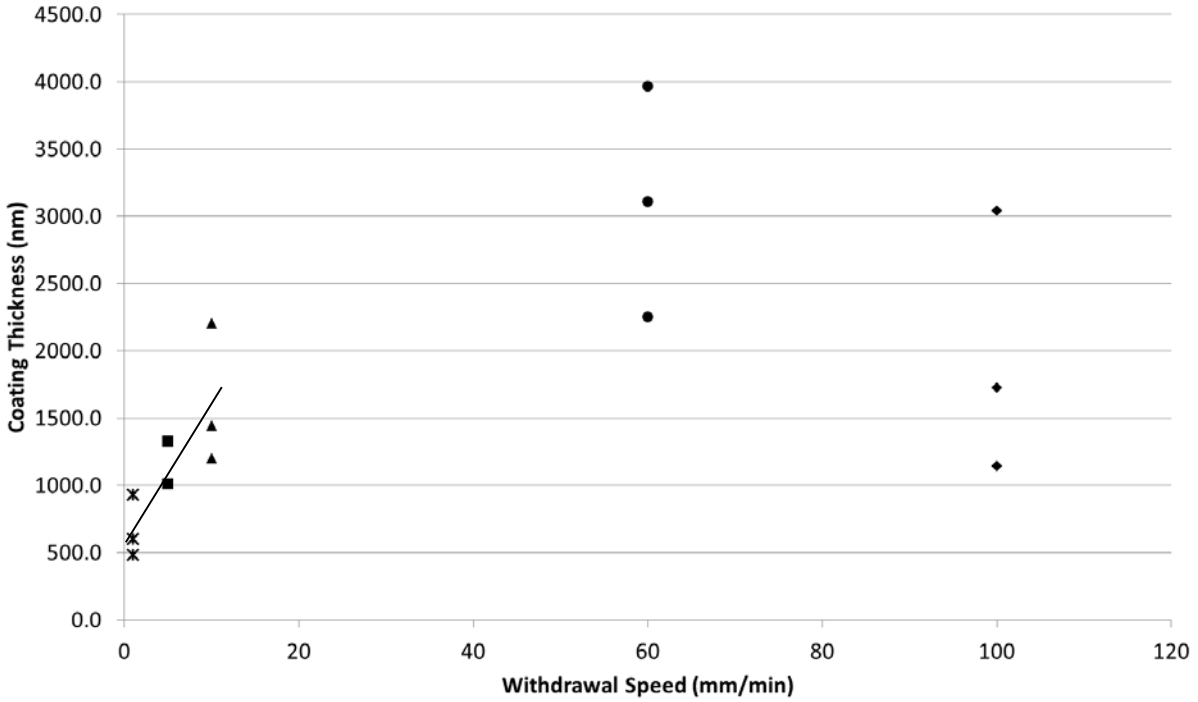

Figure 5.2: Coating thickness vs. withdrawal speed for samples dip coated in a direction parallel to the polishing lines of the stainless steel substrate.

The average roughness was also measured for each sample in order to determine whether the dip coating speed has a significant effect on the morphology of the film. Figure 5.3 shows the results for the average roughness of the samples coated in a direction perpendicular and parallel to the polishing lines. The roughness results show a slight decreasing trend in roughness with increasing withdrawal speed between withdrawal speeds of 1 and 10 mm/min. At higher speeds, the roughness increased slightly and fluctuated between 15 nm and 16 nm. Another important observation is that the roughness values of the samples dip coated in a direction parallel to the polishing lines were consistently higher than that of the samples dip coated perpendicular to the

polishing lines for withdrawal speeds between 1 and 10 mm/min. However, at speeds above 60 mm/min the roughness values for both dip coating directions have very similar roughness.

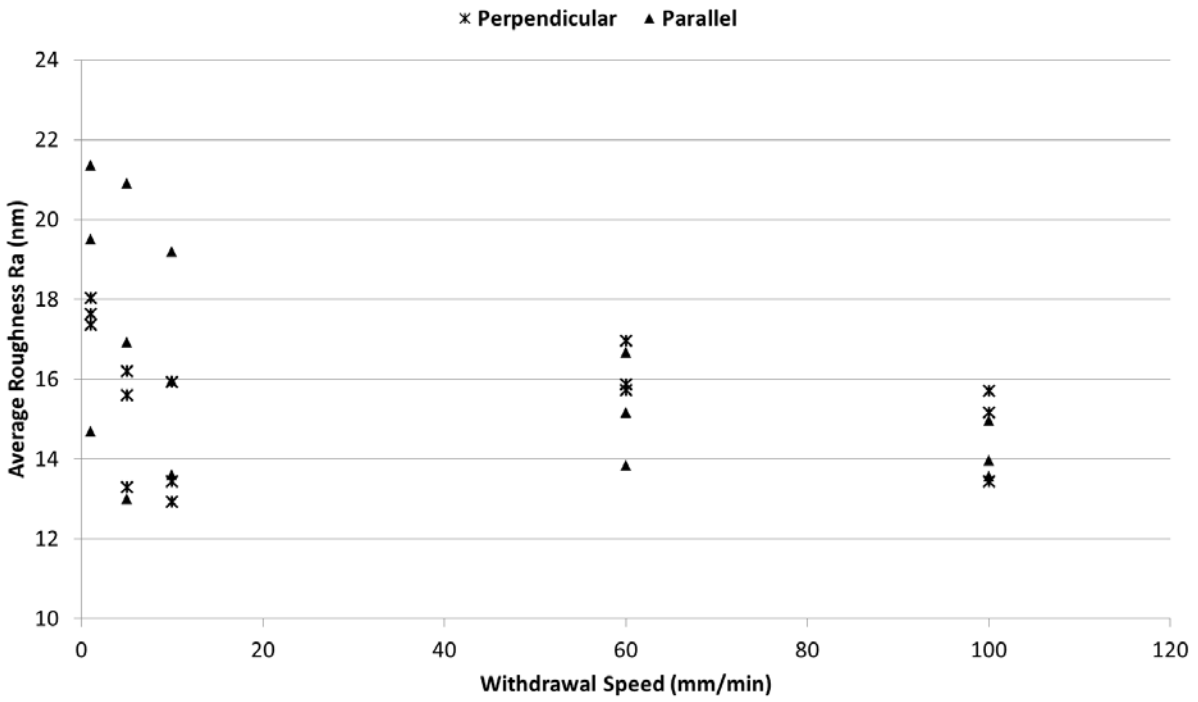

Figure 5.3: Surface roughness vs. withdrawal speed for sample dip coated in a direction perpendicular and parallel to the substrate polishing lines.

Cross-sectional profiles of the step at the leading edge of the film showed a clear peak at the edge for dip coating withdrawal speeds below 60 mm/min. Figure 5.4 (a) shows a sketch of this phenomenon. The large peak at the edge is representative of the capillary feeding effect, where the solid particles are fed to the leading edge of the film through capillary rise. These samples also showed a very even thickness in the coating after this initial peak. At higher speeds, as shown in Figure 5.4 (b), a constantly increasing thickness is observed further away from the leading edge of the film. These results showed that measuring the coating thickness at the leading edge may not be the most effective method for samples coated using faster withdrawals

speeds, even when using 4 mm long Dektak profiles. Furthermore, the changing thickness in samples coated using faster withdrawal speeds poses a risk to the accuracy of any subsequent friction tests. If three friction tests are carried out on a sample, each at a different distance from the leading edge, the friction results and also durability would be quite different for each test.

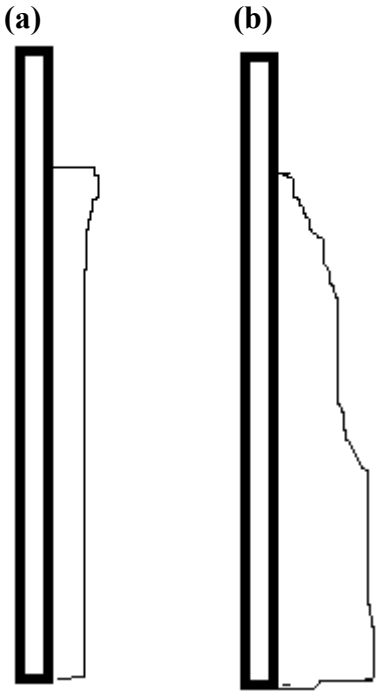

Figure 5.4: Coating morphology at speeds (a) below 60 mm/min and (b) at or above 60 mm/min.

To further study the variation in coating thickness at different locations within each sample surface, an experiment was carried out to measure the thickness of the film at predefined locations. In this experiment all samples were dip coated in a direction perpendicular to the polishing lines. However, to produce thinner films without further reducing the withdrawal speeds, the dipping solution was diluted to a 40 wt.% concentration. To measure the coating thickness, two different methods were used. First, the step height of the coating edge was measured. These measurements were taken close to the left edge, middle and right edge of the

samples, and the locations are respectively labeled 1, 2 and 3 in Figure 5.5. Second, five scratches were created by lightly running a diamond scribe over the sample surface (care was taken not to scratch the substrate surface). These scratches are labeled 4-8 in Figure 5.5. The results for the two methods were compared for each sample.

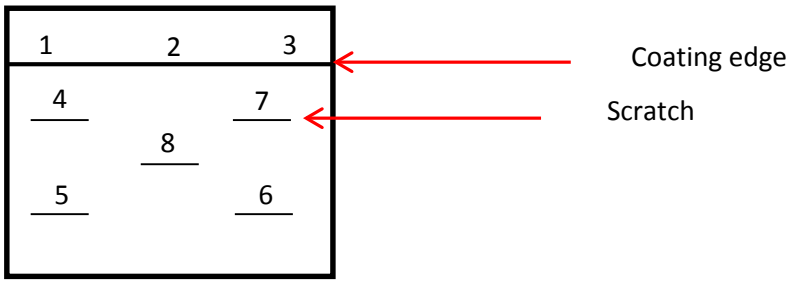

Figure 5.5: Sample coating thickness measurement location.

Table 5.1 shows the results for the individual measurements that were taken at each location. The results show that there was a trend of increasing thickness closer to the bottom of the sample. This is specially the case for samples dip coated at faster withdrawal speeds.

The graph in Figure 5.6 shows the average thickness for the measurements taken at the coating edge, and also the average thickness for the measurements taken on the 5 scratches. There is a significant difference between the results of the two methods. The thickness values for the scratches were typically higher than those for the coating edge, except at very low withdrawal speeds. This confirms the conclusions derived from Figure 5.4. The error in the scratch method is a result of the increasing thickness towards the bottom of the sample. This experiment also confirms that dipping speeds below 60 mm/min show less variation in the film thickness at different location on the same sample, as is evident from the error bars in Figure 5.6.

Table 5.1: Coating thickness measurements.

Withdraw speed	Thickness measurement [nm]							
	1	2	3	4	5	6	7	8
10 mm/min	713	745	639	507	614	664	520	573
40 mm/min	975	788	855	1097	1089	1029	1087	1159
70 mm/min	976	996	914	1060	1240	1314	1009	1286
100 mm/min	1010	1451	1002	1186	1501	1471	1248	1450

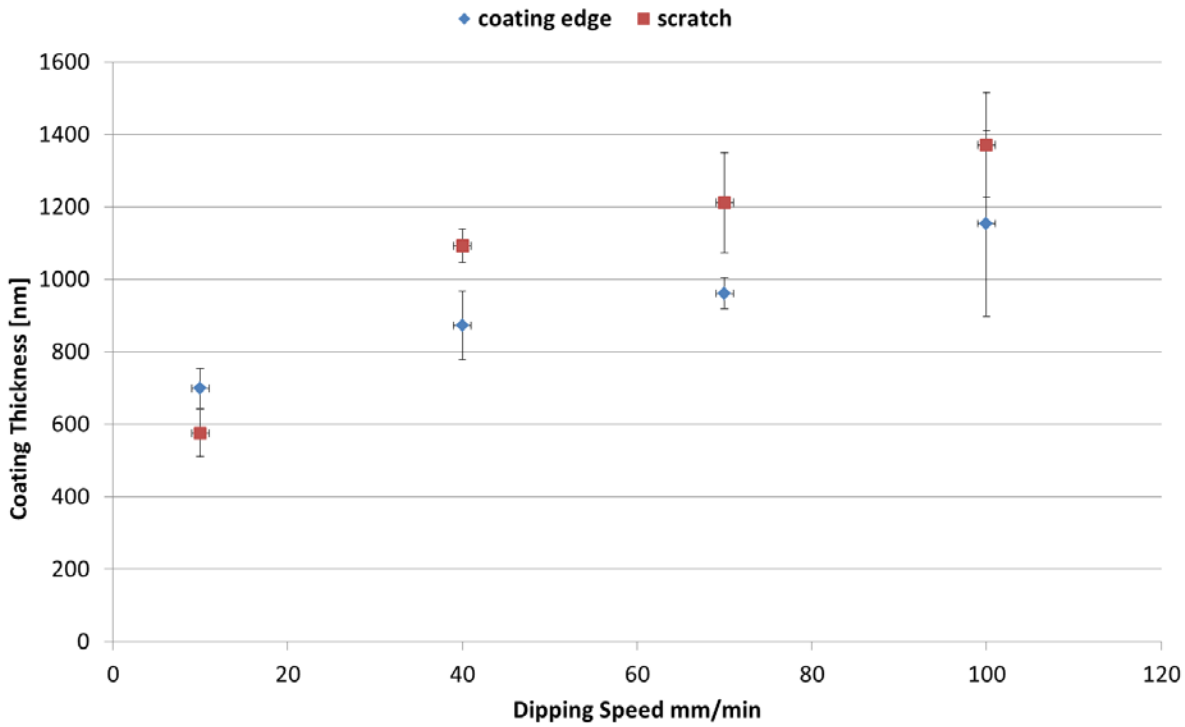

Figure 5.6: Graph of the average thickness for each measurement type.

5.4. Summary

To produce samples with even films of predictable thicknesses, dipping speeds below a withdrawal speed of 60 mm/min were selected for later studies in this investigation. This allowed the preparation of samples with less variation in coating thickness amongst each other as

well as less variation within the surface of each sample itself. In addition, it was determined that dip coating in a direction perpendicular to the polishing lines produced less variation in the film thickness between the samples. Therefore, all samples prepared in later studies were fabricated in such a manner.

Chapter 6

Wear resistant PTFE/silica nanoparticle composite film

6.1. Overview

In this study PTFE/SiO_2 nanocomposite films were fabricated on a stainless steel substrate utilizing different concentrations of colloidal SiO_2. SiO_2 was used because of its proven ability to increase the development of a transfer film on the counterface [42] as well as increasing the tensile strength, tensile modulus, and impact strength of polymer resins [67], and as a result also increasing the wear resistance of the film. Dip coating was chosen as the method of film deposition due to its low cost and simplicity. The composite films were subsequently subjected to friction tests in order to measure the COF and wear resistance of the film.

6.2. Experimental Methods

6.2.1. Sample Preparation

Pre-cleaned 0.76 mm-thick type 316 stainless steel was first cut into 2.5 cm by 2.5 cm square samples and then cleaned as described in section 5.2.1. PTFE aqueous dispersion of 60 wt.% concentration, as well as SiO_2 colloidal dispersion (Snowtex-PS-M from Nissan Chemicals) of 20 wt.% concentration, were used to produce various dip coating mixtures. The TE-3859 dispersion contains PTFE particles ranging from 0.05 to 0.5 μm suspended in water [16]. Colloidal silica is made by growing mono-dispersed, negatively charged amorphous silica particles, ranging from 18-25 nm, in water [92]. In addition to the as received pure PTFE solution, a total of three different dipping solutions were created by mixing PTFE (60 wt.%) with SiO_2 (1 wt.%, 5 wt.%, and 10 wt.%) dispersions at a 2:1 weight ratio. The resulting solutions are referred to as 0.3% SiO_2/PTFE composite, 1.7% SiO_2/PTFE composite, and 3.3% SiO_2/PTFE composite.

A dip coater was used to deposit the nanoparticle composite dispersions on the sample surfaces. Three cleaned stainless steel samples were dip-coated in each type of solution at an insertion and withdrawal speed of 10 mm/min and an immersion time of 20 sec. All samples had an insertion direction perpendicular to the polishing lines. After dip coating, the samples were dried at 120 °C (as suggested in DuPont's product information) [16] for 2 minutes using a hot plate in order to remove water. Next, the samples were baked in a furnace at 300 °C for 5 min, and finally, samples were sintered at 337 °C for 10 min.

6.2.2. Characterization of Surface Topography

A stylus surface profiler was used to measure surface roughness of the samples. The measurement was taken using a 12.5 μm radius stylus with 9.8 μN contact forces at 100 μm/s scan speed for a scan length of 1 mm. Three measurements were taken at different locations on each sample. The average roughness and root mean-square (RMS) roughness were recorded for each sample.

Scanning electron microscopy (SEM, Phillips/FEI Model XL-30) was used to characterize the surface topographies of all samples. SEM micrographs at different magnifications over several locations across each sample were taken to examine the micro-scale topography of the rubbing area as well as the uniformity of the coating in non-rubbed areas. To better show the surface topography, 45 degree oblique angle views were used for all measurements.

A non-contact 3D profiler (Talysurf CCI - lite, Taylor Hobson Precision) was used to measure the cross-sectional profiles of the wear tracks on each sample. The wear track width and the average depth of the wear track relative to the sample surface were determined from the surface profile. These measurements were performed in order to compare the amount of material removed from the wear track in each sample.

6.2.3. Friction and Wear Analysis

An automatic friction abrasion analyzer (Triboster, Kyowa Interface Science Co., Ltd.) was used to perform the friction test, measuring both the static and dynamic COFs. This apparatus provides a linear reciprocating motion and measures the friction force, which is then converted to COF by dividing by the applied normal load. The average static COF for each cycle is determined by the highest COF registered within the first 0.5 seconds of the test. The average dynamic COF for each cycle is determined by taking the average of the COF registered between 10 and 90 percent of the total stroke length.

The friction tests were performed by repetitively rubbing the test sample against a chrome steel ball (SUJ-2, Kyowa Interface Science Co., Ltd., Niiza-City, Japan) of 7 mm diameter. The test sample was mounted on the tribometer stage with a removable double-stick tape so that the chrome steel ball rested above the desired testing region of the sample. For consistency, all samples were rubbed parallel to the substrate polishing lines. Each sample was rubbed at three different locations under an applied load of 20 g, a stroke length of 15 mm, and a speed of 2.5 mm/s for 1000 cycles. It is important to emphasize that the Hertzian contact pressure resulting from a 20 g normal load is 0.335 GPa. The Hertzian contact pressure was calculated assuming contact between the ball and the substrate due to the low thickness (< 2 μm) of the coated film. The value for the Hertzian contact pressure is much higher than what is typically experienced in dry lubricated mechanical systems. This is because a ball-on-flat sliding contact is not common in mechanical systems. The high contact pressure was used to accelerate the wear process and allow comparisons to be made between samples at reasonable testing durations. To test the influence of contact pressure on the tribological performance of the samples and to further accelerate the film wear in order to compare time to failure, the friction test was repeated for an

applied load of 50 g (0.454 GPa Hertzian contact pressure). Finally, friction tests at a lower normal load of 10 g (0.266 GPa Hertzian contact pressure) were also performed on unfilled PTFE and 0.3 wt.% SiO_2/PTFE samples for a total of 6000 cycles to test the durability of the films at lower contact pressures.

6.2.4. Surface Chemical Analysis

After the friction tests, the wear tracks on each sample were analyzed using X-ray photoelectron spectroscopy (XPS, ULVAC-PHI/PHI 5000 VersaProbe). The XPS analyses were performed with a monochromatic Al K_α (1486.6 eV) source. Both XPS survey spectrum and high-energy resolution (Hi-Res) scans of the F 1s regions were acquired. The test was run at 23.5 eV pass energy, 100 μm spot size, 54.7° take off angle, 100 ms time/step, and 0.025 eV energy step for 10 repeats. In addition, the energy-dispersive X-ray spectroscopy (EDS) analysis function of the SEM was used to identify film transfer to the counterface balls during the friction tests.

6.3. Results

6.3.1. Surface Topography

Dektak measurements showed that the average roughness for the polished 316 stainless steel was 88 nm. The roughness for the chrome steel counterface was slightly smaller at 34 nm. The Dektak profiler was also used to determine the film thickness. The pure PTFE films had an average thickness of 1.8 μm and 0.3% SiO_2/PTFE composite films had an average thickness of 1.4 μm. The 1.7% and 3.3% SiO_2/PTFE composite films had the lowest average thicknesses at 0.8 μm and 1.0 μm, respectively. Because SiO_2 particles adsorb much water, it is likely that the incorporation of SiO_2 prevented higher accumulation of solid particles on the substrate surface, thus reducing the film thickness after the water was evaporated during heat treatment.

Figure 6.1 shows representative SEM micrographs (45 degree oblique angle views) of (a) bare stainless steel, (b) stainless steel coated with pure PTFE, (c) stainless steel coated with 1.7% SiO_2/PTFE composite, and (d) stainless steel coated with 3.3% SiO_2/PTFE composite. The unidirectional polishing lines characteristic of the stainless steel substrate are clearly visible from Figure 6.1 (a), while the coated samples in Figure 6.1 (b) and (c) show the presence of nanoparticles on the surfaces. There is no significant topographical difference between the pure PTFE coated samples and the samples coated with SiO_2/PTFE composite solutions. This similar topography indicates that there is a uniform dispersion of the SiO_2 particles amongst the PTFE particles in the solutions created.

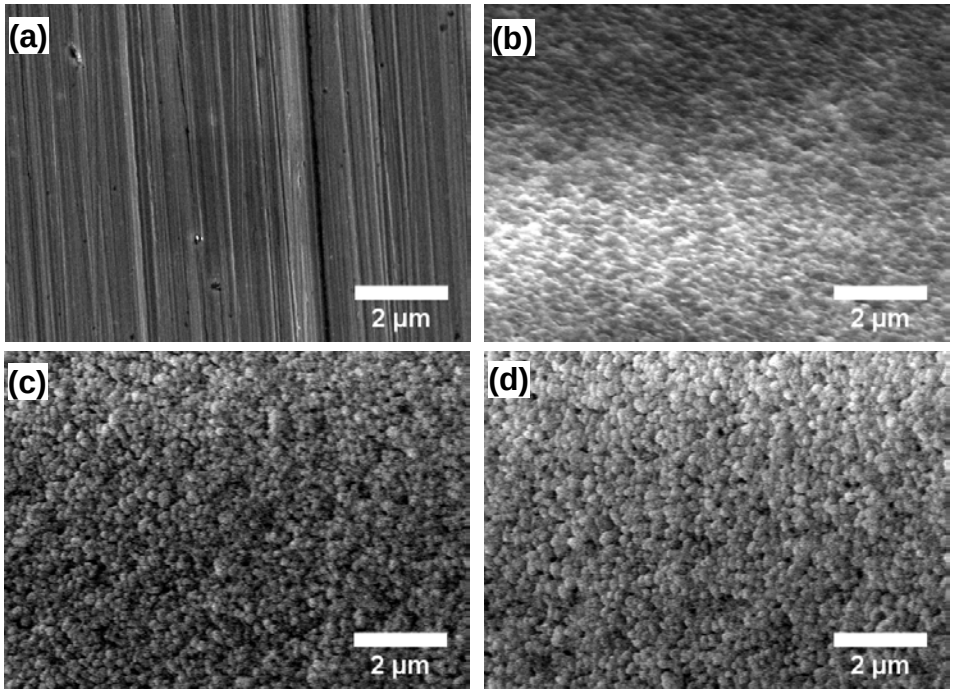

Figure 6.1: SEM micrographs (45 degree oblique angle views) of stainless steel substrate (a) uncoated, (b) coated with PTFE film, (c) coated with 1.7% SiO2/PTFE composite film, and (d) coated with 3.3% SiO2/PTFE composite film.

6.3.2. Coefficient of Friction

The plot in Figure 6.2 shows the static and dynamic COF vs. rubbing cycles of representative samples for pure PTFE, 0.3% SiO_2/PTFE, 1.7% SiO_2/PTFE, and 3.3% SiO_2/PTFE. These friction tests were performed using a 20 g applied normal load. It can be seen from both Figure 6.2 (a) and (b) that the incorporation of SiO_2 nanoparticles in PTFE films did not significantly change the steady-state COF of the films. However, the lowest concentration of SiO_2, 0.3 wt.%, did show a negative effect. This film was not able to withstand the entire 1000 cycle test, as is evident from the rise in the COF that was observed at approximately 560 cycles for the static COF and at approximately 349 cycles for the dynamic COF. This failure was characterized by a sharp increase in the COF and a high degree of fluctuation in the COF between rubbing cycles, which is a result of exposure and abrasion of the stainless steel substrate. Once the substrate was exposed, the COF rose much closer to the 1.0 and 0.8, static and dynamic COF values observed for the bare stainless steel sample. The static and dynamic COFs for pure PTFE, 1.7% SiO_2/PTFE, and 3.3% SiO_2/PTFE, on the other hand, remained constant at approximately 0.3 and 0.1, respectively.

The values for each individual friction test, performed using a 20 g normal load, are shown in Table 6.1. The average static and dynamic COF did not differ significantly between each sample type, precluding any inferences of a negative or positive correlation between the SiO_2 concentration and the COF.

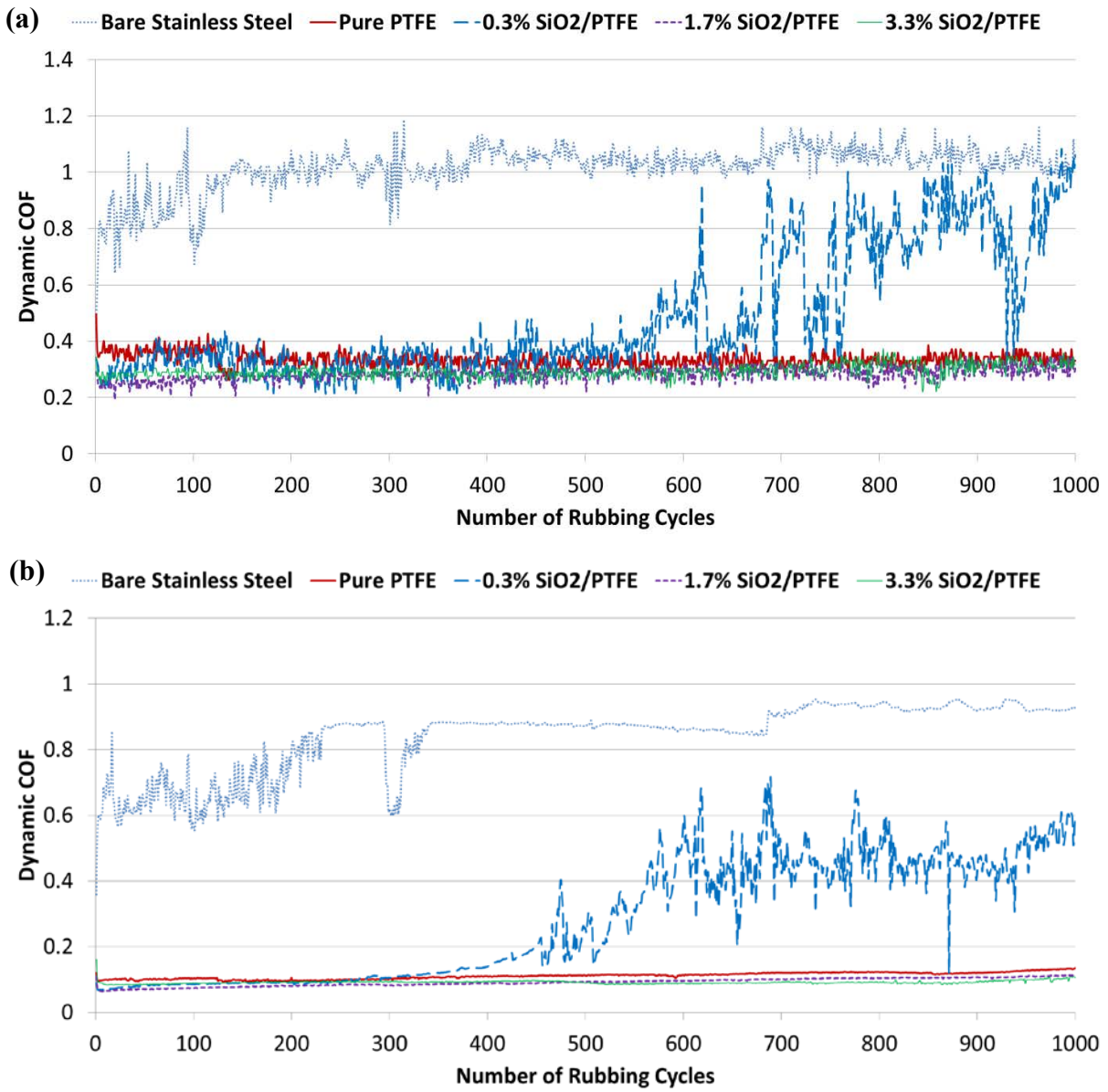

Figure 6.2: Friction test results for 20 g applied load. (a) static COF and (b) dynamic COF.

Table 6.1: Static COF, dynamic COF, and durability results for bare stainless steel, 0.3% SiO_2/PTFE, 1.7% SiO_2/PTFE, and 3.3% SiO_2/PTFE in 20g normal load friction test.

Sample	Static COF					Dynamic COF					Wear Life (No. of rubbing cycles)				
	Test 1	Test 2	Test 3	Avg.	STDEV.	Test 1	Test 2	Test 3	Avg.	STDEV.	Test 1	Test 2	Test 3	Avg.	STDEV.
Bare Stainless Steel	1.09	1.02	1.00	**1.04**	**0.050**	0.79	0.84	0.88	**0.84**	**0.046**	-	-	-	-	-
Pure PTFE	0.33	0.31	0.27	**0.30**	**0.034**	0.11	0.12	0.10	**0.11**	**0.007**	1000	1000	1000	**1000**	**0**
0.3% SiO_2/PTFE	0.32	0.29	0.28	**0.30**	**0.021**	0.09	0.10	0.08	**0.09**	**0.007**	349	266	121	**245**	**115**
1.7% SiO_2/PTFE	0.25	0.30	0.28	**0.28**	**0.022**	0.08	0.09	0.09	**0.09**	**0.005**	1000	1000	1000	**1000**	**0**
3.3% SiO_2/PTFE	0.33	0.29	0.31	**0.31**	**0.019**	0.09	0.09	0.11	**0.10**	**0.013**	1000	1000	1000	**1000**	**0**

The results for the friction test carried out using a 50 g normal load can be seen in Figure 6.3. Figure 6.3 (a) shows plots for static COF vs. rubbing cycles. For the bare stainless steel sample, the static COF started around 0.5 and slowly increased toward 1.0; this value was reached after approximately 30 cycles. For the pure PTFE coated sample, the static COF started at around 0.18 and remained at this value for the first 25 cycles. After this point the COF sharply increased and reached 0.9 within the first 40 cycles. The COF then fluctuated between 0.8 and 1.0, steadily increasing toward a steady-state value of 1.0 which was reached after approximately 550 cycles. The 0.3% SiO_2/PTFE coated sample started with a COF value of approximately 0.21. Between 200 and 300 cycles, and between 480 and 750 cycles the static COF showed a large amount of fluctuation, however, beyond this point the static COF settled back at approximately 0.2. The 1.7% SiO_2/PTFE composite sample exhibited a static COF that remained steady at approximately 0.17 for the first 115 cycles and then sharply increased, fluctuating between 0.3 and 0.7. The static COF then progressively increased to about 0.8 where it remained for the majority of the test. The 3.3% SiO_2/PTFE composite sample showed the best performance. The COF remained almost flat at 0.17 for the first 330 cycles and then slowly increased to 0.9 by 600 cycles. The COF then remains at 0.9 for the remainder of the test.

Figure 6.3 (b) shows a plot of the dynamic COF vs rubbing cycles for the 50 g normal load friction test. The dynamic COF for bare stainless steel started around 0.5, experienced a sharp rise and drop, and then slowly increased to 0.9, which was reached at about 300 cycles. The dynamic COF for the PTFE coated sample started at 0.09 and after only 24 cycles increased sharply toward 0.5 which was reached after the first 60 cycles. The COF then fluctuated as it slowly climbed to reach 0.87 after 660 cycles. The dynamic COF of the 1.7% SiO_2/PTFE composite sample started at 0.09, and increased until it reached 0.15 after 126 cycles. The COF

then decreased to 0.09 and again began to climb until it reached 0.15 at 188 cycles. After this point the COF fluctuated between 0.15 and 0.3 for the remainder of the test. The dynamic COF for the 3.3% SiO_2/PTFE composite sample started flat at 0.09 for the first 523 cycles and then slowly increased in value, fluctuating between 0.3 and 0.5 for the remainder of the test. Because the dynamic COF for pure PTFE reached a value close to that of bare stainless steel after 660 cycles, it was evident that the film had been completely removed at this point. The dynamic COF for the composite films, on the other hand, never reached the value of bare stainless steel, indicating that the film is most likely not completely removed even after 1000 cycles. Furthermore, the fact that the COF for the 3.3% SiO_2/PTFE coated sample remained at the initial value of 0.09 for 523 cycles indicates that higher concentrations of SiO_2 are more conducive to higher wear resistance. An analysis of the wear track chemical composition in section 6.3.3 clarifies if in fact the film remains present at the end of the friction test.

The reported COF for PTFE varies with contact pressure and sliding velocity, but is typically between 0.03 and 0.15 for the dynamic COF [9], which is in agreement with the test results in Figures 6.2 and 6.3. The friction force for PTFE and for the SiO_2/PTFE composite films, during the friction test, showed the presence of fluctuations of high amplitude within the first 0.5 seconds of the friction test cycle. The difference between the value of these peaks present in the first 0.5 seconds and the value of the friction force throughout the remainder of the cycle varied between 0.1 and 0.6. Therefore, the static friction was significantly higher than the dynamic friction. The values for each individual friction test performed using a 50 g normal load are shown in Table 6.2. The average static and dynamic COF between pure PTFE, 1.7% SiO_2/PTFE, and 3.3% SiO_2/PTFE did not differ significantly enough to infer that there is a negative or positive correlation between the SiO_2 concentration and the COF. However, at 0.3 wt.%

concentration of SiO_2 the average static COF had a value of 0.21 which is significantly higher than the values observed for the other samples. On the other hand, a positive correlation between SiO_2 concentration and durability/wear life of the film was very evident. The samples coated with 3.3% SiO_2/PTFE had an average wear life that was 23x that of pure PTFE and 4x that of 0.3% SiO_2/PTFE and 1.7% SiO_2/PTFE.

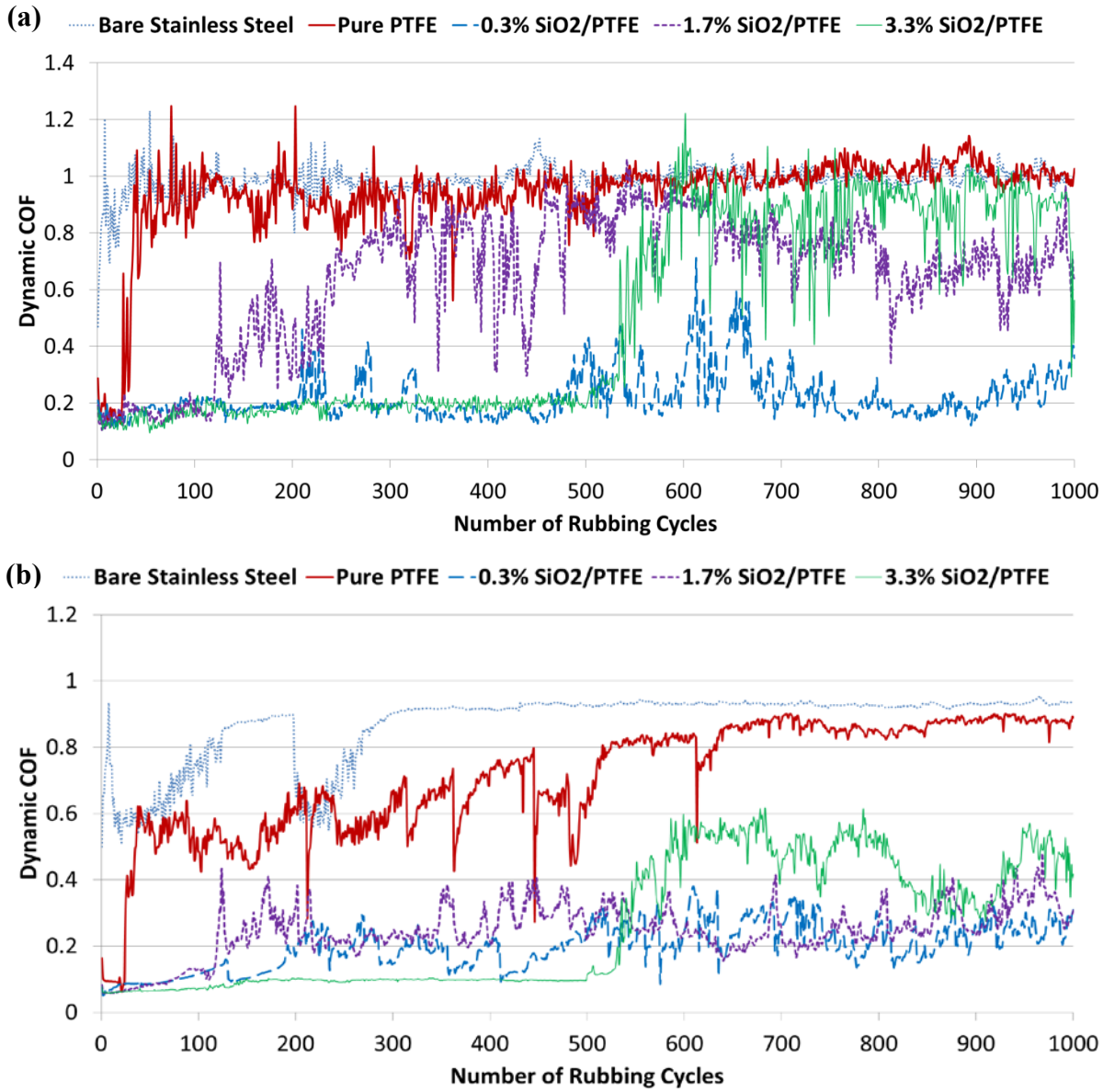

Figure 6.3: Friction test results for 50 g applied load. (a) static COF and (b) dynamic COF.

Table 6.2: Static COF, dynamic COF, and durability results for bare stainless steel, 0.3% SiO_2/PTFE, 1.7% SiO_2/PTFE, and 3.3% SiO_2/PTFE in 50g normal load friction test.

Sample	Static COF					Dynamic COF					Wear Life (No. of rubbing cycles)				
	Test 1	Test 2	Test 3	Avg.	STDEV.	Test 1	Test 2	Test 3	Avg.	STDEV.	Test 1	Test 2	Test 3	Avg.	STDEV.
Bare Stainless Steel	0.99	0.99	0.92	**0.96**	**0.040**	0.87	0.87	0.78	**0.84**	**0.054**	-	-	-	-	-
Pure PTFE	0.17	0.17	0.21	**0.18**	**0.020**	0.09	0.09	0.10	**0.09**	**0.008**	36	24	4	**21**	**16**
0.3% SiO_2/PTFE	0.17	0.18	0.28	**0.21**	**0.064**	0.09	0.09	0.09	**0.09**	**0.004**	119	168	72	**120**	**48**
1.7% SiO_2/PTFE	0.16	0.16	0.18	**0.17**	**0.011**	0.09	0.08	0.08	**0.09**	**0.006**	115	119	82	**105**	**20**
3.3% SiO_2/PTFE	0.18	0.18	0.16	**0.17**	**0.010**	0.09	0.09	0.09	**0.09**	**0.003**	320	523	604	**482**	**146**

6.3.3. Surface Chemical Composition

To confirm whether the coated film is still present after the 1000 cycle rubbing test, the samples which underwent the most severe rubbing test, 50 g load, were chosen for XPS analysis. The presence of fluorine is a clear indicator of the presence of PTFE on the wear track surface. In order to show this, a high resolution elemental scan was performed on the samples. Figure 6.4 (a) shows the XPS F1s spectrum of unscratched PTFE, 1.7% SiO_2/PTFE composite, and 3.3% SiO_2/PTFE composite. Figure 6.4 (b) shows the XPS F1s spectrum of the wear track for the same samples after the 1000-cycle rubbing tests. By comparing Figure 6.4 (a) and (b), one can see that the fluorine content significantly diminished for all three samples after the friction test. In both Figure 6.4 (a) and (b) one can observe the typical F1s peak for PTFE at a binding energy of about 689 eV. After the friction test, the 3.3% SiO_2/PTFE sample had the highest content of PTFE as shown in Figure 6.4 (b), despite the significantly lower fluorine content before wear testing, which is evident from Figure 6.4 (a). In Figure 6.4 (b) another peak at a binding energy of approximately 685 eV is observed. This peak is representative of a fluorine ion, likely from the resulting formation of FeF_2 or FeF_3 compounds [93, 94]. These compounds are formed through scission of PTFE molecules which allows the broken chains to bond with iron. The presence of this compound in the three coated samples indicates that the film has been worn down to the PTFE/substrate interface. The fact that the sample coated with pure PTFE shows the

largest peak at 685 eV inside the wear track, suggests that the PTFE molecules for this sample have suffered a higher degree of scission. This is due to the early failure of the film and high stresses resulting from contact between the counterface and the substrate. It is important to note that the spot size of 100 μm used in the XPS analysis is sufficiently small to capture only the surface within each wear track.

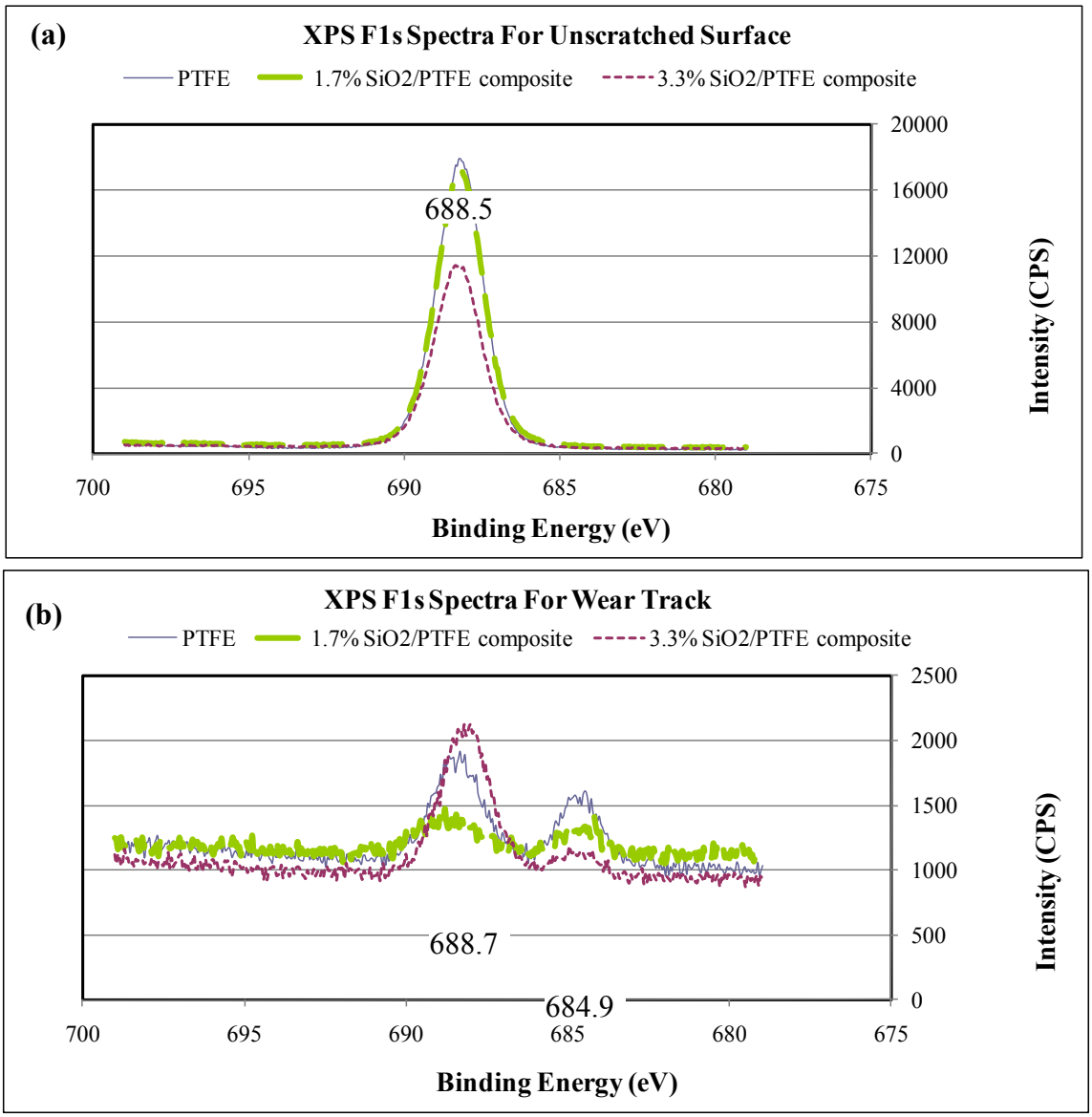

Figure 6.4: XPS F1s spectra of (a) unscratched surfaces and (b) the wear track of PTFE, 1.7% SiO2/PTFE composite film, and 3.3% SiO2/PTFE composite film coated stainless steel after 1000-cycle rubbing tests.

Figure 6.5 shows the EDS analysis performed on the chrome balls used as the counterface for the 50 g load tests. In figure 6.5 (a), the composition of chrome steel is readily visible. However, in Figure 6.5 (b), (c), and (d), the Fe is not detected; instead, O, C and F were detected. The presence of these elements indicated that a transfer film had formed on the counterface for the PTFE, 1.7% SiO_2/PTFE composite, and 3.3% SiO_2/PTFE composite samples. In Figure 6.5 (c) and (d), it can also be seen that Si was detected due to the presence of the SiO_2 filler in the sample film.

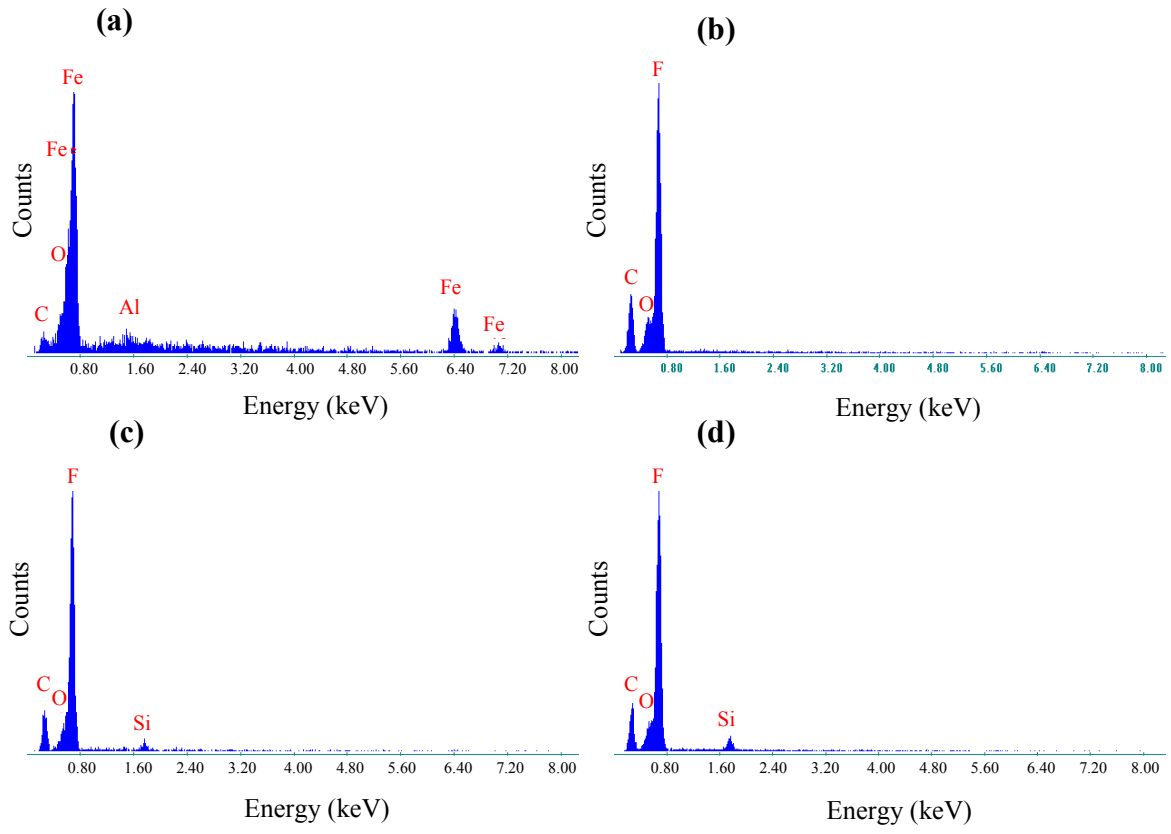

Figure 6.5: EDS spectra of (a) untested chrome balls, (b) chrome ball tested on PTFE, (c) chrome ball tested on 1.7% SiO2/PTFE composite film, and (d) chrome ball tested on 3.3% SiO2/PTFE composite film.

6.3.4. Wear

Figure 6.6 shows 100x and 1,000x magnification SEM micrographs (45 degree oblique angle views) of the wear tracks on all samples rubbed under a 50 g normal load. Micrographs of 100x magnification were used to determine the width of the wear track while 1,000x was used to identify nano- and micro-scale debris and wear grooves. From Figure 6.6 (a1) and (b1), it can be seen that bare stainless steel had a wear track width of about 500 μm and pure PTFE coated stainless steel also had a wear track approximately 500 μm wide. From Figure 6.6 (c1), it can be seen that the 1.7% SiO_2/PTFE composite had a wear track width of about 300 μm, and from Figure 6.6 (d1) that the 3.3% SiO_2/PTFE composite had a wear track width of about 200 μm. It is evident that the wear track was the widest for bare stainless steel and pure PTFE coated stainless steel, followed by 1.7% SiO_2/PTFE composite and finally 3.3% SiO_2/PTFE coated stainless steel. The broader wear track is indicative of greater wear. This result supports the hypothesis that by mixing PTFE with SiO_2 dispersions, it is possible to increase the wear resistance of the film. This result was supported by the wear on the counterface as well. The chrome ball rubbed against the 3.3% SiO_2/PTFE composite film had a wear scar of about 200 μm diameter, whereas the chrome ball on pure PTFE had a wear scar diameter of 420 μm and bare stainless steel had a wear scar diameter of 620 μm. From Figure 6.6 (b2), one can observe that after 1000 rubbing cycles, the PTFE coated surface had a large amount of small debris and that material from the counterface seemed to have transferred to the surface, as is evident by the smooth laminated material on top of the grooves, similar to that seen on bare stainless steel in Figure 6.6 (a2). This indicated that the coated film was almost entirely destroyed and that there may be material transferred from the chrome steel counterface to the substrate. On the composite film samples in Figure 6.6 (c) and (d), however, the surface topography showed

grooves with larger debris, typical of debris formed when film is transferred on and off the counterface, indicating the film is still present.

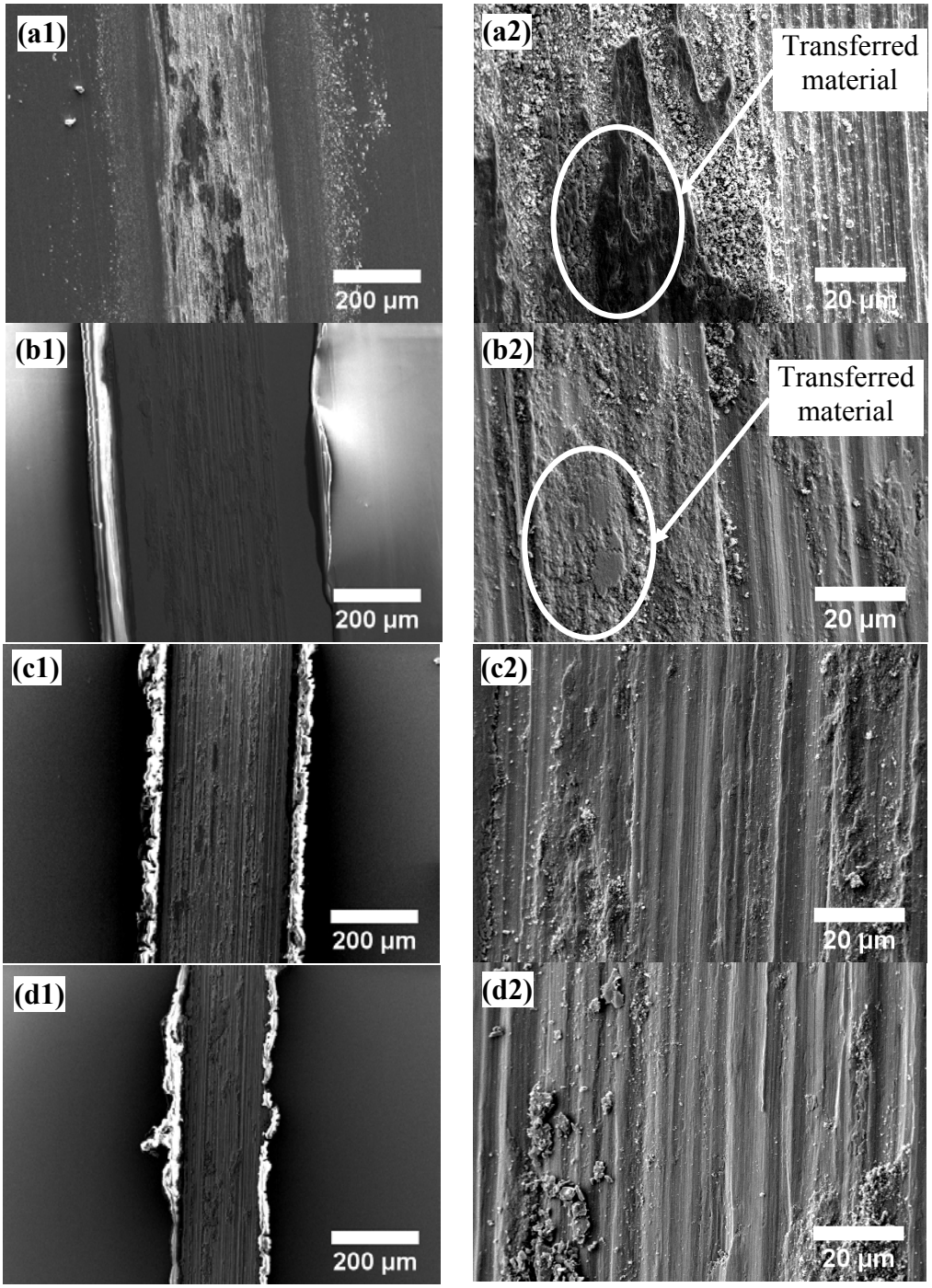

Figure 6.6: SEM micrographs (45 degree oblique angle views) of stainless steel substrate (a) uncoated, (b) coated with PTFE film, (c) coated with 1.7% SiO2/PTFE composite film, and (d) coated with 3.3% SiO2/PTFE composite film. (1: 100x and 2: 1,000x).

Figure 6.7 shows the representative cross-sectional profiles for each of the samples tested using a 50 g load, and again clearly show that the PTFE/SiO_2 composite had a much narrower wear track resulting from the friction test. In Figure 6.7 (a), for bare stainless steel, a wear track approximately 400 μm wide was observed with grooves and peaks evenly distributed about the sample surface level, the grooves reaching about 20 μm in width, consistent with the SEM observations in Figure 6.5 (a). In Figure 6.7 (b), for the PTFE film, an 830 μm wide wear track was observed with few peaks and the presence of a smooth protruding surface within the wear track, accompanied by very narrow grooves. The smooth protruding surface was most likely material delaminated from the counterface and adhered to the stainless steel surface as seen in the SEM micrograph shown in Figure 6.5 (b2). The 1.7% SiO_2/PTFE composite film, shown in Figure 6.7 (c), had a 460 μm wide wear track with evenly distributed peaks and grooves, much lower in height and depth than those seen in the two previous samples. The grooves were likely generated by the trapped nanoparticles during sliding, whereas the peaks are part of the film that had piled up on the two sides during sliding. Finally, Figure 6.7 (d) shows the cross-sectional profile for the 3.3% SiO_2/PTFE coated sample; it shows a wear track of about 330 μm wide with higher peaks and deeper grooves than the 1.7% SiO_2/PTFE coated sample. However, the grooves were much narrower and it is clear that much less material was removed from the surface. Once more, as was seen in Figure 6.5 (d1), the cross-sectional profile confirms that the 3.3% SiO_2/PTFE coated sample had the narrowest wear track.

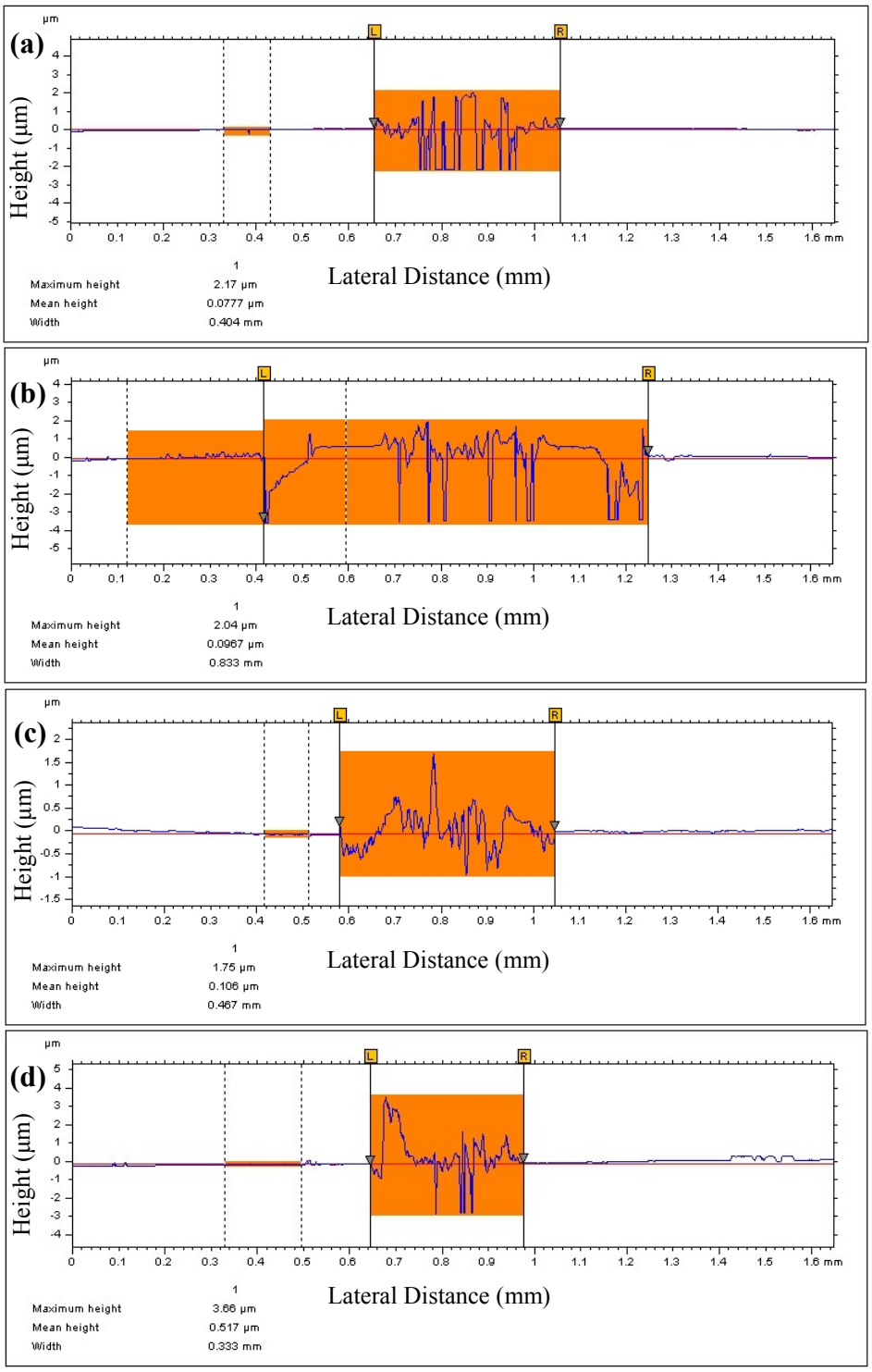

Figure 6.7: Optical profiler measurements of wear track for (a) uncoated, (b) PTFE film, (c) 1.7% SiO2/PTFE composite film, and (d) 3.3% SiO2/PTFE composite film.

Figure 6.8 shows the results of the durability test performed using a 10 g normal load for 6000 cycles. In this test, a pure PTFE coated sample was compared to a sample coated with 3.3% SiO_2/PTFE composite film. The objective of this experiment was to determine the tribological performance at lower loads for the top performing composite sample and compare it to the control. From the graph, it is clear that the COF of the pure PTFE film began to show indication of failure at approximately 4700 cycles, while the COF of the 3.3% SiO_2/PTFE composite film remained low for 6000 cycles. Again, it is evident that the incorporation of SiO_2 nanoparticle filler increased the wear resistance of the PTFE film. It should be noted that the COFs measured in the 10 g normal load friction test are higher than those observed for 20 g and 50 g friction tests. This phenomenon is typically observed in viscoelastic polymers like PTFE and is due to the time dependent relaxation of polymer chains which is affected by temperature and the speed of load application [34, 95]. At higher loads, the temperature at the contact point increases significantly, decreasing the rigidity of the film.

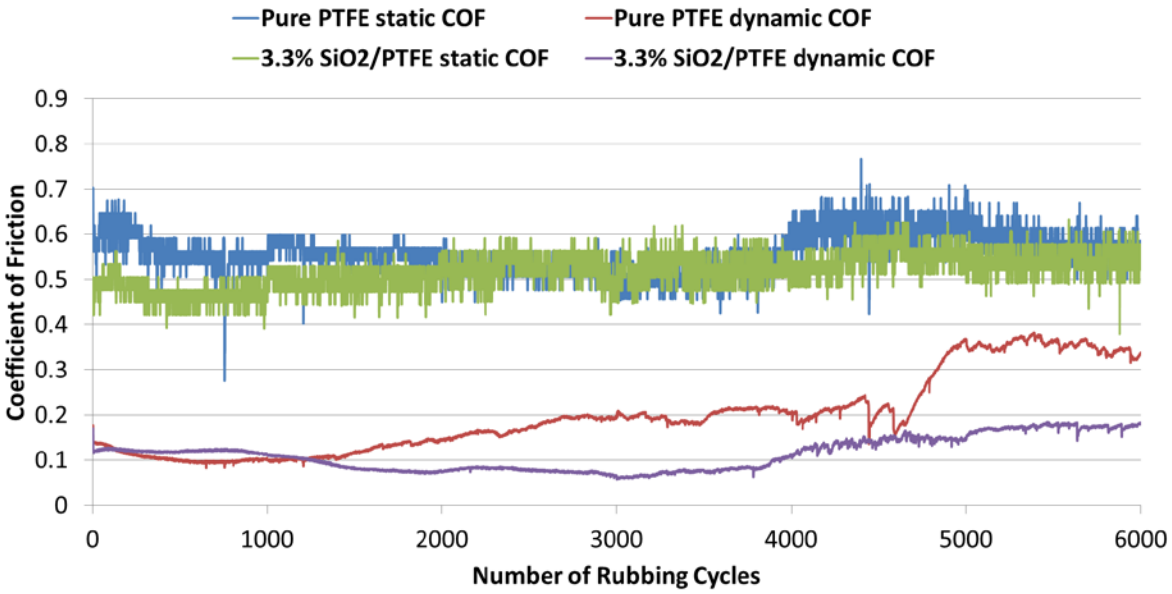

Figure 6.8: Static and dynamic COF for friction test using a 10 g applied normal load for 6000 rubbing cycles.

6.4. Summary

The results of the friction test performed using a 20 g normal load showed that pure PTFE, 0.3% SiO_2/PTFE, 1.7% SiO_2/PTFE, and 3.3% SiO_2/PTFE exhibit a similar value for both the static and dynamic COFs. However, the results showed that 0.3% SiO_2/PTFE had a lower wear resistance than the other coatings. The 50 g friction test also showed little change in COF between the coatings. The dynamic COF for all four coatings was 0.09. However, 0.3% SiO_2/PTFE exhibited an average static COF value of 0.21, significantly higher than the other three coatings. It is likely that low concentration of SiO_2 produces sparse nodes that act as defects in the film instead of changing the mechanical properties of the film as a whole. The 50 g friction test showed that the samples coated with 3.3% SiO_2/PTFE had an average wear life that was 23x that of pure PTFE and 4x that of 0.3% SiO_2/PTFE and 1.7% SiO_2/PTFE. In addition, SEM micrographs showed that the composite films with higher concentration of SiO_2 had much narrower wear tracks after the samples were subjected to the friction tests. XPS analysis showed that the composite films with higher concentration of SiO_2 contained more fluorine than their counterparts after being subjected to the friction tests. These results all indicate that, by utilizing SiO_2 as a filler in PTFE, it is possible to increase the wear resistance of the thin film, and that by increasing the concentration of SiO_2 up to 3.3 wt.%, the wear resistance can be increased while also maintaining a low COF.

Chapter 7

Use of gold Nanoparticle filled PTFE films to produce low friction and low wear surface coatings

7.1. Overview

In this study, Au nanoparticles were selected as a filler to take advantage of Au's low shear strength and consequential low COF, as well as the higher hardness of Au in comparison to PTFE. The higher hardness of the Au filler allows the film to support higher loads while experiencing less deformation. Several investigations have been carried out on the tribological properties of Au nanoparticles composites, such as in Au-a-C:H [70], Au nanoparticles within immobilized fluorinated dendrimers [71], and Au-Paraffin [96]. However, Au nanoparticle filled PTFE films have not been studied. The results of the investigation presented in this paper show that incorporating Au nanoparticles in a PTFE film increases the wear resistance by up to two times while also reducing the COF by up to 50%. It is important to note that the films produced in this investigation were very thin, ranging from 0.2 μm to 0.5 μm thick, and the concentration of the Au nanoparticle dispersion used to make the film was very small, 0.07 wt.%. Therefore, the cost of Au is not a restrictive factor for its use as a filler in PTFE for certain applications.

7.2. Experimental Methods

7.2.1. Sample Preparation

This study used the same substrate and cleaning procedure described in section 5.2.1.

A PTFE aqueous dispersion of 60 wt.% concentration was mixed with a Au nanoparticle dispersion of 0.07 wt.%. The Au nanoparticles were synthesized by reduction of $HAuCl_4$ in the presence of sodium citrate [97, 98]. The PTFE and Au composite dispersion was mixed at a 2:1 ratio by weight. This produced a final dispersion composed of 40 wt.% PTFE and 0.023 wt.%

Au. The diameter of the spherical Au nanoparticles was approximately 15 nm. Cleaned stainless steel samples were dip-coated in the dispersion at an insertion and withdrawal speed of 10 mm/min with an immersion duration of 20 sec. After dip coating, the samples were heat treated using the same conditions described in section 5.2.1.

7.2.2. Friction and Durability Test

Linear reciprocating friction tests were carried out using the Automatic Friction Abrasion Analyzer in the same manner as described in section 6.2.3. Two different sample types were investigated: PTFE coated stainless steel and PTFE + Au coated stainless steel. Both samples were tested at three different surface locations under an applied normal load of 20 g, stroke length of 15 mm and a speed of 2.5 mm/s. The 20 g normal load and 7 mm diameter ball on flat configuration provided high contact pressure which accelerated the wear process. To further accelerate the testing process, in order to compare time to failure, the test was repeated with an applied load of 50 g.

The friction tests were categorized into two different studies: durability and wear progression. First, a durability study was carried out to determine the effect of the Au nanoparticle filler on the film wear life. These tests were carried out for both a 20 g and 50 g normal load. For the durability study, the tests were performed until a sharp increase in the COF was observed. A drastic increase in the COF indicated that the film on the sample had been sufficiently worn away so as to expose the stainless steel substrate to the counterface. As a result, the number of rubbing cycles until this point represented the wear life or durability of the film. As the friction test progresses, PTFE experience thermally activated structural transformation as well as chain scission [99]. This caused the friction to slowly rise over time, often above the typical COF range of 0.05 – 0.10, before the film was completely removed from

the surface. However, the increasing rate resulting from these structural changes was very low, unlike the sharp increase observed when stainless steel was exposed.

Second, a 50 g normal load friction test was run for 30 and 60 cycles to observe the wear progression at both stages on each sample. The purpose of this test was to examine changes in surface morphology, measure the wear progression, and determine the wear mechanism affecting each sample type.

7.2.3. Sample Characterization

A Stylus Surface Profiler was used to determine the coating thickness and wear track cross-sectional profile on each sample. The coating thickness and cross-sectional profiles were measured using a 12.5 μm radius stylus with 3 mg contact force, 600 μm scan length, and scan duration of 30 sec. The wear track profile was established by running the stylus along the width of each wear track. The samples were only partially coated with the film, leaving a small area of uncoated stainless steel on each sample. The coating thickness was determined by running the stylus across the coating edge, measuring the height difference between the uncoated stainless steel and coated film. The average coating thickness for each sample was determined by taking an average of 3 measurements taken at different location along the coating edge.

Scanning electron microscopy was used to characterize the surface topography and wear of all samples using the same parameters described in section 6.2.4. In addition, an atomic force microscope (AFM; Dimension Icon, Bruker, Santa Barbara, CA) was used to measure the surface roughness on each sample.

7.3. Results and Discussion

7.3.1. Surface Topography

Two material surfaces were evaluated in this investigation, stainless steel coated with PTFE and stainless steel coated with a PTFE + Au composite film. Each was characterized by SEM and compared to a bare stainless steel surface. Figure 7.1 (a), (b) and (c) show the SEM micrograph for bare stainless steel, stainless steel coated with PTFE, and stainless steel coated with PTFE + Au, respectively. For the bare stainless steel surface, the unidirectional polishing lines were clearly visible. On the other hand, for the PTFE coated sample, small rod-like structures oriented along a horizontal plane and measuring approximately 200 - 500 nm in length were noticeable, as shown in Figure 7.1 (b). These structures were the product of PTFE particles that had fused together as a result of heat treatment at 337 °C [100]. The PTFE + Au sample, shown in Figure 7.1 (c), had a fibrillar network on the film surface. The formation of the fibrillar network suggested that the PTFE nanoparticles had not only fused together into discrete agglomerates, but formed an interconnected network. It was evident that the film had undergone a higher degree of melting as a result of the presence of Au nanoparticles within the PTFE matrix. Studies have shown that Au nanoparticles can have significantly lower melting points than bulk gold, as low as 171 °C [101]. In addition, when these particles are incorporated into a PTFE matrix, they have shown to decrease the softening temperature of PTFE as observed by Yeshenko et al. [101]. The lower softening temperature and melting point is a significant factor behind the formation of the interconnected network observed in the PTFE + Au sample.

AFM measurements showed that stainless steel had an average roughness R_a value of 77.2 nm, root mean square roughness R_q value of 107.5 nm, and a peak to valley distance R_z value of 571.1 nm. The PTFE coated sample had an average roughness R_a value of 20.4 nm, root mean

square roughness R_q value of 25.1 nm, and a peak to valley distance R_z value of 83.4 nm. The PTFE + Au coated sample had an R_a value of 17.2 nm, R_q value of 19.9 nm, and an R_z value of 54.2 nm. These results indicate that the PTFE film had a significantly higher surface roughness than PTFE + Au. This difference in surface roughness resulted from the higher degree of melting in the composite film, which allowed the film to spread and produce a more even film. In addition, the large difference in surface roughness between the substrate and coating surfaces shows that the coatings did not conform to the topography of the substrate surface, but instead fill in the deep valleys present in the substrate.

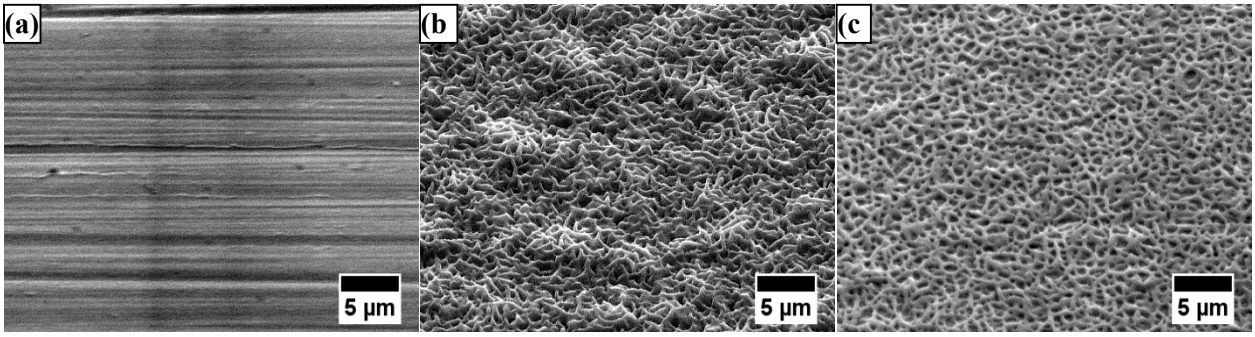

Figure 7.1: SEM micrographs (45 degree oblique angle views) of stainless steel substrate (a) uncoated, (b) coated with PTFE film, and (c) coated with PTFE + Au composite film.

The coating thickness measurements show that there is a relatively wide range of resultant coating thickness amongst the fabricated samples (between 0.21 µm and 0.48 µm). To compare the tribological performance between samples, it was critical to match up samples of similar coating thickness. The PTFE samples selected for the durability study had an average thickness of 0.45 µm and the PTFE + Au samples had an average thickness of 0.47 µm. The samples selected for the wear progression study had an average coating thickness of 0.25 µm for the pure PTFE sample and 0.24 µm for the PTFE + Au sample.

7.3.2. Friction an Durability 20g Normal Load Test

The durability test performed under a 20 g normal load was repeated three times for each sample type. The results show that under a 20 g normal load, the PTFE film was able to withstand an average of 307 cycles before failure, with a standard deviation of 197. The PTFE + Au sample, on the other hand, was able to withstand an average of 608 cycles before failure, with a standard deviation of 347. These results indicate that by incorporating Au nanoparticles, even at the low concentration of 0.07 wt.%, it was possible to improve the wear resistance of the PTFE film twofold.

Figure 7.2 shows the dynamic COF vs. rubbing cycles for the top performing PTFE and PTFE + Au samples in the 20 g normal load durability study. For PTFE, the COF started off at a value of 0.01 at the first cycle and quickly increased to about 0.07 after 15 rubbing cycles. The value then slowly trended upward with increasing rubbing cycles until it reached 0.2 at 532 cycles. At this point, a sharp increase in the COF was observed, indicating that the PTFE film had been sufficiently rubbed off to expose the stainless steel substrate. The average dynamic COF for the PTFE film, before failure, was 0.10. The PTFE + Au sample, on the other hand, began with a COF value of approximately 0.04, quickly increased to 0.08 and then gradually decreased to a value of 0.02 after 263 rubbing cycles. The COF then progressively increased until it reached a value of 0.11 at 1000 rubbing cycles. The test was stopped at this point due to equipment limitations; the Triboster Automatic Friction Abrasion Analyzer can only store data for up to 1000 consecutive rubbing cycles. However, the fluctuating COF values at this point indicated that the sample might be close to failure. Therefore, 1000 cycles was established as the failure point for this test. The average dynamic COF for the PTFE + Au film, before failure, was 0.05. Thus, the difference in average COF, before failure, between both sample types was

approximately 0.05. These results show that incorporating Au nanoparticles as a filler not only increased the film's wear resistance, but also reduced the average COF by up to 50%.

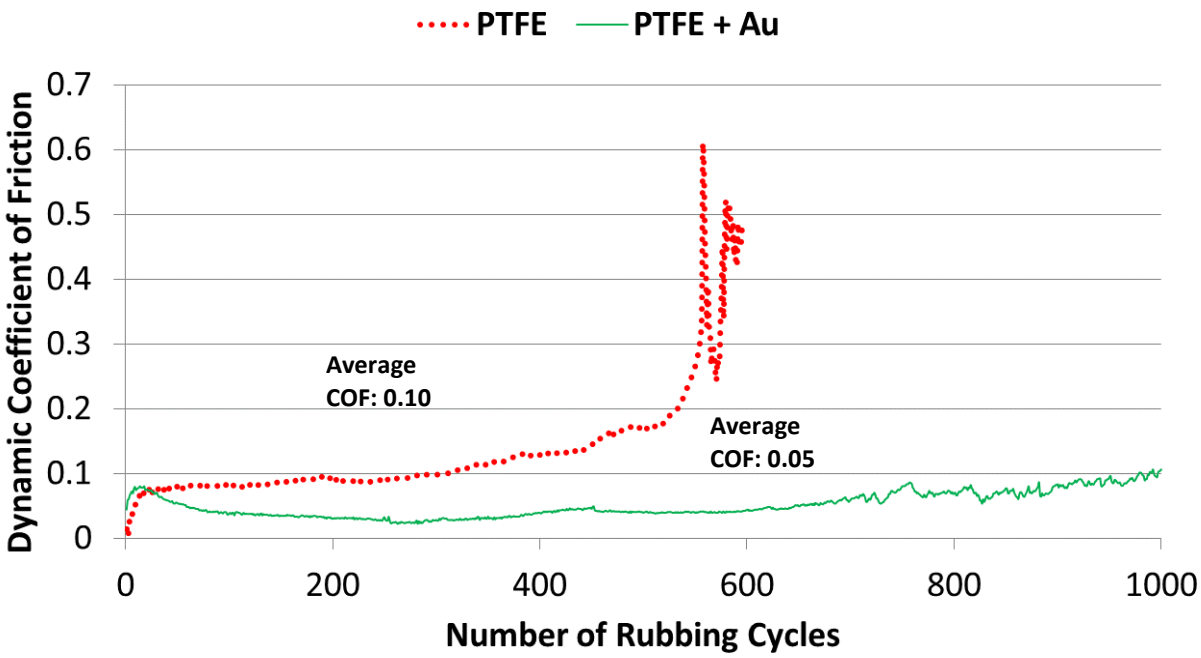

Figure 7.2: Dynamic COF values for PTFE and PTFE + Au in 20g normal load friction test.

SEM micrographs of the wear tracks resulting from the durability test were captured to observe the wear extent and wear mechanism on the sample surfaces. Figure 7.3 shows the SEM micrographs for PTFE and PTFE + Au coated samples that represent the typical performance of the 20 g durability test. Figure 7.3 (a) shows the wear track on PTFE. The micrograph shows that the wear track was approximately 81 µm wide and had a large amount of built up material at the wear track edges (dark area adjacent to wear track). This build-up showed the presence of corrugations indicative of film delamination and also showed areas where the film has suffered tearing, as shown by the dashed outline in Figure 7.3 (a). The tearing observed at the edges of the wear track is an indication that adhesive wear is the dominant wear mechanism [102]. In this

wear mode, the film adheres to the counterface and is torn off producing slabs of material as debris. Figure 7.3 (a) also shows the presence of deep grooves inside the wear track which indicated that the film was removed enough to allow the counterface to plough into the substrate.

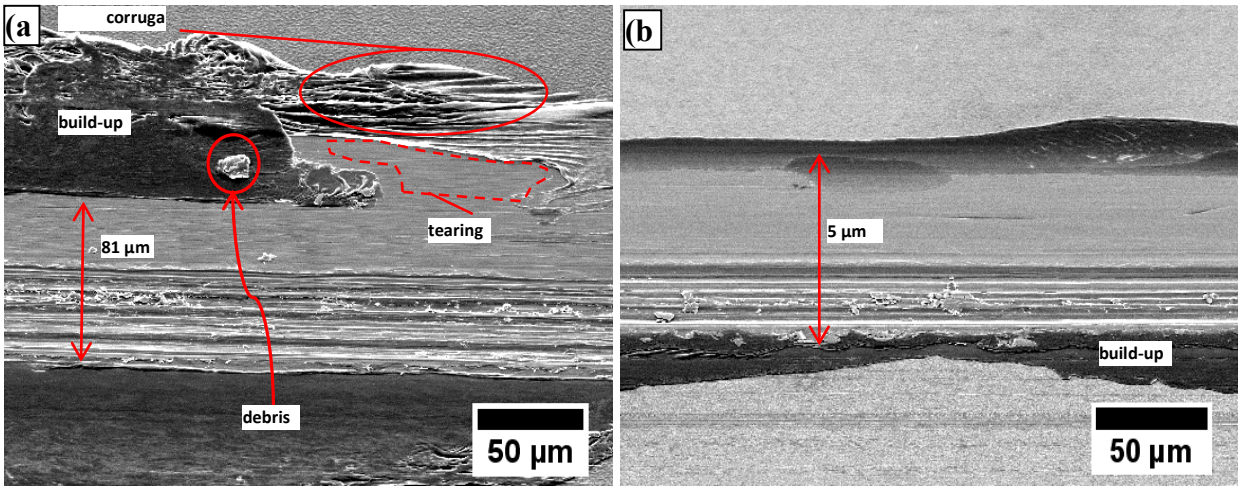

Figure 7.3: SEM micrographs of (a) PTFE wear track and (b) PTFE + Au wear track for 20g normal load friction test carried out until film failure.

Figure 7.3 (b) shows the wear track on PTFE + Au. The wear track was approximately 85 µm wide. The image shows a significantly smaller build-up (darker area) for PTFE + Au as compared to pure PTFE. The morphology observed inside the wear track of PTFE + Au was that of a smooth surface with deep grooves present at the point of failure. There was no evidence of tearing or corrugations. The absence of corrugations indicates the film was not delaminating from the substrate as was the case for the PTFE sample. The adhesion between the film and the substrate has improved as a result of the higher degree of melting in the composite film. Additionally, the absence of tearing and large debris indicates that adhesive wear was no longer the principal wear mode. Similar to what was reported by Wang et al. for nano-La_2O_3 filled PTFE, the incorporation of Au nanoparticles in PTFE likely increased the rigidity of the film, reducing deformation and, as a result, also reducing the real contact area. This reduction in

contact area lessened the adhesion between film and counterface, decreasing the effect of adhesive wear on the surface [102].

The cross-sectional profiles for the wear tracks in Figure 7.3 were measured using a Dektak stylus profiler and are shown in Figure 7.4. It is evident that the PTFE sample, shown in a dashed line, indeed exhibited large build-up and corrugations as indicated by the multiple peaks at the edge of the wear track (circled area). Because the build-up was much larger than the area inside the wear track, it is clear that the majority of the build-up was not material removed from inside the wear track, but was rather folds of delaminated film. The average wear track depth for PTFE is approximately 170 nm, but grooves as deep as 727 nm are observed on the left hand side of the wear track. These grooves, which were deeper than the film thickness of 450 nm, indicated that the wear had reached the substrate level and the film had failed. For the PTFE + Au sample, shown in a solid line, the wear track shows little build-up and has an average depth of 130 nm with grooves as deep as 866 nm. Because of the deep grooves, it is also clear that the coating had also failed.

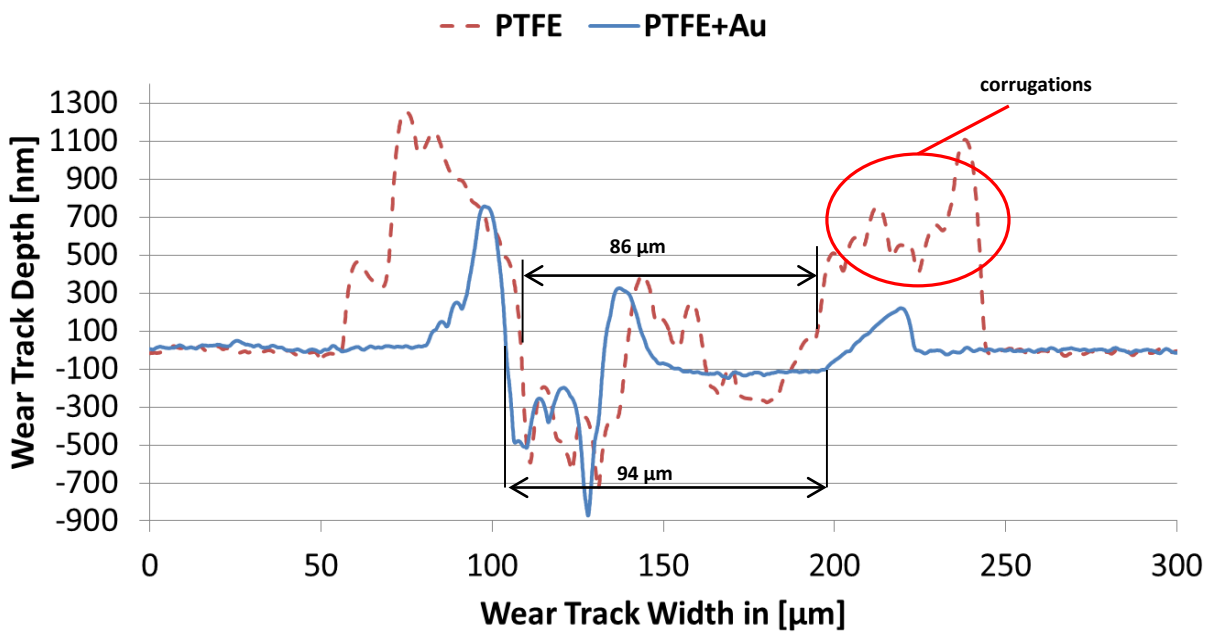

Figure 7.4: Dektak cross-sectional profiles of PTFE and PTFE + Au for 20 g normal load friction test.

7.3.3. Friction and Durability 50g Normal Load Test

The results for the durability study performed using a 50 g normal load show that the average failure point for PTFE dropped to an average of 174 cycles, with a standard deviation of 38, as a result of the higher contact pressures. For PTFE + Au, the average failure point also dropped to an average of 263 cycles, with a standard deviation of 83. It is evident that even at this high contact pressure, PTFE + Au still exhibits higher wear resistance than PTFE.

The average COF of each cycle vs. rubbing cycles for the top performing samples in the 50 g normal load durability study are shown in Figure 7.5. Similar to what was observed for the 20 g normal load test, it can be seen that PTFE + Au had a COF value that was lower than pure PTFE. For pure PTFE shown in a dashed line, the COF value began at 0.04 and quickly increased to 0.08 after 13 rubbing cycles. At this point, the COF gradually dropped to a value of 0.07 at 23 cycles, at which point it began to show an increasing trend. The COF reached 0.17 after 218

cycles (average COF of 0.09 for first 218 cycles) where it showed a sharp increase in value, indicating that the film had been removed. The COF for PTFE + Au, shown in a solid line, startsd at a value of 0.05, quickly increased to 0.07, and then slowly decreased until it reached a value of approximately 0.06 after 28 rubbing cycles. At this point the COF value showed an increasing trend until it reached a value of 0.11 at 352 cycles (average COF of 0.07 for first 352 cycles). Here the COF increased sharply, indicating that the film had been removed. A difference of 0.02 is observed in the average COF before failure between PTFE and PTFE + Au, indicating that the Au nanoparticle filler has reduced the COF of the PTFE film by 22%.

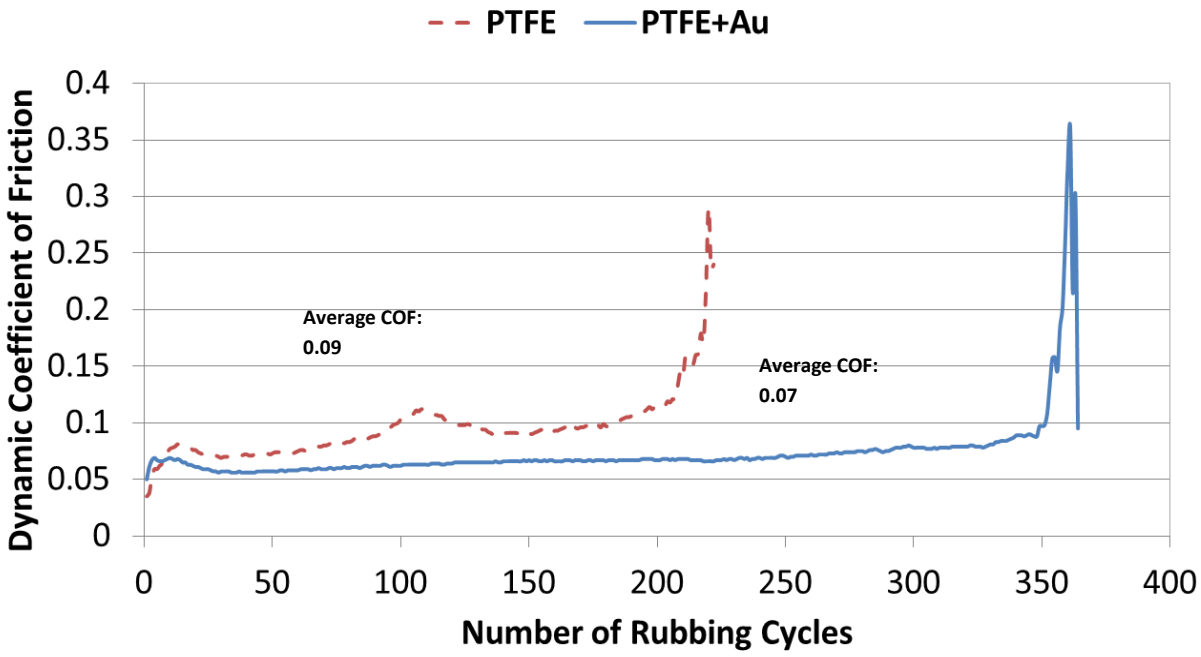

Figure 7.5: Dynamic COF values for PTFE and PTFE + Au in 50g normal load friction test.

Figure 7.6 shows the SEM micrographs of the wear tracks resulting from the 50 g friction test. PTFE and PTFE + Au are shown in Figure 7.6 (a) and (b), respectively. PTFE had a wear track width of 106 µm and PTFE + Au had a wear track width of 94 µm. The build-up on the

edges of the wear track was also wider for PTFE than for PTFE + Au. The total wear track width including the build-up for PTFE was 155 µm, while the total wear track width for PTFE + Au was only 114 µm. Fewer corrugations were observed for PTFE in the 50 g study compared to the 20 g study. However, small corrugations and some tearing were still present as shown by the circled area in Figure 7.6 (a). It is evident that delamination and adhesive wear still occur in the PTFE sample, although to a much lesser degree than was observed for the 20 g test. In addition, both PTFE and PTFE + Au exhibit deep grooves inside the wear track indicating that both films had been removed sufficiently to expose and abrade the substrate.

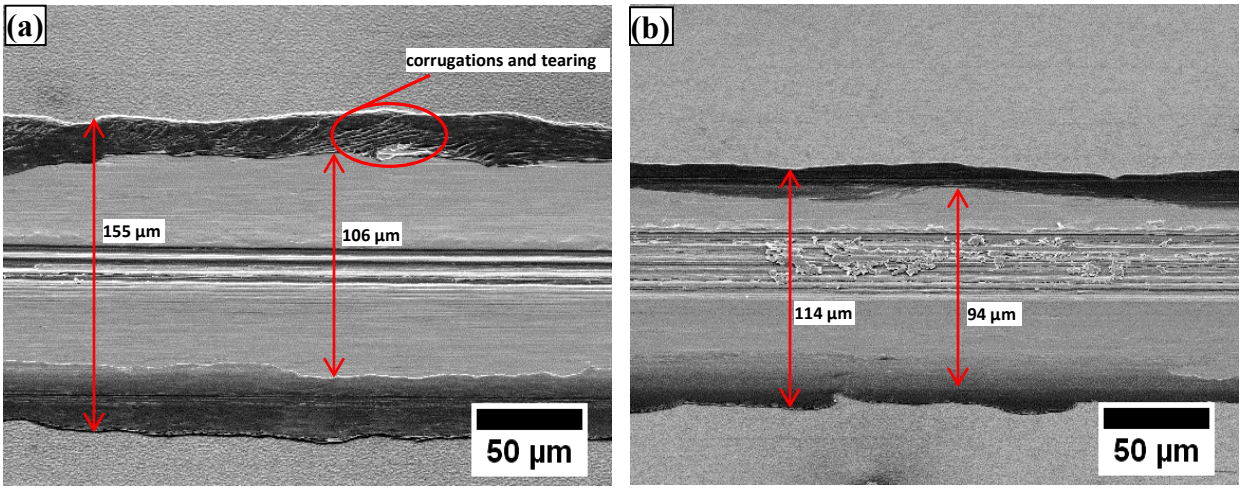

Figure 7.6: SEM micrographs of the wear tracks for (a) PTFE and (b) PTFE + Au for 50g normal load friction test carried out until film failure.

The cross-sectional profile in Figure 7.7 confirms the findings of Figure 7.6. It shows a smaller wear track width for PTFE + Au than for PTFE. According to the cross-sectional profile, the PTFE wear track had a width of 115 µm and the PTFE + Au had a width of 103 µm. The profile also shows that the build-up at the edge of the wear track for PTFE was twice as broad as that of PTFE + Au. Finally, the large peaks and valleys at the center of the wear tracks are representative of large grooves resulting from abrasion of the substrate by the counterface.

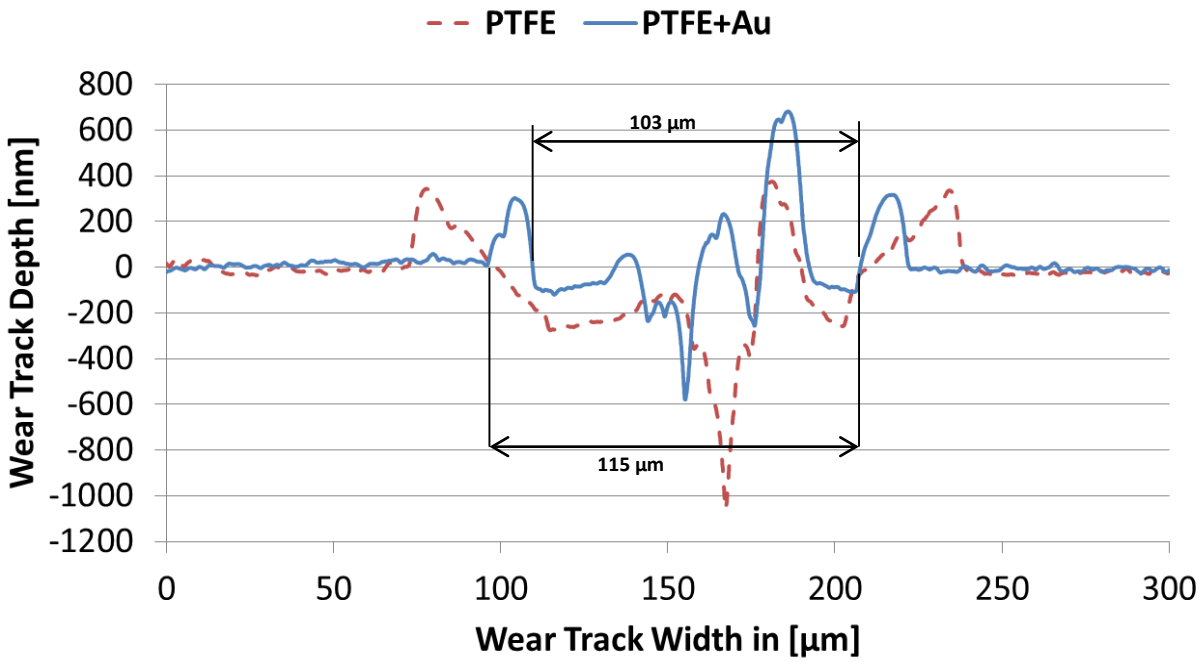

Figure 7.7: Dektak cross-sectional profiles of PTFE and PTFE + Au for 50 g normal load friction test.

7.3.4. Wear Progression

Figure 7.8 shows the dynamic COF for the 50 g normal load wear progression study. The results for the PTFE sample rubbed for 30 and 60 cycles are shown in dotted and dashed lines, respectively. The results for PTFE + Au rubbed for 30 and 60 cycles are shown in a thin and thicker solid line, respectively. Pure PTFE failed almost immediately in both 30 and 60 cycle tests. However, PTFE + Au remained at a low and stable COF for the entire duration of both 30 and 60 cycle runs. Note that the coating thickness of both sample types was lower for the wear progression study compared to the durability study. The coating thicknesses for PTFE and PTFE + Au in this study were 250 nm and 240 nm, respectively.

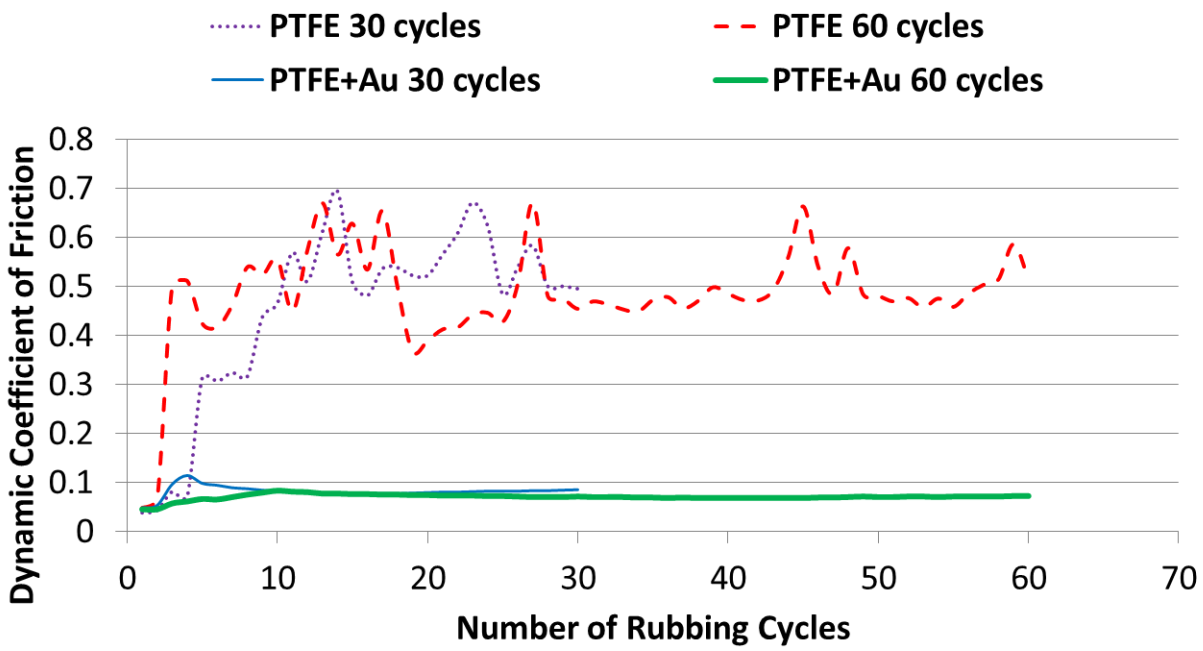

Figure 7.8: Dynamic COF of PTFE and PTFE + Au samples in 50 g normal load friction test carried out for 30 and 60 cycles.

SEM micrographs for the 30 and 60 cycle tests were captured to show the wear progression. Figure 7.9 (a) shows an SEM micrograph of the PTFE sample after the 30 cycle test. It is easy to see grooves in the middle of the wear track that indicate the substrate had been abraded. The inside of the wear track was approximately 63 µm wide and the total width including the build-up on the edges was 117 µm. Figure 7.9 (b) shows the wear track after 60 rubbing cycles. The deep grooves are present throughout the entire wear track and have reached the wear track edge. The width of the inside of the wear track was 120 µm at this point, slightly larger than the total width of 117 µm observed at 30 rubbing cycles. Figure 7.9 (b) also shows that outside of the wear track were corrugations resulting from delamination. These corrugations were much more pronounced than was observed for the durability study. They were approximately 275 µm in length and were caused by large adhesive forces resulting from contact between the counterface and the substrate after film failure. The film at the edge of the wear track/contact area is caught

between the two opposing metal surfaces and is pulled in the direction of sliding. A higher magnification SEM micrograph can be seen in Figure 7.9 (c). This micrograph clearly shows the large plate-like debris typical of adhesive wear in metal on metal contact.

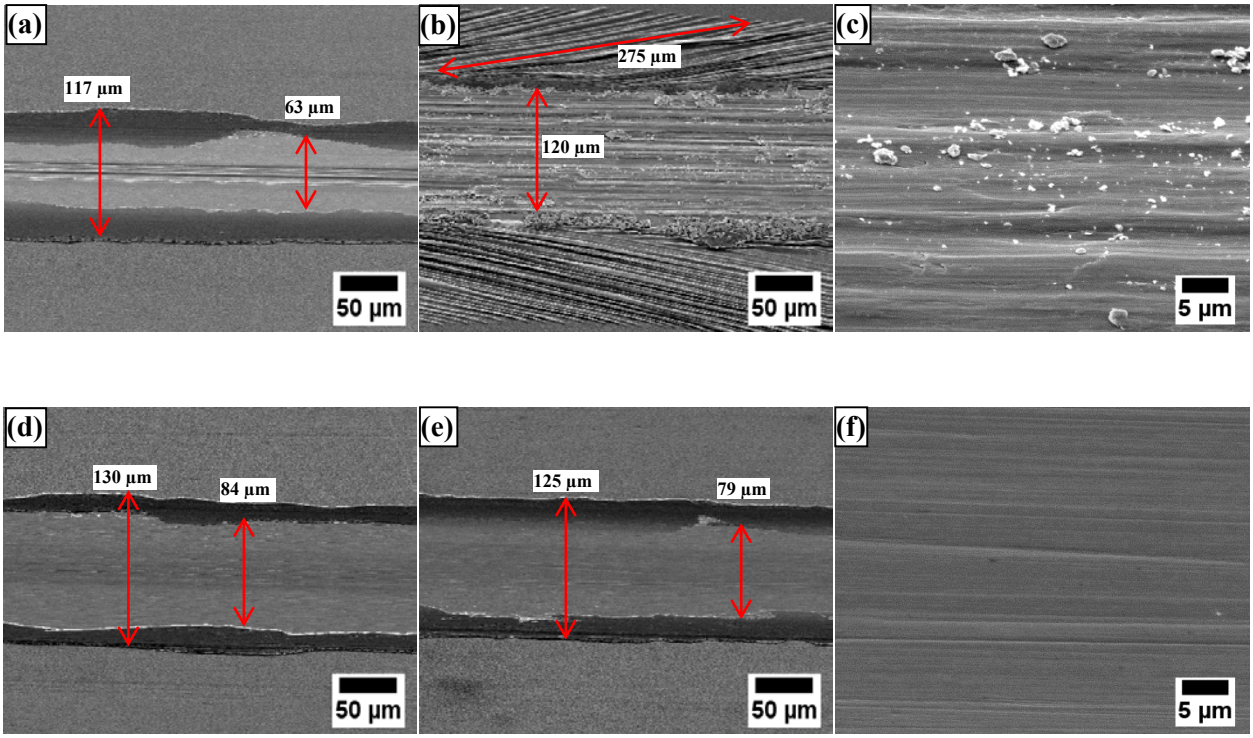

Figure 7.9: SEM micrographs of 50 g normal load friction test for PTFE carried for (a) 30 cycles, (b) 60 cycles, (c) higher magnification micrograph of 60 cycles, and for PTFE + Au carried out for (d) 30 cycles, (e) 60 cycles, and (f) higher magnification micrograph of 60 cycles.

Figure 7.9 (d) shows the SEM micrograph of the PTFE + Au sample after the 30 cycle test. The inside of the wear track was approximately 84 µm wide, and the total width (including build-up) reached 130 µm. The width of the inside of the wear track is significantly wider than the width observed for the PTFE sample in Figure 7.9 (a). However, it is clear again that the build-up for PTFE was much larger than for PTFE + Au. The SEM micrograph of the PTFE + Au sample after the 60 cycle test is shown in Figure 7.9 (e). Comparing Figure 7.9 (d) and (e), it can be seen that the width of the wear track for PTFE + Au remained similar for both the 30

cycle and 60 cycle tests. The lack of corrugations and tearing indicated that adhesive wear was not the principal mode of wear in this film. Figure 7.9 (f) shows the center of the wear track for PTFE + Au at a higher magnification. The surface of the wear track was very smooth with little signs of debris, which indicated that the film was likely being compacted and also polished as small asperities were removed by the counterface. The smooth surface confirms that unlike for PTFE, adhesive wear is not the principal wear mode for the composite PTFE + Au film.

7.4. Summary

This study has shown that adding Au nanoparticles of approximately 15 nm diameter, at a very low concentration of 0.07 wt.%, significantly improves the tribological performance of PTFE films. The results for the durability study under both 20 g and 50 g normal loads show that PTFE + Au was able to withstand between 1.5 to 2 times the number of rubbing cycles observed for pure PTFE. In addition, the COF for PTFE + Au was up to 50% lower than pure PTFE when tested under a 20 g normal load, and up to 22% lower under a 50 g normal load. Finally, both the durability and wear progression studies show that the dominant wear mechanism was different for the two sample types. PTFE suffered delamination as a result of poor adhesion of the film to the substrate and tearing resulting from a dominant adhesive wear mode. PTFE + Au, on the other hand, showed no sign of delamination or adhesive wear. The film surface is instead compacted and polished by the counterface. This change in wear mode caused by the addition of Au nanoparticles significantly increases the wear resistance and durability of PTFE.

Chapter 8

Wear resistant PTFE thin Film Enabled by a Polydopamine Adhesive Layer

8.1. Overview

In order to increase the wear resistance of PTFE thin films without the use of surface roughening and thick coatings, it is important to find a material with a strong affinity to both PTFE and the substrate. Lee found that PDA adheres well to both organic and inorganic materials, including PTFE [53]. PDA is synthesized through an oxidative reaction. It is rich in 3,4-dihydroxy-L-phenylalanine (DOPA) and lysine peptides. Although the exact mechanism behind the adhesive property of PDA is not known, it is believed that the catechol functional groups in DOPA and amine in lysine play a significant role in the process [53]. These properties of PDA have only recently been discovered [53] and thus, there are very few tribological studies on PDA films.

Ou et al. studied the mechanical properties and tribological performance of PDA multilayer composite films. PDA was used as an adhesive layer to deposit functional films on the surface using a nonelectrostatic layer-by-layer assembly technique. One of the composite films investigated was a ZrO_2/PDA nanocomposite multilayer film; it was determined that the PDA layer increased the packing density of the nano film by removing nanovoids in the ZrO_2 layer, and thus increased the hardness and modulus of elasticity of the composite film [103]. PDA/graphene oxide/PFDTS films were also studied and showed a COF as low as 0.16 and better wear resistance than PFDTS films alone [104]. However, the COF measured for these films was still higher than what is observed for PTFE films under similar testing conditions.

In this investigation, the influence of a PDA adhesive layer on the tribological performance of a thin PTFE top coat was studied. The results show a similar COF of approximately 0.06 for a

PDA/PTFE film compared to a PTFE film alone. However, due to the strong adhesion between PTFE and PDA, the PDA/PTFE film was able to withstand approximately 600 times more rubbing cycles than the PTFE film alone. More importantly, the majority of the rubbing cycles took place at the interface between the counterface and a remaining film of approximately 160 nm thickness which adhered tenaciously to the substrate. This tenacious layer was a result of the strong adhesion between PTFE and PDA, and contributes to the durability of the film. Because of the relatively low thickness of the film, it shows great potential to be used in applications where thin, durable PTFE films are required.

8.2. Experimental Methods

8.2.1. Sample Preparation

Two different sample types were evaluated in this investigation. The first sample type consisted of stainless steel coated with a PTFE film only. The second sample type consisted of an adhesive PDA layer and a PTFE top-coat and will subsequently be referred to as PDA/PTFE. The objective of this investigation was to determine the friction and durability of PDA/PTFE films and compare them to a film composed of PTFE only. The substrate selected for this study was by 2.5 x 2.5 cm squares of 0.76 mm-thick stainless steel type 316. The first step was to clean the substrates using the process described section 5.2.1.

The following step was to mix two separate dipping solutions, PDA and colloidal PTFE. For the PDA solution, Trizma base (T1503, Sigma Aldrich, St. Louis, MO) and dopamine hydrochloride (H8502, Sigma Aldrich, St. Louis, MO) were combined to produce a PDA pH 8.5 solution. First, the Trizma base was mixed with DI water to produce a 10 mM concentration of tris buffer solution. Second, dopamine hydrochloride was mixed into the tris buffer solution at a concentration of 2 mg/ml to initialize the polymerization process [105].

For the PTFE solution, a PTFE nanoparticle aqueous dispersion was used. This dispersion has a PTFE solids concentration of 60 wt.% as-received and particles ranging from 50 to 500 nm in size. In order to produce thinner coats of PTFE, the concentration of the as-received PTFE dispersion was diluted to a 40 wt.% concentration using DI water.

For the first sample type, PTFE only, stainless steel square sheets were dip coated in the PTFE solution at an insertion and withdrawal speed of 10 mm/min and immersion duration of 20 sec using a dip coater. For the second sample type, PDA/PTFE, the stainless steel sheets were first dip coated into the PDA solution for 24 hrs. at an insertion and withdrawal speed of 10 mm/min. The samples were subsequently rinsed in DI water in an ultrasonic bath for 5 minutes and dried using nitrogen gas. The final top coat of PTFE was deposited using a 10 mm/min dip coating insertion and withdrawal speed and immersion duration of 20 sec. Once dip coating was completed, the samples were dried on a hot plate at 120 °C for 2 min and then heat treated in a furnace at a temperature of 250 °C for 10 min.

In order to compare the performance of one sample type to the other, both sample types were coated with PTFE using the same dip coating parameters. The PTFE only samples had an average film thickness of approximately 580 nm, while the PDA/PTFE samples had an average thickness of 720 nm, measured using a stylus surface profiler. The film thickness of the PDA layer was approximately 120 nm, measured using an AFM. Subtracting the PDA film thickness from the total thickness of PDA/PTFE reveals a PTFE top coat thickness of about 600 nm, which is consistent with the film thickness of the PTFE only samples.

8.2.2. Tribological Testing

Tribological testing of the samples was performed using an automatic friction abrasion analyzer. The counterface used was a 7 mm diameter chrome steel ball, and the test was

performed under a 50 g normal load, 2.5 mm/s sliding speed, and 15 mm stroke length. To maintain consistency, all tribological tests were performed by rubbing the samples in a direction parallel to the polishing lines of the stainless steel substrates.

Two different tribological studies were carried out. The first study was a friction and durability study. From this study, the COF of the films, under the testing conditions, as well as the number of rubbing cycles at which the film is sufficiently rubbed off/damaged to produce a sharp increase in the COF (failure point) were determined. The number of rubbing cycles before failure can therefore be used as a measure of the durability of the film. The second study allowed the observation of the wear progression on each film. For PTFE only, four separate friction tests were carried out for 1, 10, 60 and 1000 cycles. For PDA/PTFE, the friction tests were carried out for 1, 10, 60, 1000, and 4000 cycles. Each wear track's cross-sectional profile was then used to analyze the wear progression. In all experiments, each testing condition was repeated three times to ensure the repeatability of the testing results.

8.2.3. Surface Characterization

An optical microscope (model XJP-H100, American Scope, Irvine, CA) was used to characterize each sample and counterface. Optical images were captured to qualitatively compare the wear tracks between sample types and for different rubbing durations, as well as to identify film transferred to the counterface after the rubbing tests. The wear track cross-sectional profiles on each sample were characterized using a Dektak stylus surface profiler. These wear track profiles were determined by running the stylus across the width of each wear track. In addition, a Dimension Icon AFM was used to characterize the surface nanotopography on each sample.

Scanning electron microscopy was used to characterize the surface of each sample type after friction tests of various rubbing cycles. The topography of each sample and wear characteristic was carefully analyzed to determine the wear mechanism on the different samples.

Surface chemical compositions of the films before and after the tribological tests, as well as transfer films on the counterface, were investigated using X-ray photoelectron spectroscopy The XPS spectra were obtained using a monochromatic Al K_α (1486.6 eV) source with a 100 μm spot size. Both XPS survey spectrum and high-energy resolution (Hi-Res) scans were acquired. Because PTFE is an insulator, dual-beam neutralization was used to avoid charge build up on the samples. Additionally, all spectra were shifted based on adventitious carbon at a binding energy of 284.8 eV to allow for comparison between spectra.

8.3. Results and Discussion

8.3.1. Friction and Durability

Figure 8.1 shows the results for the COF as a function of rubbing cycles. The sample coated with PTFE only, shown in solid line in Figure 8.1 (a), presented a low COF of approximately 0.06 at the onset of the test, but the COF quickly rose to approximately 0.65 after only 10 rubbing cycles. These results indicated that the film had failed, and the stainless steel substrate was now exposed to the counterface. The sample with a PDA adhesive layer and PTFE top coat, on the other hand, showed a COF that remained stable at approximately 0.06 for 1000 rubbing cycles. To test the durability of this film, the friction test was repeated for a longer duration. The COF in Figure 8.1 (b) showed a slightly increasing trend from 0.06 to 0.1 over 5370 cycles, with a sharp increase in the COF at 5370 cycles, indicating film failure.

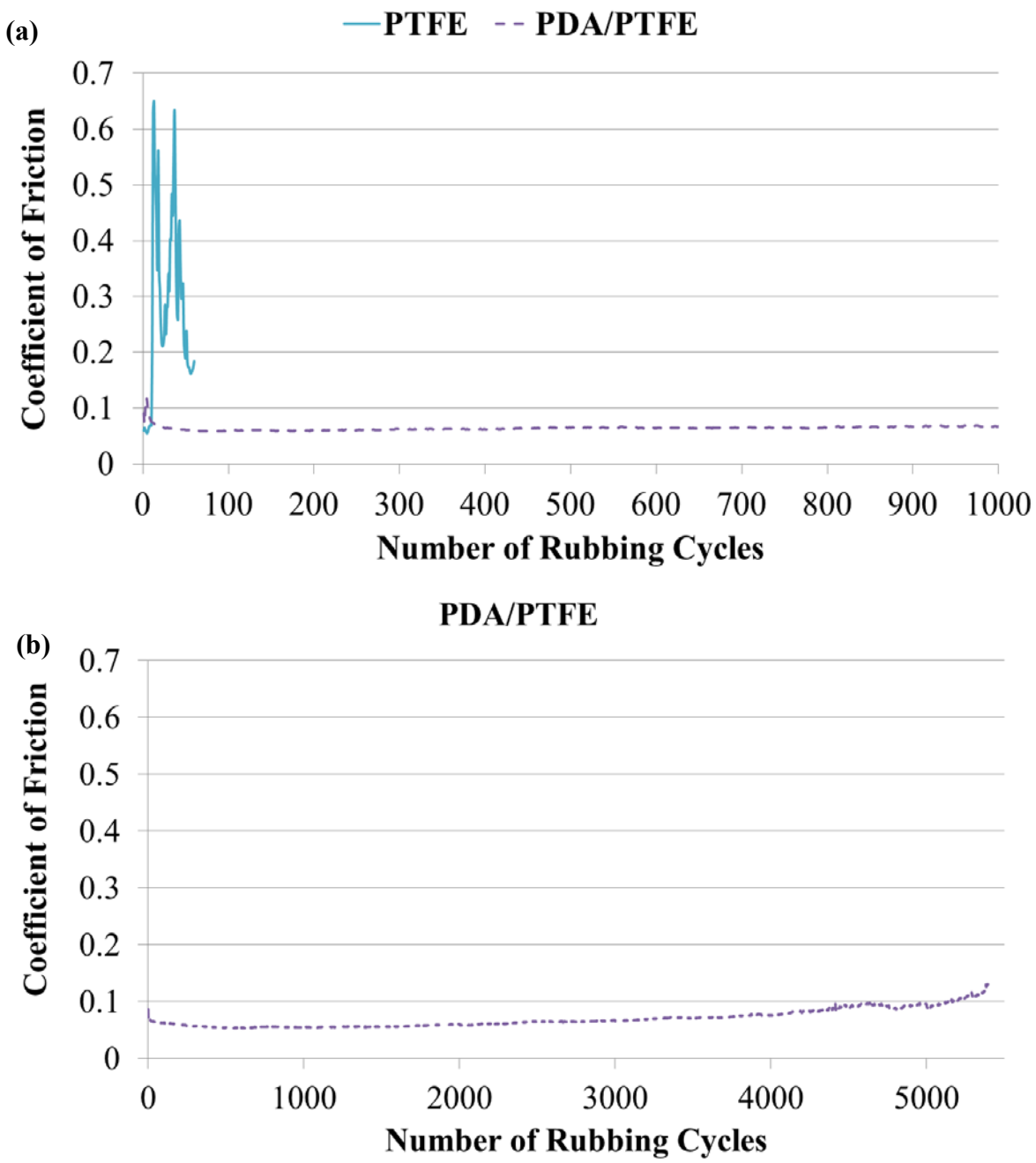

Figure 8.1: COF vs. rubbing cycles for (a) PTFE film and PDA/PTFE film rubbed for 1000 cycles, and (b) PDA/PTFE rubbed for 5400 cycles. The testing conditions are: 50 g normal load, 2.5 mm/s speed, 15 mm stroke, 7 mm diameter chrome steel ball counterface, linear reciprocating test.

Table 8.1 shows the individual results for each test carried out in the durability study. On average PTFE exhibited a dynamic COF of 0.8 and PDA/PTFE a dynamic COF of 0.07. The

average wear life/durability for PTFE was 7.33 cycles, while for PDA/PTFE the average wear life was 4690 cycles. These results show that on average the PDA/PTFE film was able to withstand more than 600 times the number of rubbing cycles of a PTFE only film.

Table 8.1: Dynamic COF, and durability results for PTFE and PDA/PTFE in 50g normal load friction test.

Sample	Dynamic COF					Wear Life (No. of rubbing cycles)				
	Test 1	Test 2	Test 3	Avg.	STDEV.	Test 1	Test 2	Test 3	Avg.	STDEV.
PTFE	0.06	0.11	0.07	**0.08**	**0.03**	10	5	7	**7.3**	**2.5**
PDA/PTFE	0.08	0.07	0.07	**0.07**	**0.01**	4150	5370	4550	**4690**	**622**

8.3.2. Transfer Film

It has been established, in prior investigations of bulk PTFE composites, that the formation of a well bonded transfer film on the counterface plays a crucial role in the wear performance of PTFE. The well adhered transfer film allows the PTFE composite to essentially rub against itself [31, 41]. In order to test whether this is also true for PDA/PTFE thin films, an image of the counterface was captured after friction tests carried out for 1, 10, 60 and 1000 rubbing cycles. As shown in Figure 8.2 (a1) and (b1), PTFE only and PDA/PTFE both formed a transfer film on the counterface after only the first rubbing cycle. The thick, discontinuous nature of the transfer film observed in Figure 8.2 for both sample types, suggests that the transfer film is likely a build-up of material, repetitively formed and removed, with little adhesion strength to the counterface [106]. In both sample types, the transferred material did not accumulate progressively on the counterface as the number of cycles increased. After 60 cycles, as shown in Figure 8.2 (a3), the sample with PTFE only had already failed. Part of the transfer film had been removed from the counterface as a result of contact between the counterface and the substrate. After 1000 cycles, as shown in Figure 8.2 (a4), the damage to the counterface was significant, and deep grooves

were visible inside the contact area. The PDA/PTFE sample, on the other hand, showed no damage to the counterface for up to 1000 cycles. These results suggest that the formation of a transfer film, by itself, does not ensure wear resistance of the film.

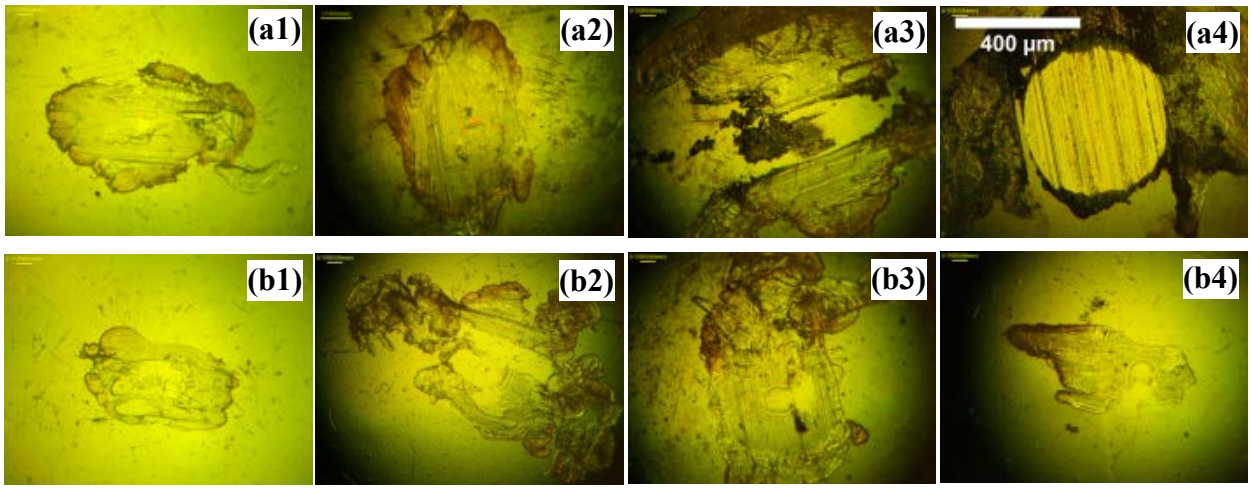

Figure 8.2: Optical microscope images of the chrome steel balls rubbed against PTFE film for (a1) 1 cycle, (a2) 10 cycles, (a3) 60 cycles, (a4) 1000 cycles and against PDA/PTFE film for (b1) 1 cycle, (b2) 10 cycles, (b3) 60 cycles and (b4) 1000 cycles at 10x magnification. The scale bar in (a4) applies to each image.

8.3.3. Wear

Optical images of the wear tracks on the samples after friction tests carried out for 1, 10, 60 and 1000 rubbing cycles can be seen in Figure 8.3. For the PTFE only sample, the wear track width after the first cycle was 220 µm, as seen in Figure 8.3 (a1), and increased progressively with successive rubbing cycles. After 60 rubbing cycles, it is evident from the dark area in the middle of the wear track, as shown in Figure 8.3 (a3), that the substrate was exposed and abraded. After 1000 cycles, shown in Figure 8.3 (a4), the surface was significantly damaged, showing an even wider abraded area. However, the abraded area is only present at the center of the wear track, resulting from the counterface ploughing through the surface of the substrate. Adjacent to this abraded area, the film had also delaminated from the substrate due to the high

shear forces produced during the rubbing test and weak adhesion between the film and substrate. The delamination of the film, which was confirmed using the Peak Force Quantitative Nanomechanics function of the Dimension Icon AFM, left an area of exposed but undamaged stainless steel and produced a total wear track width of approximately 640 µm.

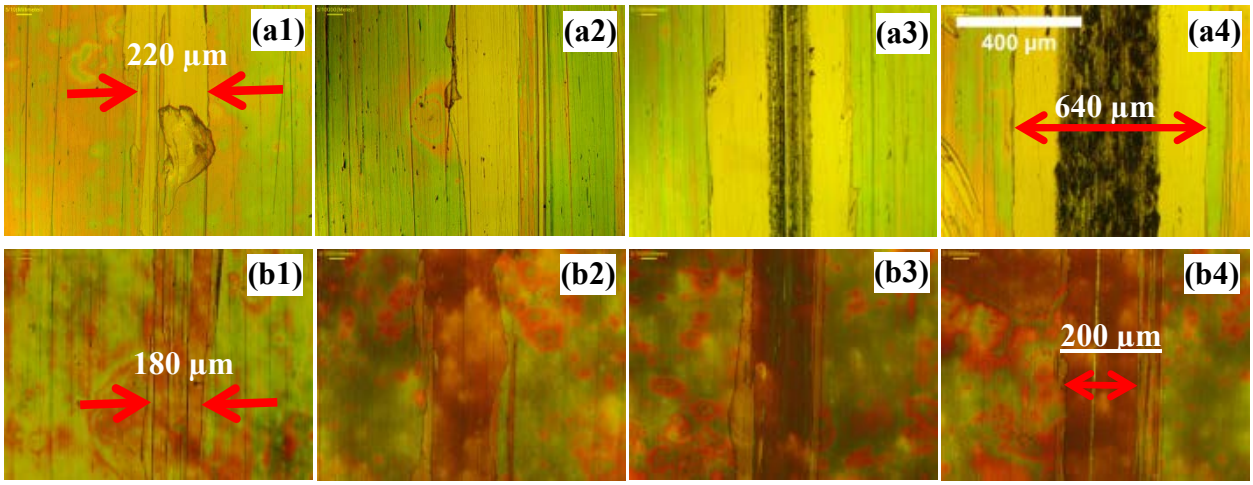

Figure 8.3: Optical microscope images of the wear track on PTFE film sample rubbed for (a1) 1 cycle, (a2) 10 cycles, (a3) 60 cycles, (a4) 1000 cycles and on PDA/PTFE film sample rubbed for (b1) 1 cycle, (b2) 10 cycles, (b3) 60 cycles and (b4) 1000 cycles. The scale bar in (a4) applies to each image.

Optical images of the wear tracks on PDA/PTFE after friction tests carried out for 1, 10, 60 and 1000 rubbing cycles can be seen in Figure 8.3 (b1-b4). The wear track for PDA/PTFE reached a width of about 180 µm after the first cycle, as shown in Figure 8.3 (b1), and then slowly progressed to only 200 µm after 1000 rubbing cycles, as seen in Figure 8.3 (b4). The minimum change in wear track width from the first cycle through 1000 cycles indicates that, after the first rubbing cycle, the wear of PDA/PTFE progressed much slower than for PTFE only.

The progression of the wear, indicated by the cross-sectional profile for each wear track, was measured using a Dektak stylus profiler. Figure 8.4 shows the wear track cross-sectional profile for 1, 10, 60 and 1000 rubbing cycles on PTFE only. The depth of the wear track reached the

film thickness of approximately 570 nm in the first cycle. The profile shows that after the first cycle, the wear track had a width of about 200 µm, and, as the cycles progressed, the width increased to about 650 µm. The peaks and valleys of high amplitude, which appear in the center of the wear track profile after 60 rubbing cycles, indicate that the counterface has dug into the stainless steel substrate. This shows that the film has been removed sufficiently to expose the substrate, allowing it to be abraded by the counterface.

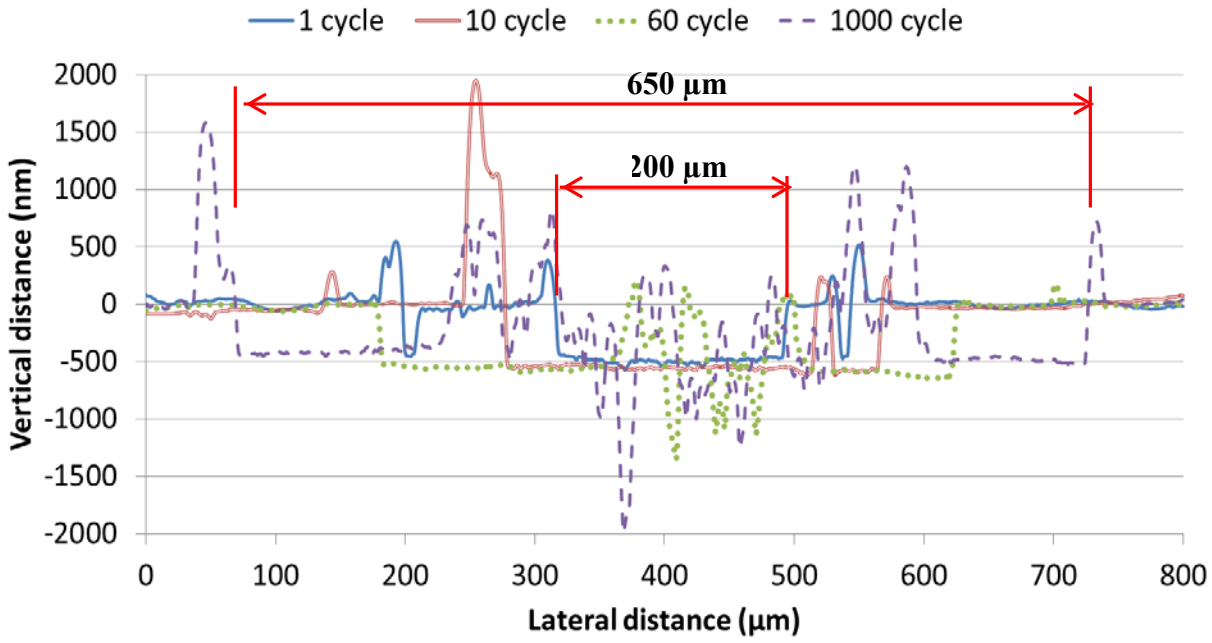

Figure 8.4: Cross-sectional profiles of the wear tracks for 1, 10, 60 and 1000 cycle friction tests on PTFE film.

The cross-sectional profiles for the PDA/PTFE sample wear tracks after 1, 10, 60, 1000, and 4000 rubbing cycles are shown in Figure 8.5. The width of the wear track, measured from the cross-sectional profile, started at approximately 150 µm after 1 cycle, increased to 190 µm after 1000 cycles and finished at 230 µm after 4000 cycles. The depth of the wear track reached 560 nm after only the first rubbing cycle and remained more or less the same for up to 4000 cycles.

Comparing the depth of the wear track to the initial film thickness of 720 nm indicates that a film of approximately 160 nm (about 40 nm PTFE and 120 nm PDA) remained on the substrate for the majority of the rubbing test. These results shows that the majority of the top coat is removed in the first pass of the counterface and also that the majority of the PTFE top coat is unaffected by the incorporation of PDA. However, once the wear track reaches a depth just above the PDA coat, the wear progression slows down dramatically. The fact that the COF also remains low and stable for over 5370 cycles suggests that a thin tenacious layer of PTFE remains at the interface with PDA. This thin layer of PTFE is well bonded to the PDA and allows the PDA/PTFE sample to withstand a significantly larger number of rubbing cycles than PTFE only.

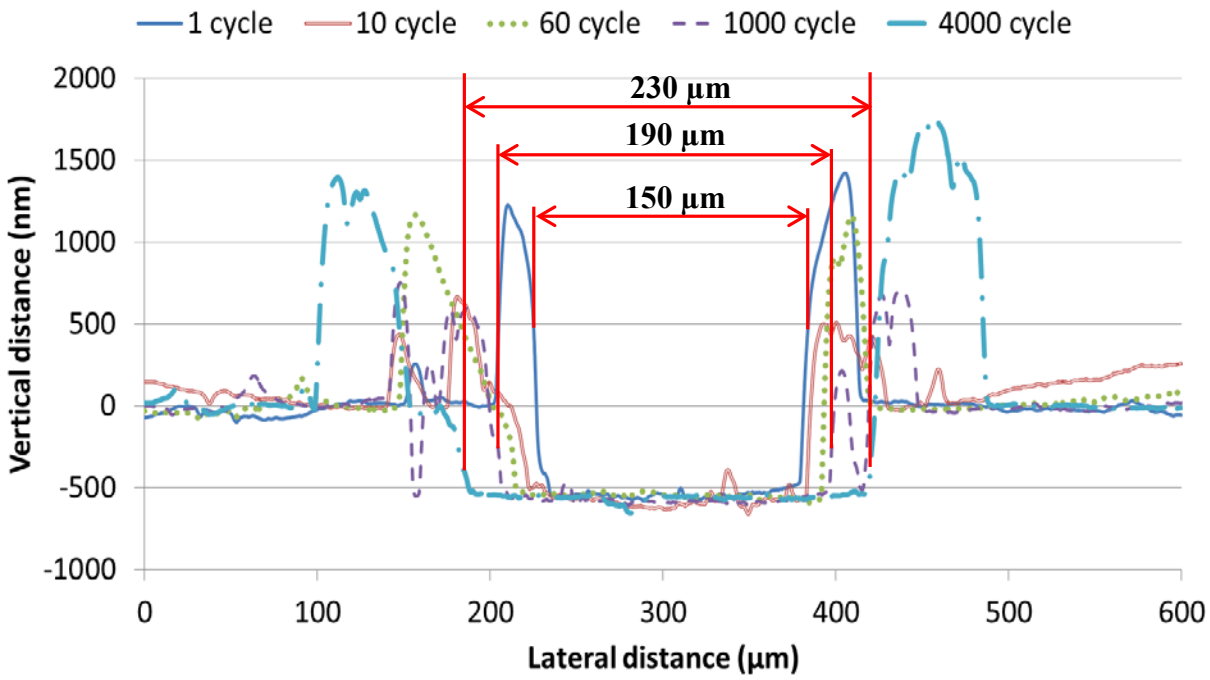

Figure 8.5: Cross-sectional profiles of the wear tracks for 1, 10, 60, 1000 and 4000 cycle friction tests on PDA/PTFE film.

8.3.4. Surface Topography

The surface topography of both PTFE and PDA/PTFE coated films were characterized using AFM. Figure 8.6 (a) and (b) show AFM images that depict the PTFE nanoparticles present in both films. Each PTFE nanoparticle is pebble shaped with lengths ranging between 100 to 400 nm, which is comparable to the nominal value of 50 – 500 nm provided by the manufacturer. In addition, as a result of the heat treatment process during the sample fabrication, it is evident that the individual nanoparticles have begun to fuse together. There is very little discernible difference between the surface topography of the two sample types. PDA/PTFE had an average surface roughness, Ra, of approximately 20.8 nm, while PTFE had a Ra value of about 21.6 nm. The root mean square roughness Rq was also similar for both sample types with a value of 24.6 nm for PDA/PTFE and a value of 28.5 nm for PTFE.

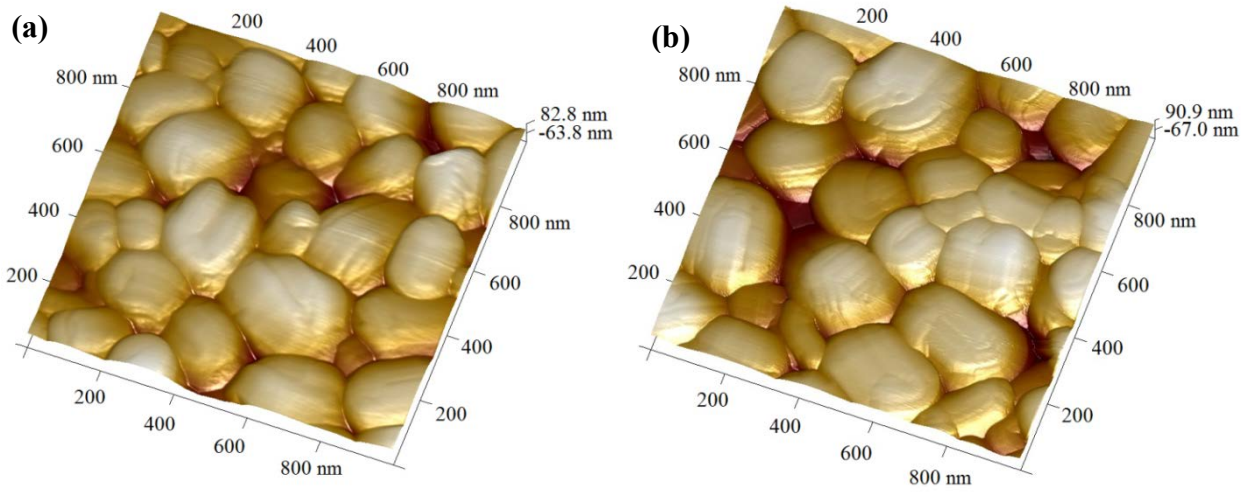

Figure 8.6: AFM images of (a) PTFE and (b) PDA/PTFE film topography.

The topography was also characterized using SEM. The SEM micrographs in Figure 8.7(a1) and (b1) show the coated surface for the PTFE only sample and PDA/PTFE sample, respectively. For both sample types PTFE nanoparticles of approximately 200 nm in diameter are clearly

observable on the intact surface of the samples. Figure 8.7 (a2) and (b2) show the surface of the wear track edge after 10 rubbing cycles. In Figure 8.7 (a2), which shows the PTFE only sample, it can be seen that the PTFE film has been completely removed from the wear track and a high pile up of PTFE particles can be observed at the wear track edge. On the other hand, in Figure 8.7 (b2), for PDA/PTFE, it can be seen that the PTFE particles have been compressed and have fused together to form a more cohesive film. Figure 8.7 (a3) and (b3), taken at the center of the wear tracks after 10 rubbing cycles confirm this. In Figure 8.7 (a3) it is clear that the PTFE particles have been removed and the polishing lines of the stainless steel substrate have been exposed. In Figure 8.7 (b3), on the other hand, it can be seen that the majority of the PTFE film is present; however, striations have begun to form where the film has begun to detach from the sample. After 1000 cycles, as shown in Figure 8.7 (a4) the PTFE only sample suffered significant wear, down to the substrate, and debris is present throughout the wear track. However, in Figure 8.7 (b4), which shows the PDA/PTFE sample wear track after 1000 cycles, the compacted film is still present inside the wear track with the presence of a few voids which show intact PTFE nanoparticles underneath. In addition, the striations are no longer as prevalent as they were after 10 rubbing cycles. It seems that these areas have a tendency to be filled in as film transferred to the counterface is re-deposited onto the wear track surface.

The striation present in the PDA/PTFE sample as shown in Figure 8.7 (a3), are an indicator of the improved adhesion of the PTFE film to the substrate, resulting from the incorporation of the PDA adhesive layer. The particles are no longer easily displaced from the substrate surface; instead, a tearing effect is observed over time.

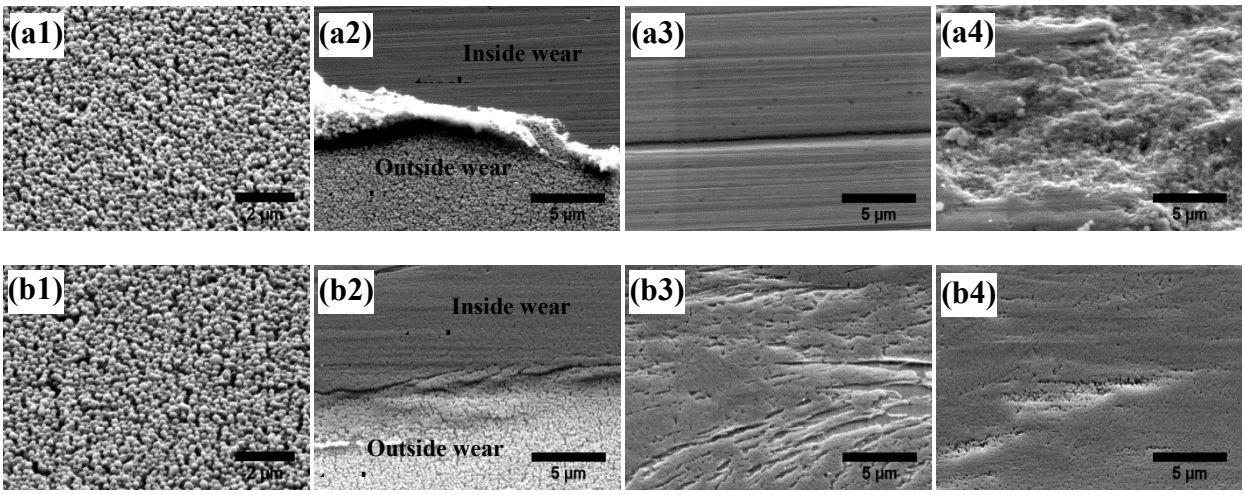

Figure 8.7: SEM micrographs of PTFE coated sample (a1) intact surface, (a2) 10 rubbing cycles, edge of the wear track, (a3) 10 rubbing cycles, center of the wear track, and (a4) 1000 rubbing cycles, center of the wear track, as well as SEM micrographs of PDA/PTFE coated sample (b1) intact surface, (b2) 10 rubbing cycles, edge of the wear track, (b3) 10 rubbing cycles, center of the wear track, and (b4) 1000 rubbing cycles, center of the wear track.

8.3.5. Chemical Analysis

In order to confirm the presence of a tenacious PTFE layer on PDA after extensive rubbing, an analysis of the chemical composition inside and outside the wear track was performed for both sample types using XPS. Each sample was analyzed after the durability test. The PTFE sample used was rubbed for 10 cycles, and testing was stopped as soon as the COF rose above 0.1. The PDA/PTFE sample was rubbed for 5400 cycles, and testing was also stopped as soon as the COF rose above 0.1. For the sample coated with PTFE only, a typical PTFE spectrum with a C1s peak at a binding energy of 292 eV and an F1s peak at 689 eV was observed outside the wear track, as shown in Figure 8.8 (a). To determine what chemical reactions may be taking place at the rubbing contact area, an XPS survey spectrum was also obtained inside the wear track. The spectrum, as shown in Figure 8.8 (b), revealed that the intensity of the F1s peak decreased in comparison to the F1s peak outside the wear track, and a Fe 2p3 peak was now present at 711 eV. This indicates that there was less fluorine content inside the wear track and

that the substrate was partially exposed. In addition, an oxygen peak at approximately 531 eV was also present inside the wear track. This peak is representative of the oxide layer formed on the exposed stainless steel surface. These results show that for the PTFE only sample, after only 10 rubbing cycles, the film was sufficiently penetrated to expose the substrate underneath it.

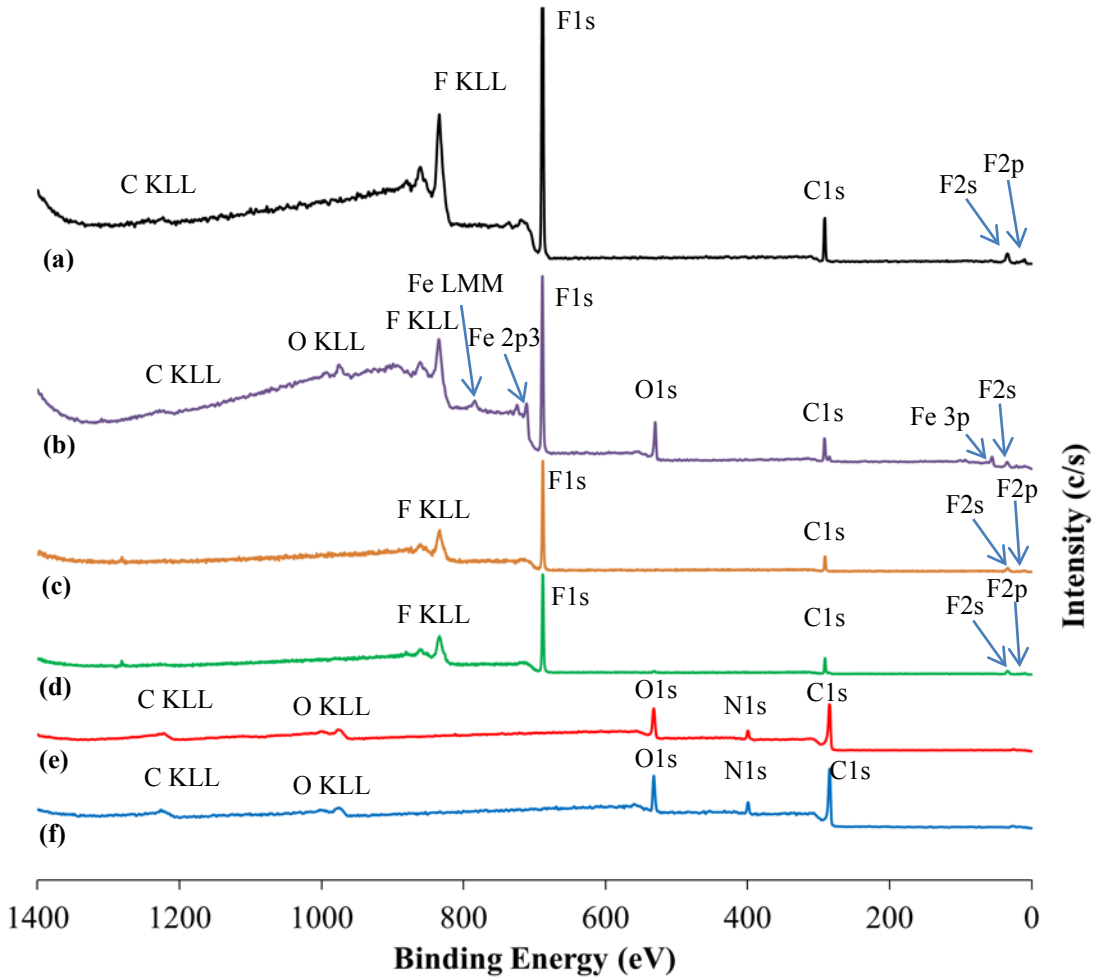

Figure 8.8: XPS survey spectra obtained (a) outside and (b) inside the wear track of PTFE coated stainless steel, (c) outside and (d) inside the wear track of PDA/PTFE coated stainless steel, as well as for stainless steel coated with PDA only (e) heated at 250°C and (f) with no heat treatment (all spectra are the same scale).

The XPS survey spectra obtained for PDA/PTFE are shown in Figure 8.8 (c) and (d). The spectrum for the PDA/PTFE surface outside the wear track exhibited C1s and F1s peaks

typically present in PTFE. Inside the wear track of PDA/PTFE, after a 5400 cycle rubbing test, these same peaks were also present, but at slightly lower intensities, confirming the PTFE film was still present inside the wear track. In addition, the absence of Fe peaks indicates that the substrate was not exposed. Even after 5400 rubbing cycles, a PTFE film of at least 10 nm thick (photoelectron escape depth of XPS) was still present inside the PDA/PTFE wear track.

XPS analysis was also performed on PDA-only films with no heat treatment and PDA-only films heated at 250 °C, as shown in Figure 8.8 (e) and (f), respectively. This analysis was performed to test the effect of the heat treatment procedure on the PDA film and to confirm that the film had not degraded after heat treatment at 250 °C for 10 min. The survey spectra for both PDA with no heat treatment and PDA heat treated at 250 °C had similar peaks with only a slight decrease in intensity for the heat treated surface. The spectra show the presence of O1s peaks at a binding energy of 532 eV, N1s peaks at 399 eV and C1s peaks at 285 eV, typical of PDA. Because the spectrum for heated PDA does not show the presence of new peaks resulting from the formation of new radicals, it is not likely that the film has degraded significantly.

For both PTFE and PDA/PTFE after 10 and 5400 respective rubbing cycles, high-resolution XPS scans in the C1s region were obtained inside the wear track to closely observe if new radicals may have been formed as a result of the high pressure rubbing. Figure 8.9 (a) shows the C1s spectrum for the PTFE wear track. The spectrum shows 5 peaks at binding energies of 291.8 eV, 291.4 eV, 288.5 eV, 286.2 eV and 284.8 eV, corresponding to CF_3-CF_2-, -(CF_2-CF_2)-, -(CF-CF)-, C-F and adventitious carbon, respectively [107, 108]. These peaks are characteristic of deconvoluted PTFE C1s spectra. This shows that, as a result of the high pressure rubbing, the PTFE chains have undergone scission, producing free radicals.

Figure 8.9 (b) shows the spectrum for PDA/PTFE. The spectrum shows the same peaks as those observed for PTFE only, in addition to a peak at 289.5 eV corresponding to -CF-CF_2- [107, 108]. This peak in the spectrum for PDA/PTFE is also typically found for deconvoluted PTFE C1s spectra and may not have been present for the PTFE only sample because of the large difference in rubbing cycles between the two samples. In other words, with more rubbing cycles, a higher degree of scission of PTFE chains will occur and a larger variety of radicals will be formed. Furthermore, PDA/PTFE also shows a significantly larger area, 78.76, under the peak for -(CF_2-CF_2)-, which is the representative peak for unbroken PTFE chains. The PTFE only sample, on the other hand, shows an area of only 24.83 for this peak. This shows that there was still a larger concentration of intact PTFE within the PDA/PTFE wear track, compared to PTFE only, despite the large difference in rubbing cycles.

8.4. Summary

This study shows that the addition of PDA as an adhesive layer before depositing a PTFE top-coat has a significant impact on the durability of the PTFE film. Under high contact pressures, a PDA/PTFE film of approximately 720 nm, on average, was able to withstand friction test durations of 4690 cycles, approximately 600 times the average durability of a PTFE film alone. More importantly, the majority of the test took place at the interface between the counterface and about 160 nm of remaining film. This is because a tenacious layer of PTFE was strongly adhered to the PDA and not easily removed, contributing to the durability of the film. Because of the relatively low thickness of the PDA/PTFE film, it shows great potential to be used in applications where durable, thin PTFE films are desirable.

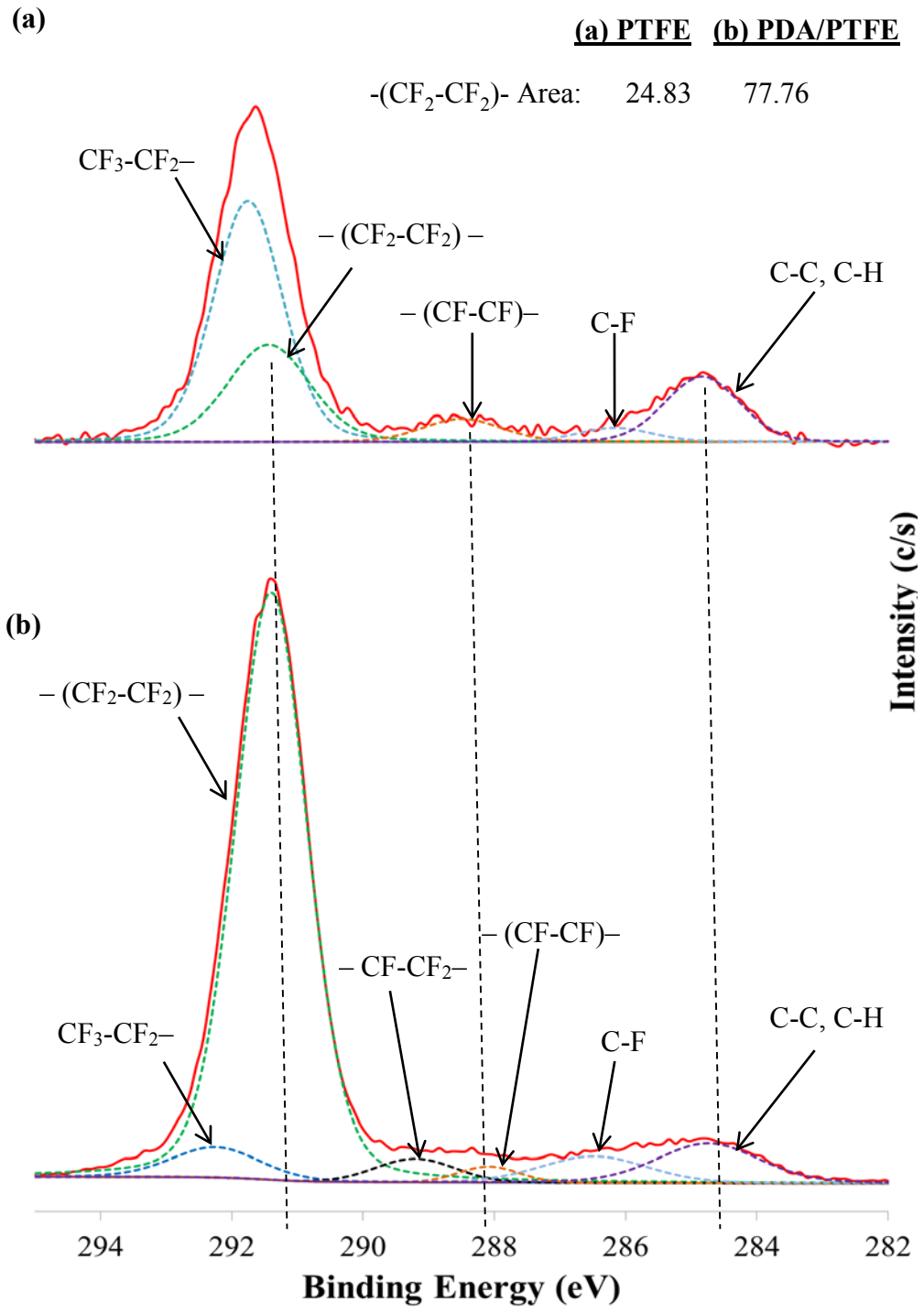

Figure 8.9: XPS high-resolution C1s spectra for the wear tracks on (a) PTFE film (10 cycles) and (b) PDA/PTFE film (5400 cycles).

Chapter 9

Combined effect of incorporating polydopamine as an adhesive layer and Copper nanoparticle filler in PTFE

9.1. Overview

To make PTFE more suitable for use in tribological application, much focus has been placed in reducing its wear rate. Various fillers and polymer blends have been used to reduce the wear rate of PTFE such as: glass fiber [38], alumina [39], graphite [40], and PEEK [109]. Fillers have shown to affect PTFE in the following ways: increasing the crystallinity, improving the ultimate strength, increasing elongation to failure, and improving toughness [9]. As a result of these investigations a great deal of progress has been made in reducing the wear rate of PTFE as a bulk material.

In the last two decades, with the emergence of MEMS technology and advances in film deposition methods, a great deal of focus has shifted to the study of thin films. In the field of tribology, thin films have drawn interest for use as solid lubricants. Various polymers, ceramics and metals have been investigated to determine their friction and wear properties. However, very little focus has been placed on the tribological performance of PTFE thin films [21].

The work presented in this chapter builds on the previous study on the influence of a PDA adhesive layer on the tribological performance of a thin PTFE top coat, which was presented in Chapter 8. The previous study showed that the use of PDA increased the wear life of PTFE films by over 600x, without producing a detrimental effect on the COF of PTFE [110]. The current work studies the combined effect of using Cu nanospheres as a filler in PTFE in addition to the use of the PDA adhesive layer. It was observed that the incorporation of Cu nanospheres

increased the wear life of the PDA/PTFE film by 2x, even at very low concentrations, and significantly reduced the COF of the film.

9.2. Materials and Methods

9.2.1. Sample Preparation

Two surface coatings were evaluated in this study. The first coating consisted of an adhesive PDA layer and a PTFE top-coat. The second coating consisted of an adhesive PDA layer and a PTFE/Cu nanospheres composite top-coat. The objective of this investigation was to evaluate the friction and durability of these films and determine the influence of the Cu nanoparticle filler.

The substrate selected for this investigation was 0.76 mm-thick Corrosion Resistant stainless steel sheets type 316. These sheets were first cut into 5 cm by 5 cm square samples and then cleaned using the procedure described in section 5.2.1.

Trizma base, dopamine hydrochloride, PTFE nanoparticle aqueous dispersion, and Cu nanoparticle dispersion were used to prepare the dip-coating solutions. The Cu nanospheres were synthesized in Chen Lab by reducing the Cu precursors using amines [111]. The preparation and deposition of PDA is explained in in Chapter 7. The solutions for the PTFE and PTFE/Cu top-coats were prepared as follows:

1. PTFE top-coat solution - The TE-3859 dispersion has a PTFE solids concentration of 60 wt.% as-received. In order to produce thinner coats of PTFE, the concentration of the as-received PTFE dispersion was diluted with DI water to produce a PTFE dispersion of 40 wt.% concentration.
2. PTFE/Cu nanoparticle top-coat solution – PTFE dispersion was mixed with a Cu nanoparticle solution to produce a final composite dispersion of 40 wt.% PTFE and 0.01 wt.% Cu nanoparticles.

Both surface coatings were deposited by dip coating at an insertion and withdrawal speed of 10 mm/min and immersion duration of 20 sec using a dip coater.

The heating procedure for this final study was modified from the experiments mentioned in earlier chapters in order to optimize the tribological performance of the film. Dupont typically suggests heating samples above the crystalline melting point of PTFE of 337 °C. The suggested process is as follows. After dip coating, the samples should be dried at 120 °C (as suggested in DuPont's product information) for 2 minutes in order to remove water from the film [16]. Next, the samples were to be baked in a furnace at 300 °C for 10 min, and finally, sintered at 337 °C for 10 min. These conditions proved not to be ideal for all components in the composite film. Thermogravimetric analysis of PDA showed that the polymer underwent a significant mass loss at approximately 200 °C, as seen in Figure 9.1. However, significant degradation is not likely to be happening until temperatures above 400 °C where a dramatic drop in mass is observed. It is believed that at 200 °C smaller molecules composed of self-assembled 5,6-dihydroxyindole, which are also produced in the polymerization of dopamine, may degrade. In order to prevent detrimental effects as a result of heat treatment, the heating process was optimized to produce the best results.

In order to effectively fuse a PTFE film to a substrate, Dupont also suggested heating it to temperatures ranging between 360 °C and 400 °C. Preliminary experiments were carried out that showed that a minimum temperature of 372 °C produced the best tribological results. At this temperature the film was observed to change from a milky color to a transparent film. The next step was to select the optimal duration of heat treatment at this temperature. The duration was varied between 1 min to 10 min at 372 °C, of which a 4 minute duration showed the best tribological results. Therefore, the final procedure for heat treatment was chosen to be as

follows: first, the sample was heated on a hot plate at 120 °C for 3 min, next the samples were heated in a furnace at 300 °C for 4 min and finally the film was sintered in a furnace at a temperature of 372 °C for 4 min.

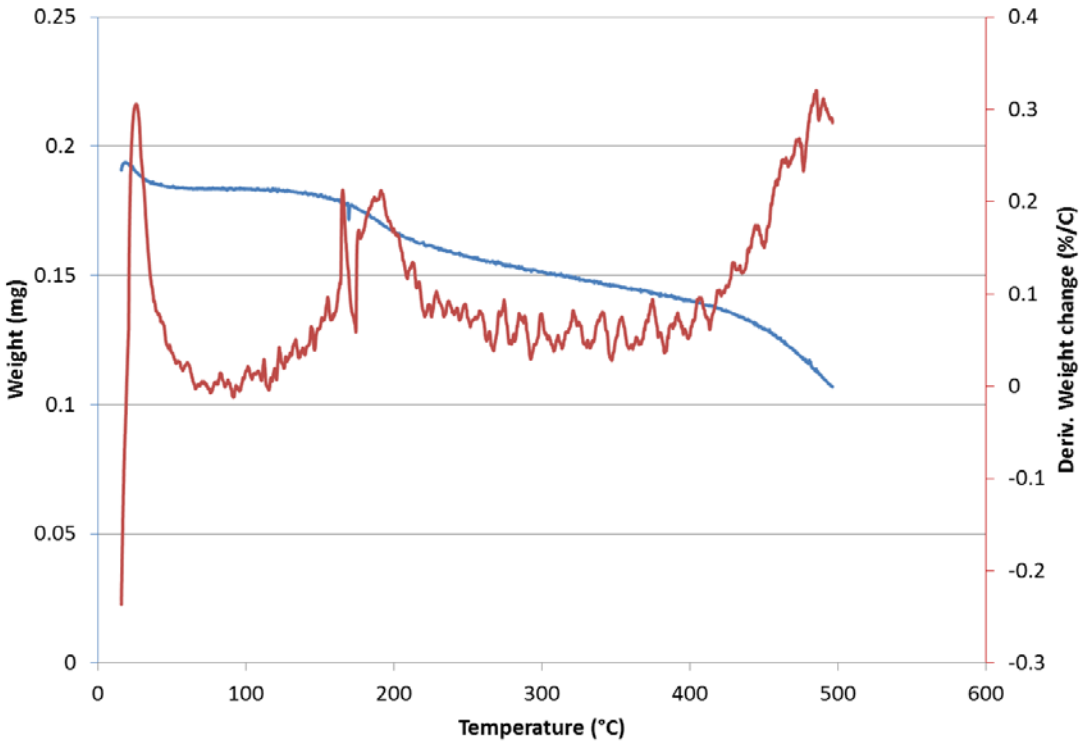

Figure 9.1: Thermogravimetric analysis of Polydopamine.

These heating conditions produced a transparent PTFE top coat with optimal tribological properties. The resulting coating thicknesses were measured using a stylus surface profiler. The average coating thickness for the PDA/PTFE films was 1.32 µm and the average coating thickness for the PDA/PTFE + Cu films was 1.17 µm as shown in Figure 9.2.

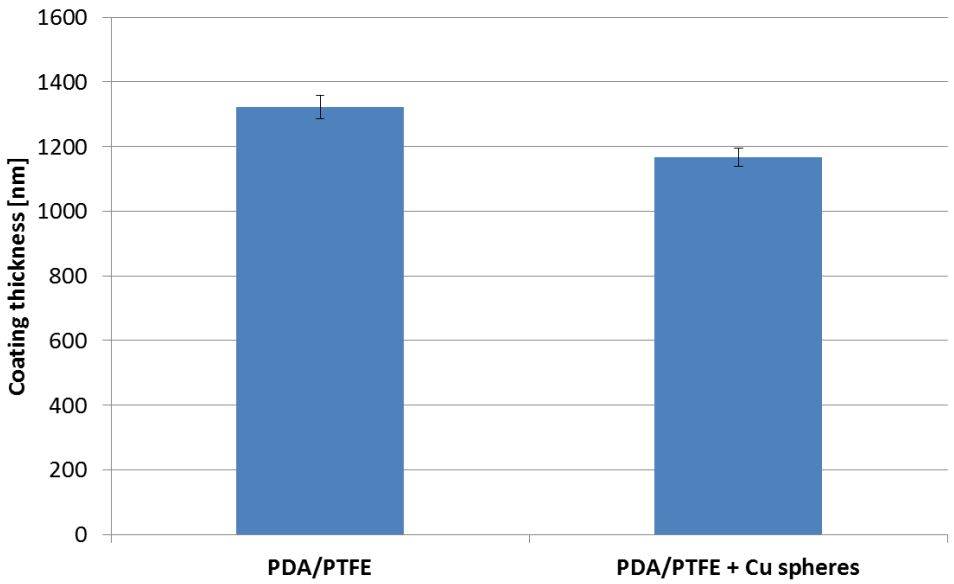

Figure 9.2: PDA/PTFE and PDA/PTFE + Cu Film thicknesses.

9.2.2. Friction and Durability

A Nano + Micro Tribometer (UMT-2, Bruker, Santa Barbara, CA) was used to perform linear reciprocating friction tests and measure static and dynamic COFs simultaneously. The test was performed by repeatedly sliding a 7 mm diameter chrome steel ball against the test sample, mounted on the tribometer stage. The friction tests were repeated at three different surface locations under an applied normal load of 50 g, a stroke length of 15 mm and a speed of 2.5 mm/s.

The friction tests were categorized into three different studies: durability, wear progression, and a linearly increasing load scratch test. First, a durability study was carried out to determine the effect of the Cu nanoparticle filler on the film wear life. The friction test was performed until a sharp increase in the COF was observed. A sharp increase in the COF indicates that the film on the sample has been sufficiently worn away so as to expose the stainless steel substrate to the counterface. As a result, the number of rubbing cycles until this point represents the wear life or durability of the film.

Second, a friction test was repeated for 1, 10, 60 and 1000 cycles to allow the examination of the wear track at each of these rubbing durations on each sample. The purpose of this test was to examine changes in surface morphology, measure the wear progression, and determine the wear mechanism affecting each sample type.

Finally, the linearly increasing load scratch test was carried out by using the UMT Tribometer to slide a 7 mm chrome steel ball across the surface of each sample at a constant speed and linearly increasing normal load. The load was increased from 0 to 460 mN in a distance of 20 mm. This test was repeated three times for each sample.

9.2.3. Sample Characterization

A stylus surface profiler was used to determine the wear track cross-sectional profile on each sample. The cross-sectional profiles were measured using a 12.5 μm radius stylus with 3 mg contact force, 600 μm scan length, and scan duration of 30 sec. The wear track profile was established by running the stylus along the width of each wear track.

Scanning electron microscopy was used to characterize the surface topography and wear of all samples. Several SEM micrographs at different surface locations were captured to examine the micro-scale topography of the coated surface and inside the wear tracks. In addition, an AFM was used to produce topographical images of the samples and measure the surface roughness.

9.3. Results and Discussion

9.3.1. Copper Particles

The Cu nanospheres, shown in Figure 9.3 (a) had diameters ranging from 5 to 20 nm. For the most part, Cu nanospheres appeared to be evenly distributed in their dispersion without much agglomeration. However, some batches showed more agglomeration than others as seen in

Figure 9.3 (b). The batches which were selected to form the coating solutions were those which showed better dispersion.

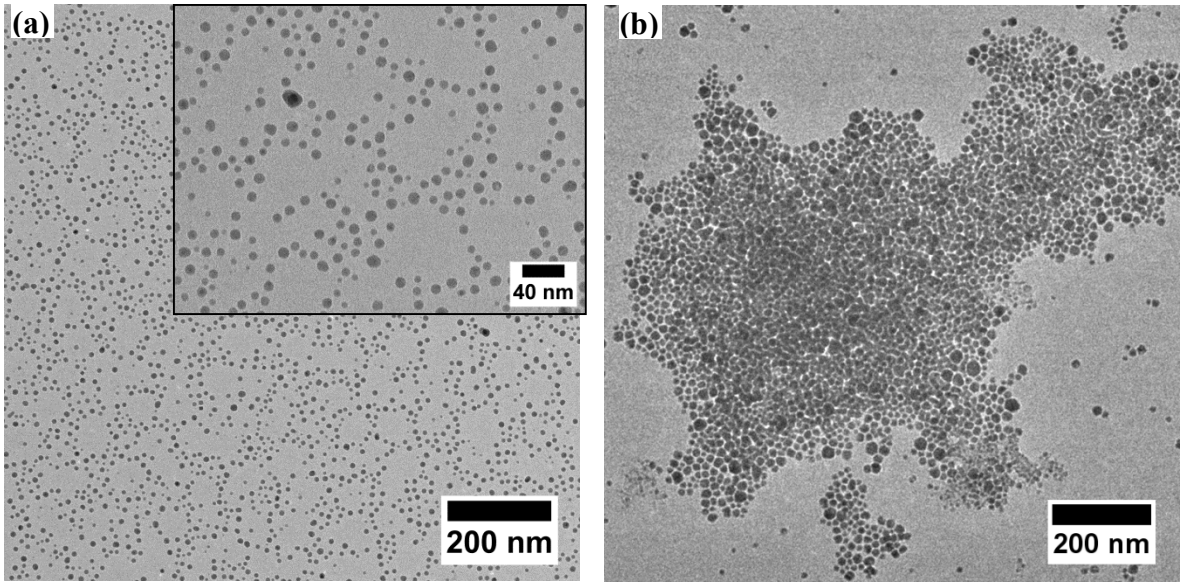

Figure 9.3: TEM of Copper (a) well dispersed nanospheres, and (b) agglomerated nanospheres.

Although Cu nanosphere dispersions with even distribution of nanoparticles were selected to mix with PTFE dispersions, the final coated samples all showed agglomeration of Cu nanospheres. As seen in Figure 9.4, the Cu particles agglomerated into clusters of approximately 2 to 10 μm. The image in Figure 9.4 was captured using a 3D Laser Scanning Microscope. The blue areas in the image represent portions of the surface that possessed a different reflectance. This allowed the identification of the metallic nanoparticles within the film. It is clear from the image that the particles have agglomerated into large clusters within the film.

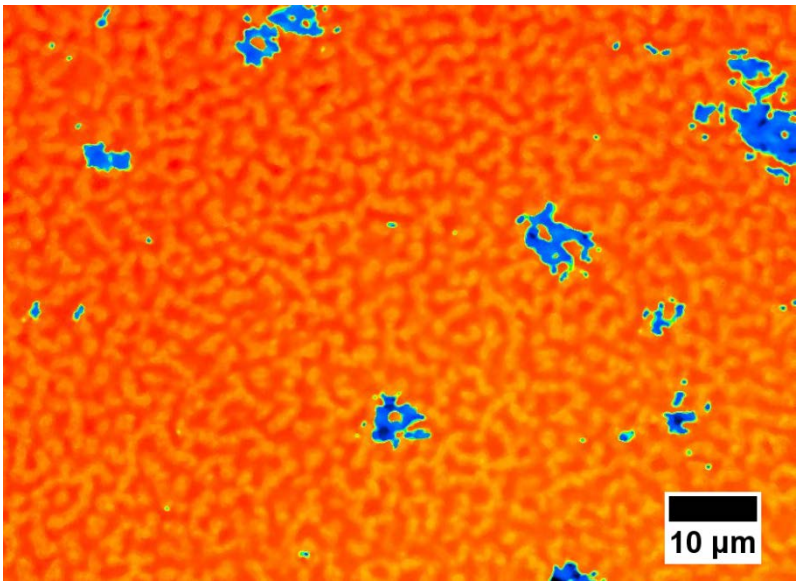

Figure 9.4: 3D Laser Scanning Microscope image of PDA/PTFE + Cu film surface.

Figure 9.5 (a) and (b) shows AFM images of PDA/PTFE and PDA/PTFE + Cu films, respectively. From the image it appears that the PDA/PTFE + Cu film is denser. As was the case with PTFE + Au studied in Chapter 7, it is likely that the metallic nanoparticles may aid in the spreading of the film by reducing the melting point. The lower thickness of these films also confirms that they are more compact than PDA/PTFE films. PDA/PTFE + Cu films also had a R_a and R_q surface roughness that was approximately 8 nm higher than those of the PDA/PTFE films.

9.3.2. Friction and Durability

Both PDA/PTFE and PDA/PTFE + Cu films showed similar COF values which averaged 0.07, as shown in Table 9.1. The three tests carried out for each sample type had very little variation, both having a standard deviation of 0.01. However, on average PDA/PTFE + Cu films were able to withstand 19,854 rubbing cycles, while PDA/PTFE films only lasted for 10,082 cycles. This is an average increase in wear resistance by about 2x. In addition, when comparing

the PDA/PTFE film results for this study to those observed in section 8.3.1, it is clear that the PDA/PTFE samples prepared with the new heating procedure used in this study show a significant increase in durability. In section 8.3.1 it was observed that PDA/PTFE had an average durability of 4690. However in this study, PDA/PTFE shows an average durability of 10082 cycles. That is an increase in durability of more than 2x. This increase in durability is largely due to better sintering of the PTFE nanoparticles through heat treatment at a higher temperature.

The top performers for each sample type are shown in Figure 9.6. Both sample types typically experienced a slight increase in COF as the friction test progressed. This increase in friction is a result of changes in the chemical properties of PTFE as a result of the high shear forces. As was determined through chemical analysis in Chapter 7, the PTFE molecules underwent scission and crosslinked with each other, reducing the wear rate of the film with successive cycles but also increasing the COF. From Figure 9.6, the spike in friction representing failure of the film is clearly visible. This is the approximate point at which each test was stopped to allow observation of the worn surface. The drop in friction observed at approximately 11,000 and 18,000 cycles for the PDA/PTFE + Cu film is typically observed after a defect or tear in the film is covered with material transferred from the counterface back to the sample surface. When a large tear or hole is produced in the film as a result of the sliding motion, the friction increases at that specific location. This localized increase in friction raises the value for the average COF for that cycle. As that hole or tear increases in size the COF trends upward. Once that hole is patched by material retransfered from the counterface, the average COF value quickly drops producing an inverse spike in the plot.

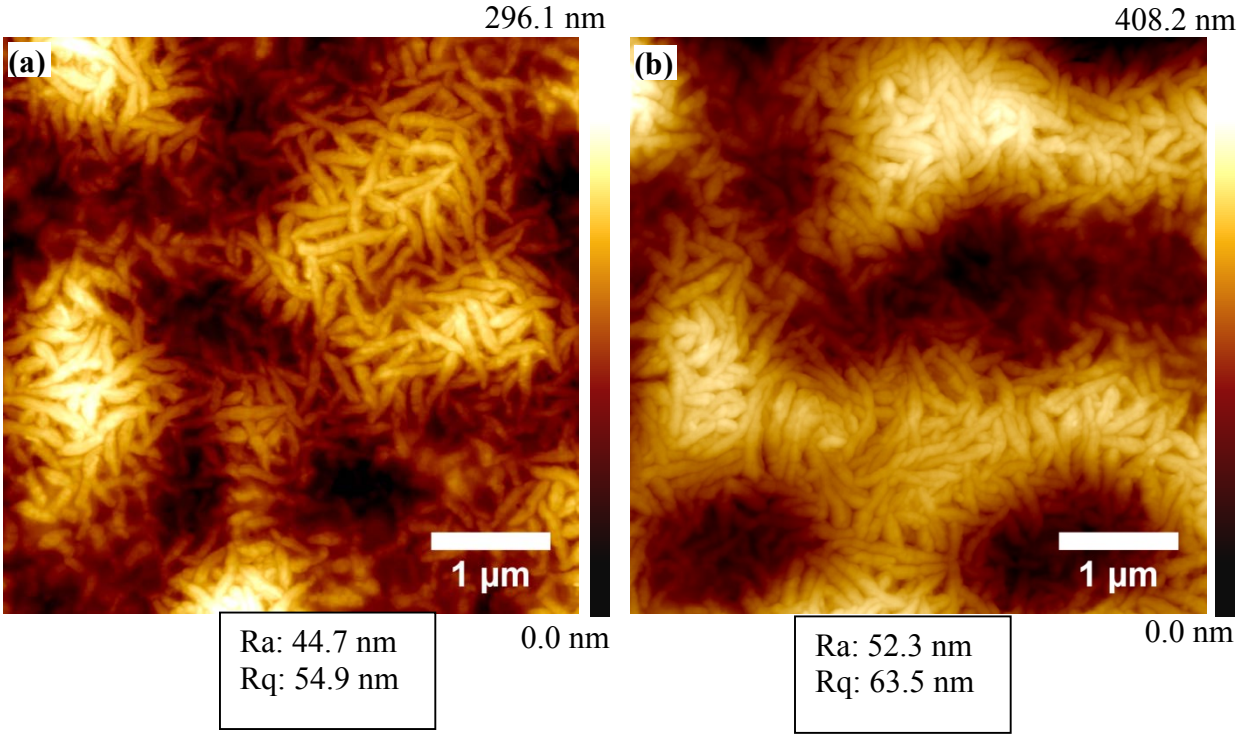

Figure 9.5: AFM topographical images and surface roughness values for (a) PDA/PTFE and (b) PDA/PTFE + Cu films.

Table 9.1: Durability and friction test results for PDA/PTFE and PDA/PTFE + Cu.

Sample	**Test 1**	**Test 2**	**Test 3**	**Avg.**	**STDEV.**
	Number of Cycles				
PDA/PTFE	10649	11158	8439	10082	1445
PDA/PTFE + Cu	19571	16543	23447	19854	3461
Average COF					
PDA/PTFE	0.07	0.06	0.07	0.07	0.01
PDA/PTFE + Cu	0.07	0.08	0.07	0.07	0.01

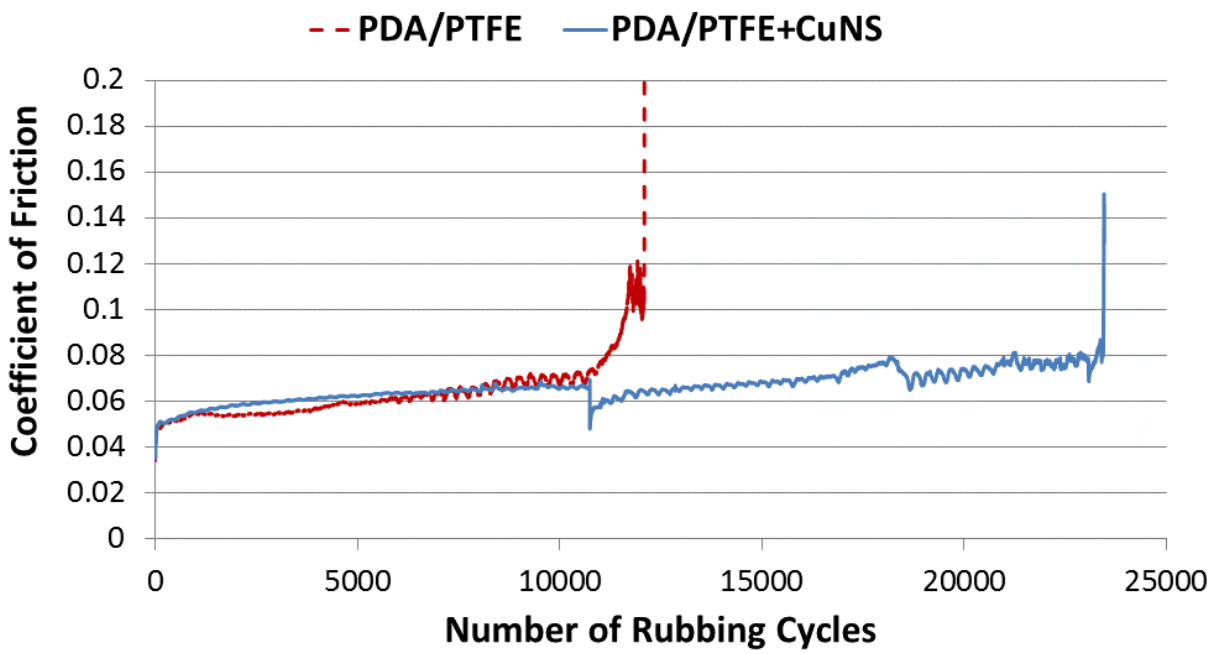

Figure 9.6: Friction test results for PDA/PTFE and PDA/PTFE + Cu films.

Figure 9.7 shows SEM micrographs of the wear tracks of the two top performing samples which were discussed above. It is clear from Figure 9.7 (a) and (e) that at the end of the friction test both films had been removed sufficiently to expose the substrate, as was evident from the grooves present at the center of the wear track. A higher magnification of these grooves is shown in Figure 9.7 (b) and (f). A high magnification of the area inside the wear track, adjacent to the grooves, is shown in Figure 9.7 (c) and (g). It is evident that the film had been compacted as a result of the friction test. Figure 9.7 (g) shows a plate like slab of PTFE which had likely been deposited back on the surface of the sample after the formation of a transfer film on the counterface. This is commonly seen in PTFE coatings. Figure 9.7 (d) and (h) were captured at the periphery of the wear track to show the topography of the build-up which accumulated at the edges of the wear track during the friction test. Both samples types show fibrils and striation that are typically observed in PTFE films. A key difference, however, for PDA/PTFE + Cu shown in Figure 9.7 (h), is the presence of micro-cracks. These micro-cracks reduce debris size or

similarly prevent large amounts of film from being removed with each pass of the counterface as was the case with unfilled PDA/PTFE.

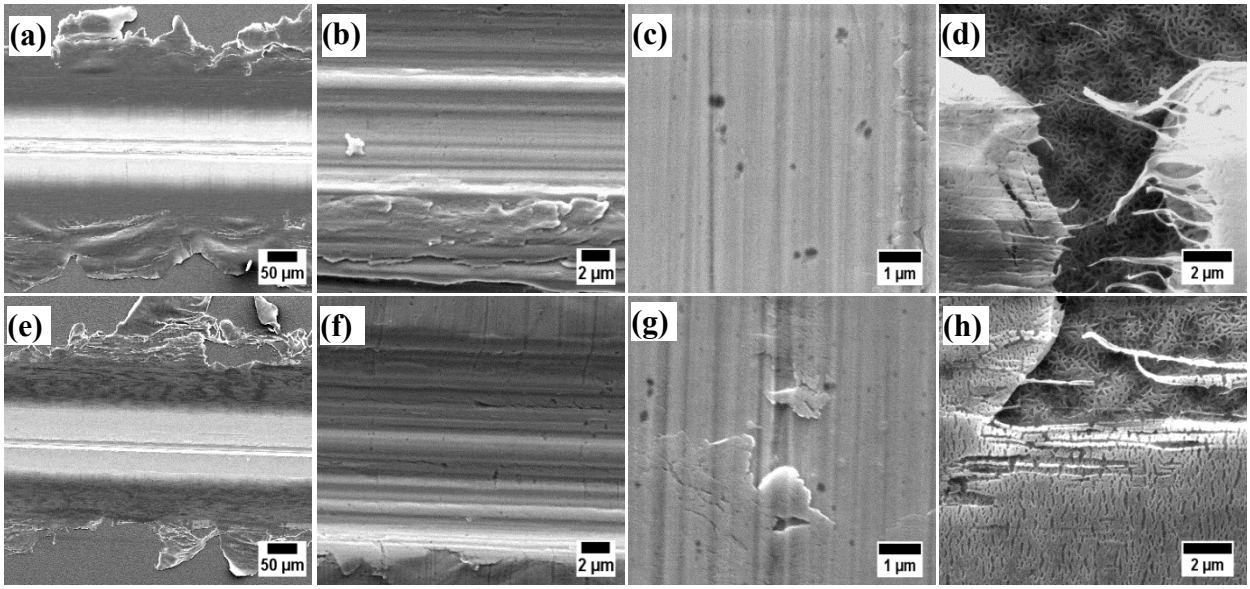

Figure 9.7: SEM micrographs of the wear tracks in (a-d) PDA/PTFE and (e-h) PDA/PTFE + Cu films.

9.3.3. Wear Progression

This portion of the investigation consisted of repeating the friction test above for a specific number of cycles and the wear progression at each point was analyzed. The friction tests were carried out for 1, 10, 60, and 1000 cycles. Figure 9.8 shows SEM micrographs of each wear track resulting from 1, 10, 60, and 1000 rubbing cycles. PDA/PTFE shown in Figure 9.8 (a-d) had a wear track width of 80 µm after 1 cycle. The wear track width then increased to 102 µm after 10 cycles, 134 µm after 60 cycles and finally 247 µm after 1000 cycles. PDA/PTFE + Cu, shown in Figure 9.8 (e-h), had a wear track width of 72 µm after the first cycles, 93 µm after 10 cycles, 138 µm after 60 cycles, and 153 µm after 1000 cycles. Based on the wear track width,

the initial wear of both sample types is quite similar; however, between 60 and 1000 cycles the wear of PDA/PTFE + Cu film is much less than that of PDA/PTFE.

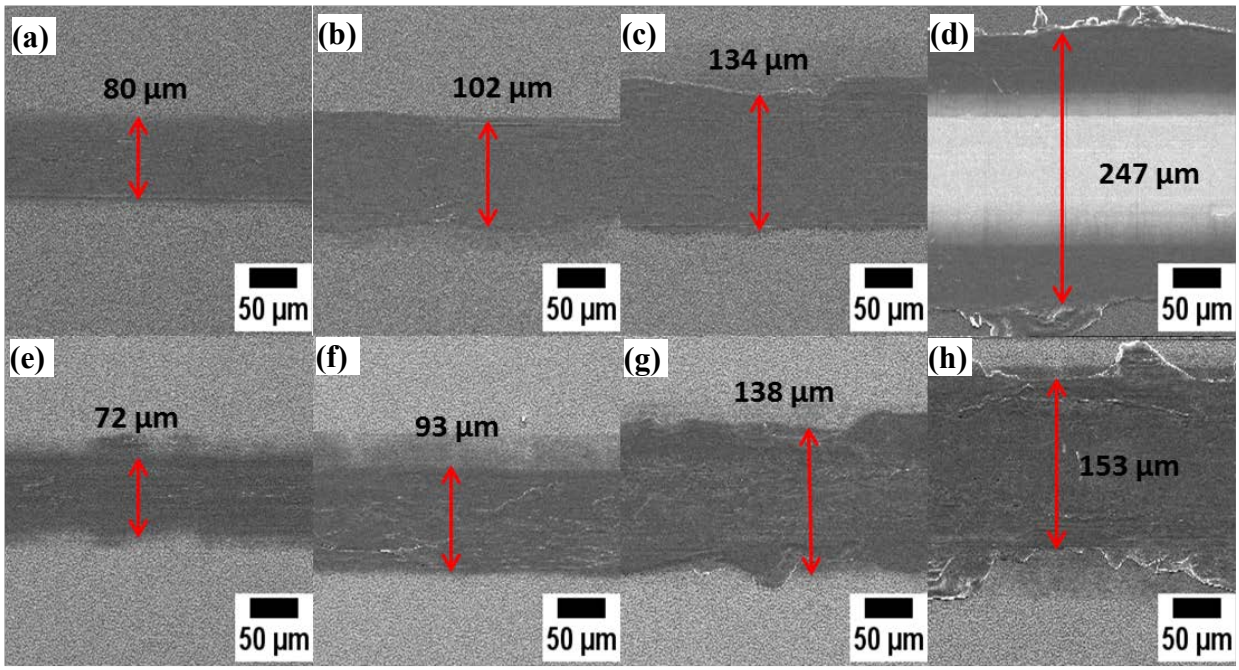

Figure 9.8: SEM micrographs of the wear tracks in PDA/PTFE film tested for (a) 1 cycle, (b) 10 cycles, (c) 60 cycles, and (d) 1000 cycles, and wear tracks in PDA/PTFE + Cu film tested for (e) 1 cycle, (f) 10 cycles, (g) 60 cycles, and (h) 1000 cycles.

The slower wear progression of PDA/PTFE + Cu films determined from the width of the wear tracks above was confirmed through cross-sectional profiles of the wear tracks. The cross-sectional profiles permitted the observation of the wear depth at 1, 10, 60, and 1000 rubbing cycles. Figure 9.9 shows the cross-sectional profiles for PDA/PTFE film and Figure 9.10 shows the cross-sectional for PDA/PTFE + Cu film. The difference in wear progression after 1000 cycles was again very clear. The depth of the wear track progresses similarly for both sample types up to 60 cycles; however, after 1000 cycles the depth of PDA/PTFE is approximately 1000 nm, while the depth of PDA/PTFE + Cu is only about 350 nm - very little increase from the wear

depth after 60 cycles. This difference in depth confirms that PDA/PTFE + Cu has higher wear resistance than PDA/PTFE and is thus more durable.

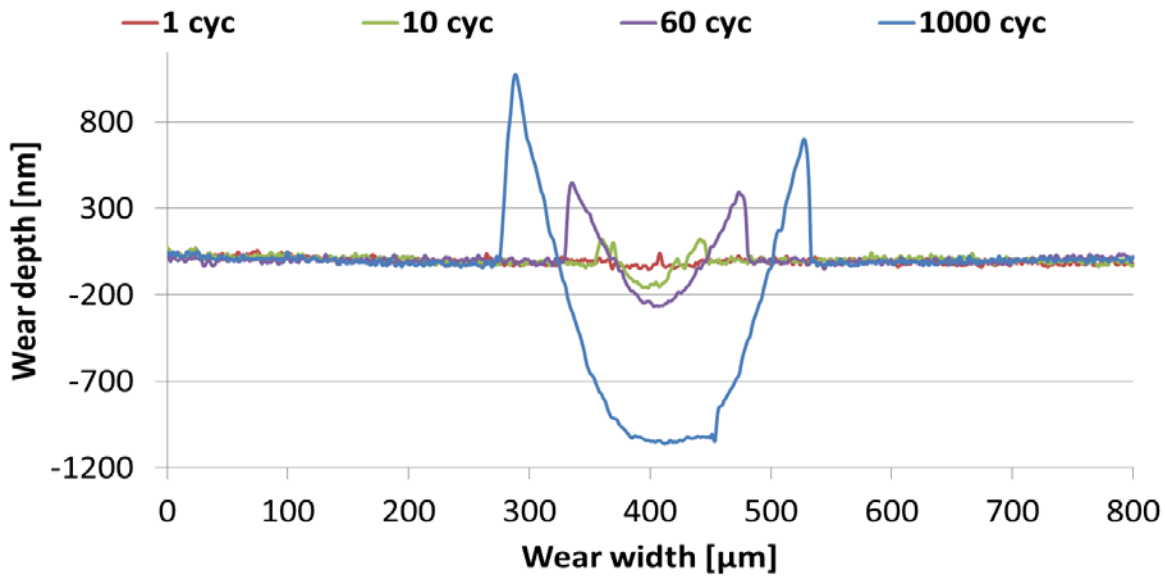

Figure 9.9: Dektak cross-sectional profile for PDA/PTFE film wear progression study.

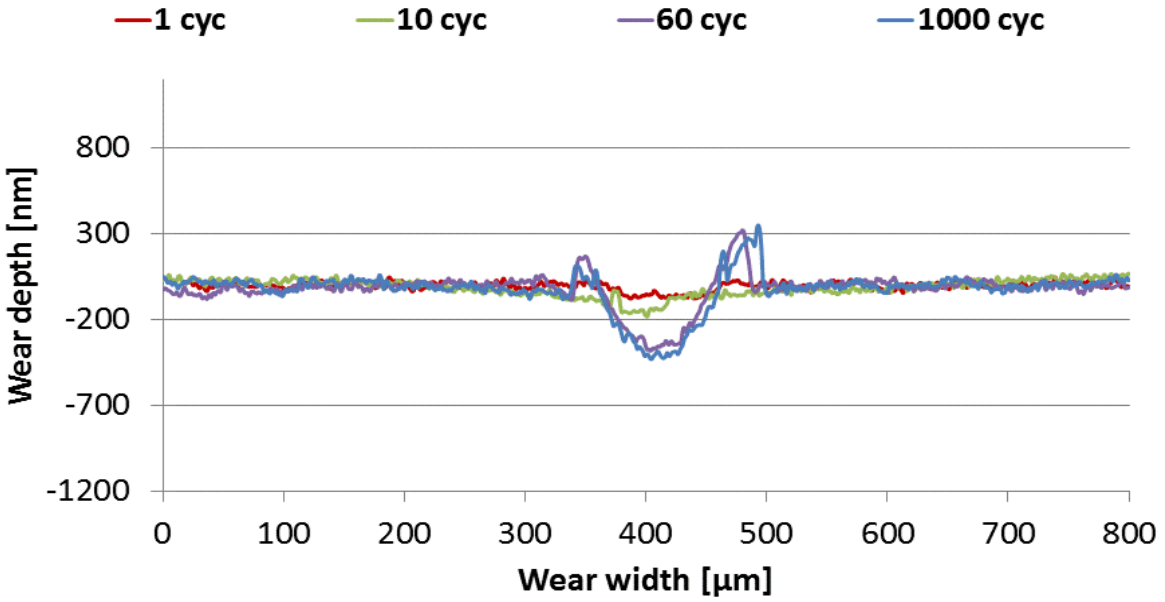

Figure 9.10: Dektak cross-sectional profile for PDA/PTFE + Cu film wear progression study.

Figure 9.11 shows optical microscope images of the chrome steel ball counterfaces used for the wear progression study. Figure 9.11 (a-d) are images of the chrome steel ball rubbed against the PDA/PTFE film for 1, 10, 60, and 1000 cycles, respectively. Figure 9.11 (e-h) are images of the ball rubbed against the PDA/PTFE + Cu sample for 1, 10, 60, and 1000 cycles, respectively. The balls rubbed against PDA/PTFE for 1, and 10 cycles showed little to no signs of a transfer film present on the surface. The ball used for 60 cycles did show transferred film on the surface, although only a minimal amount. For 1000 cycles again there was no presence of a transfer film. For balls rubbed against PDA/PTFE + Cu films, on the other hand, it was evident that after 10 rubbing cycles a significant amount of transfer film has formed. The transfer film appeared to be sufficiently thick to create a barrier between the ball and the sample surface and had a circular shape that surrounded the contact area. It is appears that the majority of the transfer film was deposited at the front center and front edges of the contact area as the ball slid forward and likewise at the back of the contact area as the ball slid in the reverse direction. The transfer film was also present for 60 and 1000 rubbing cycles. The formation of this film explains the change in wear progression after 60 cycles that was observed in the cross-sectional profile of the wear track. It is evident that the presence of the nanoparticle filler has a strong effect on the formation of the transfer film. The nanoparticle filler may initially act as an abrasive third body at the interface between the two opposing surfaces. Cu nanospheres will fuse more readily to the chrome steel than PTFE, and carry PTFE debris along with it to form a transfer film. Another explanation is the possibility of a chemical reaction between the Cu nanospheres and PTFE resulting from the high shear stresses. As stated in section 1.1.6, Bahadur suggested that it is the decomposition of the filler, generating reaction products between PTFE and the filler, which can

improve the bonding of a transfer film to the counterface, and thus enhances the wear resistance of PTFE [41].

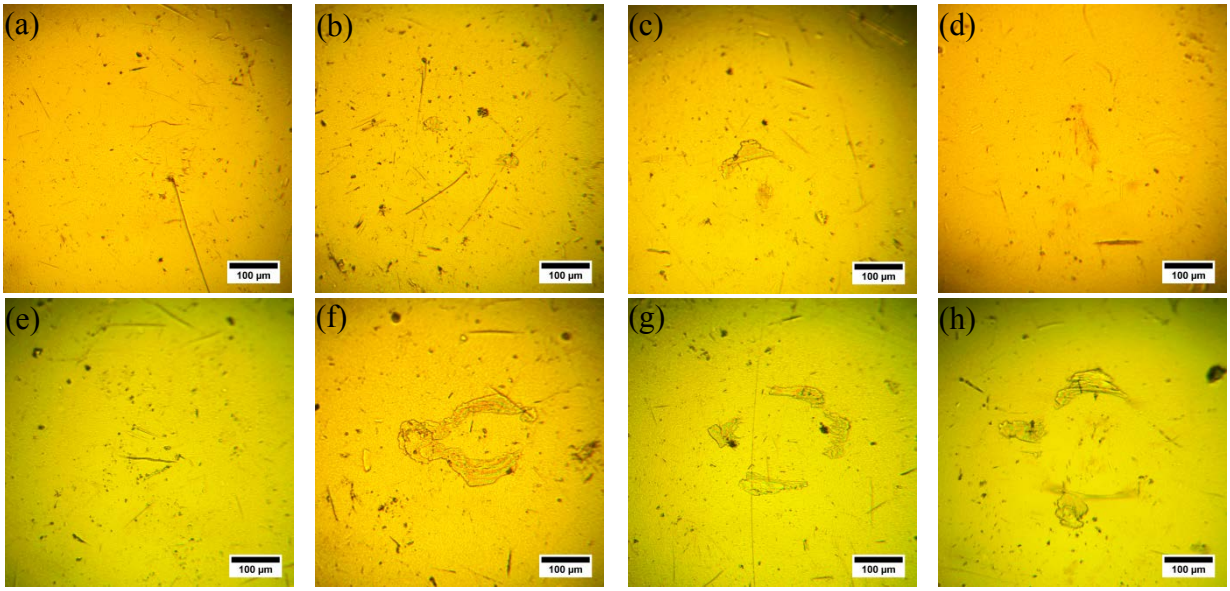

Figure 9.11: Optical microscope images of the chrome steel balls rubbed against PDA/PTFE films for (a) 1, (b) 10, (c) 60, (d) 1000 cycles, and chrome steel balls rubbed against PDA/PTFE + Cu films for (e) 1, (f) 10, (g) 60, and (h) 1000 cycles.

9.3.4. Linearly Increasing Load Scratch Test

The results for the linearly increasing load scratch tests are shown in Figures 9.12 and 9.13. The PDA/PTFE film, shown in Figure 9.12, was detached from the substrate after the test progressed for a distance of approximately 15 mm where the normal load reached a value of 370 mN. Optical images of the scratch show the different stages of wear. Figure 9.12 (a) represents the portion of the scratch up to a distance of 5 mm where the COF is relatively stable and has a value of about 0.09. Figure 9.12 (b) represents the portion of the scratch between 5 and 15 mm. In this section the COF intermittently jumps between 0.07 and 0.11. This stick-slip behavior is caused by the film building up in front of the counterface as it slides against it. At first the COF increases because the ball is pushing against the film, accumulating material in front of it. Once the accumulation of the film in front of the ball is large enough, it forces the ball to slide over the

build-up, exhibiting slip behavior. This stick-slip behavior continuously repeats for this section of the scratch. One of the sections of accumulated material is shown in Figure 9.12 (b). The distance between these areas of accumulated film is approximately 100 μm, which is the same as the distance between the peaks and valleys observed in the COF plot. Figure 9.12 (c) represents the portion of the scratch between 15 and 20 mm. Here the stick-slip behavior is more pronounced and it is evident from the optical image that there are segments of the scratch where the PTFE top coat has detached from the PDA.

Figure 9.13 shows the scratch produced on the PDA/PTFE + Cu film. Figure 9.13 (a) represents a small portion of the scratch between 0 to 2.5 mm. In this segment the COF is stable but shows a slight increasing trend from 0.08 to 0.10. Figure 9.13 (b) represents a small portion of the scratch between 2.5 to 8 mm where material accumulates in front of the counterface as was observed in Figure 9.12 (b). In this segment the COF intermittently jumps between 0.07 and 0.12. Figure 9.13 (c) shows a portion of the scratch between 8 and 18 mm. In this section, accumulation of material can be seen; however, the accumulation is smaller and closely spaced producing a stable COF that remains at about 0.10. Figure 9.13 (d) represents the section between 18 and 20 mm where the stick-slip behavior is very pronounced. Again, from the image it is evident that the PTFE top coat had detached in certain areas of the scratch. The areas where the PTFE had detached, exposed PDA to the counterface. As the counterface slid over these areas, the COF increased producing a sharp increase in the plot in Figure 9.13 (e). Then as the counterface moved over an area where PTFE was still present, the COF dropped back down. This is why a stick-slip behavior is observed. The linearly increasing load scratch test has revealed that the sample with Cu nanospheres withstands significantly higher normal loads before detachment of the film. For PDA/PTFE the film detached at a distance of about 15 mm

and normal load of 370 mN, whereas PDA/PTFE + Cu reached a distance of 18 mm and a load of about 420 mN before the film detached from the PDA layer. These results indicate that the Cu nanospheres may increase the shear strength of the PTFE film and also improve adhesion to the PDA primer. The scratch tests were repeated 3 times on each sample and showed similar results in each test. Both films failed before the normal load reached 500 mN, which is the load that was used for the durability tests. This is, in part, a result of the high friction forces observed at lower loads, but mainly because part of the mechanism that adheres the PTFE film to the PDA primer is the compaction resulting from friction tests at higher loads. The strong bond between PTFE and PDA is, in part, a tribo-induced effect resulting from high contact pressure. This effect is not as pronounced for lower loads.

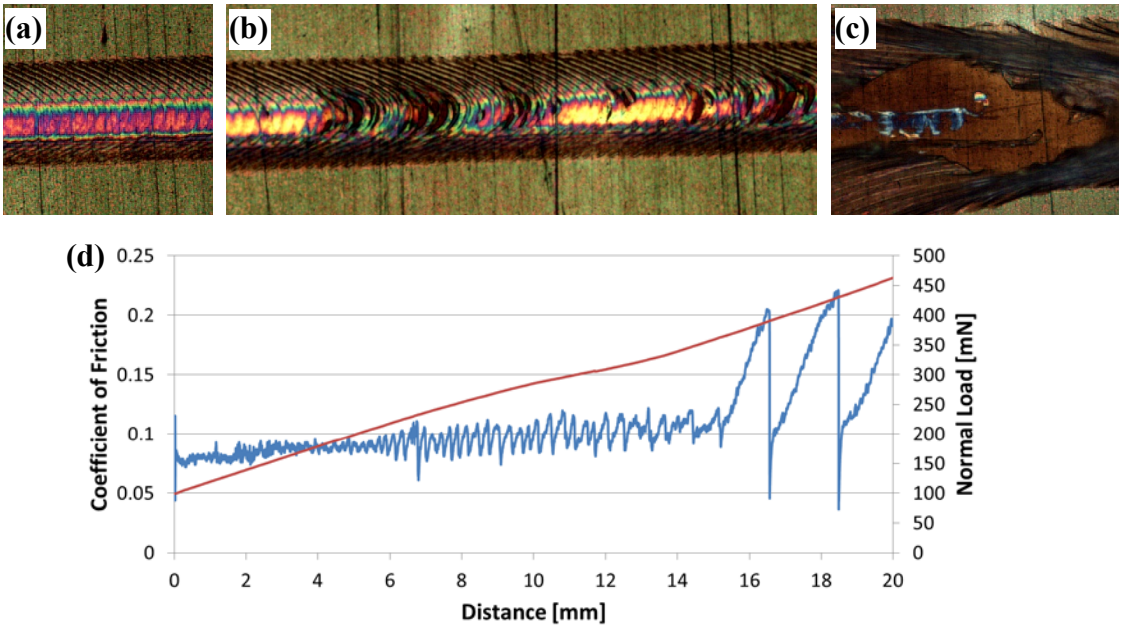

Figure 9.12: Optical Images of scratch representative of segment (a) 1 to 5 mm, (b) 5 to 15 mm, (c) 15 to 20 mm, and (d) a plot of COF and Normal Load vs. Distance for linearly increasing load scratch test on PDA/PTFE film.

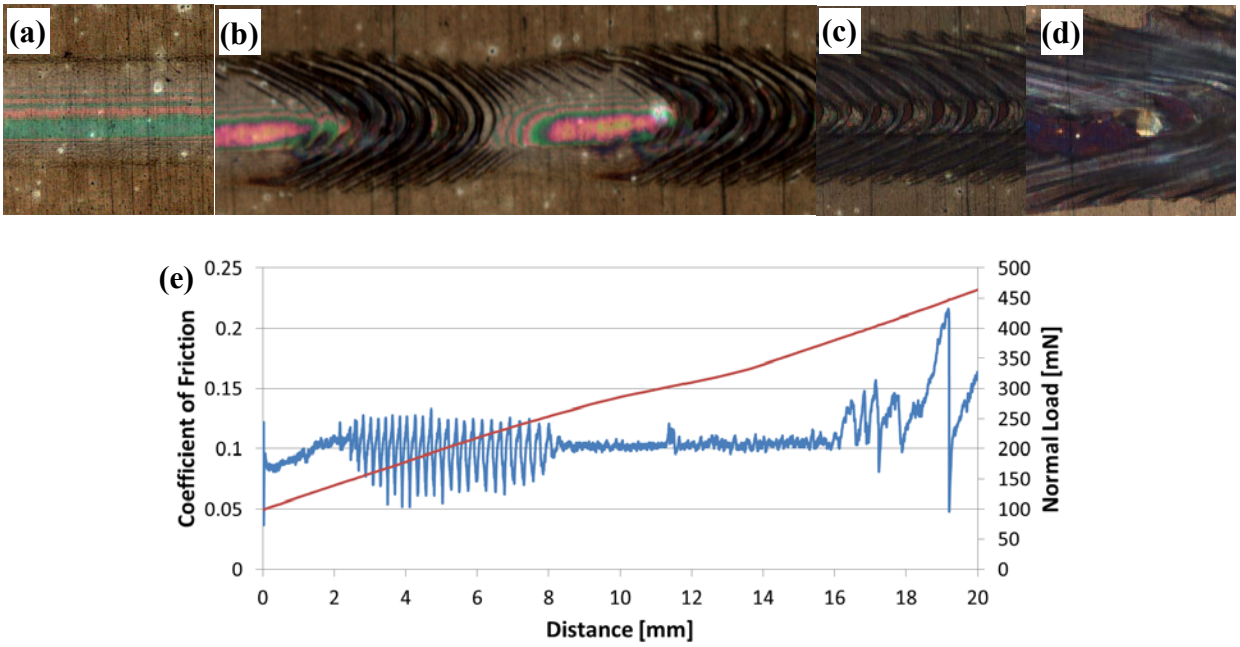

Figure 9.13: Optical Images of scratch representative of segment (a) 1 to 2.5 mm, (b) 2.5 to 8 mm, (c) 8 to 18 mm, (d) 18 to 20 mm, and (e) a plot of COF and Normal Load vs. Distance for linearly increasing load scratch test on PDA/PTFE + Cu film.

9.3.5. Comparison to state-of-the-art

A final 50 g friction test was performed to compare PDA/PTFE to a commercially available low friction, high durability coating. The coating which has the trademark Emralon 333 was selected as the coating of choice due its nominally low COF and excellent durability. Emralon 333 is manufactured by Henkel Corporation and is advertised as follows:

> "*BONDERITE S-FN 333 DRYFILM COATING ACHESON is a blend of fluorocarbon lubricants in an organic resin binder and solvent system designed for applications beyond the scope of conventional fluorocarbon coatings. Its low coefficient of friction, hardness, adhesion, resiliency, and cure conditions allow application of BONDERITE S-FN 333 DRYFILM COATING ACHESON in a multitude of places where pure sintered PTFE coatings are unsuitable.* [112]"

This coating is advertised as having a static and dynamic COF between 0.09 and 0.10, and much higher durability than traditional PTFE coatings [113].

To prepare samples with Emralon 333, 0.76 mm-thick type 316 stainless steel sheets were first cut into 2.5 cm x 2.5 cm squares and then sent to DECC Company which specializes in deposition of industrial coatings. The coated samples which were returned had a nominal coating thickness of 25 μm. The PDA/PTFE sample was prepared using the same process described in section 9.2.1 with two differences. In contrast to previous samples, this sample was dip coated into the PTFE dispersion at an immersion/withdrawal speed of 40 mm/min. Additionally, the dilution of PTFE was changed to result in a final PTFE concentration of 45 wt.% in solution in contrast to the previously used 40 wt.%. This produced a film of approximately 1.2 μm thickness.

The friction test was carried out using the same conditions described in section 9.2.2. The results are shown in Figure 9.14. At onset of the friction test, Emralon 333 exhibited an average dynamic COF of approximately 0.08. At approximately 9000 cycles, the COF began to rise and reached a value of about 0.15 after 23,000 rubbing cycles. The PDA/PTFE film, on the other hand, had an average COF of 0.05 at onset of the test and the COF remained below 0.06 until the test reaches 22,983. At this point the COF spiked up to a value of 0.15 before decreasing to a value of 0.09 again. The friction test was stopped at this point to allow analysis of the wear track before significant damage to the substrate. It is evident from these results that PDA/PTFE outperformed Emralon 333. It is also important to note that the optimized dip coating parameters used for the sample that was compared to Emralon 333, produced a PDA/PTFE film that was 2x more durable than observed for PDA/PTFE films discussed earlier in this chapter. The higher

dip coating speed and higher PTFE concentration likely resulted in denser PTFE films with better wear resistance.

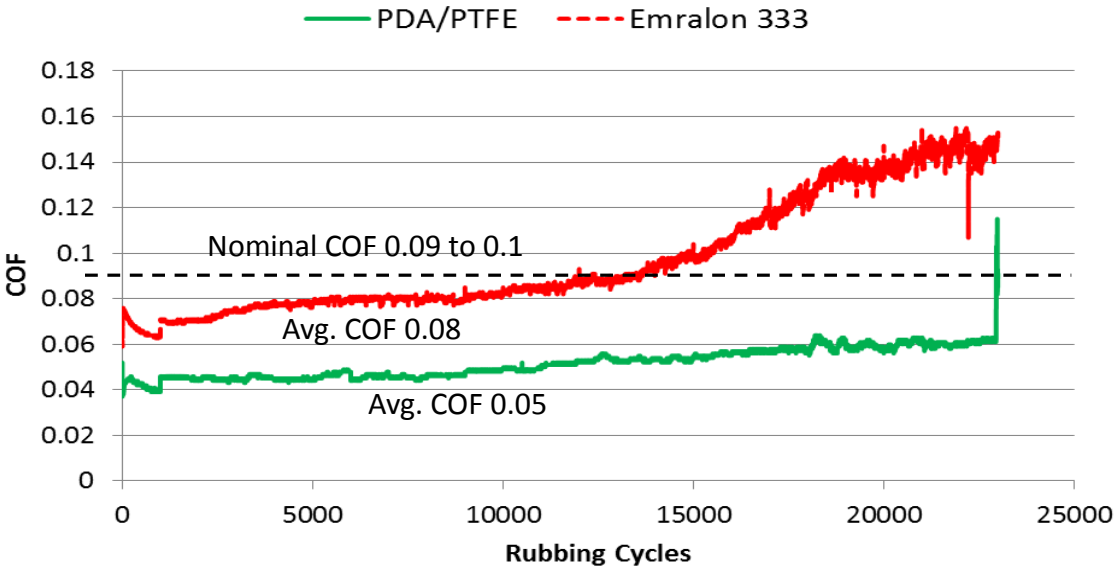

Figure 9.14: Dynamic COF vs rubbing cycles for a PDA/PTFE coated sample and an Emralon 333 coated sample.

To study the wear produced as a result of the friction test above, the chrome steel ball counterface and the sample surface were both characterized using an optical microscope. The optical images are shown in Figure 9.15 (a) and (b). Both films had a wear track that was approximately 260 µm wide, however, the counterface used on PDA/PTFE showed the presence of a transfer film and very little wear. The counterface tested on Emralon 333, on the other hand, showed significant damage. These results indicate that the PDA/PTFE film has better tribological performance than Emralon 333 under these testing conditions.

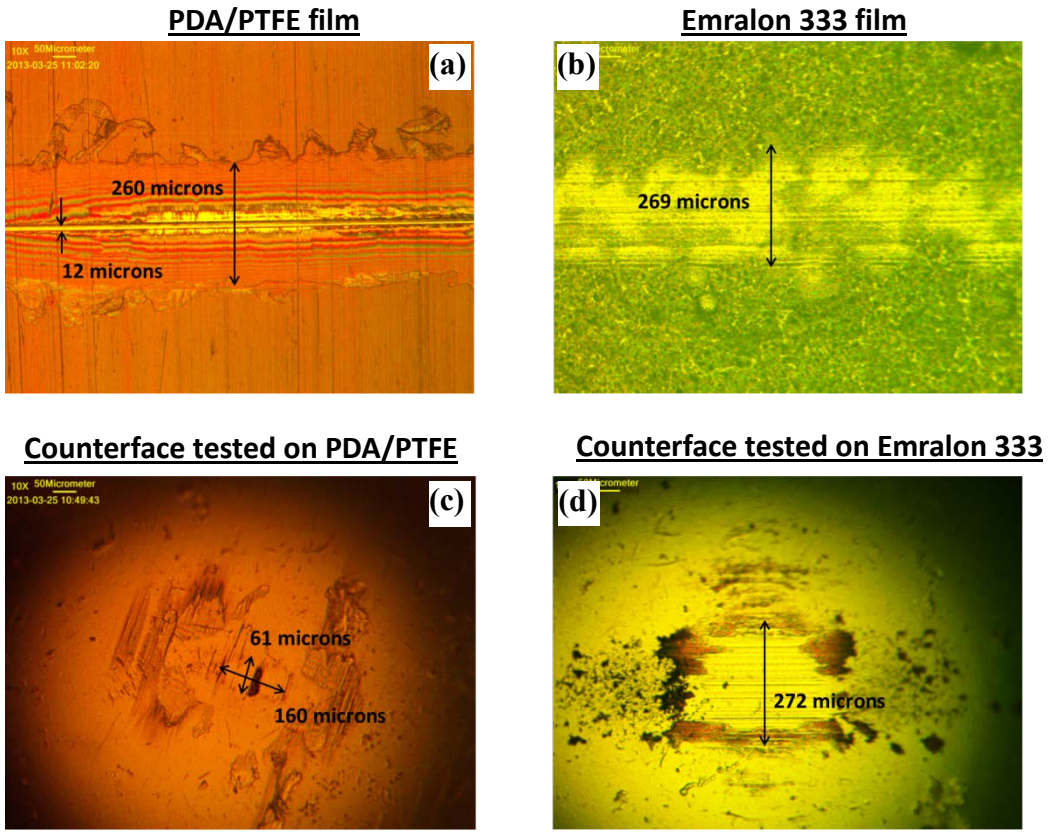

Figure 9.15: Optical images of the wear track produced on (a) PDA/PTFE film, (b) Emralon 333 film, and images of the counterface tested on (c) PDA/PTFE and (d) Emralon 333.

9.4. Summary

This study shows that the addition of Cu nanospheres as a filler in PTFE increases the durability of PDA/PTFE films. The results showed that PDA/PTFE + Cu films had a durability that was, on average, more than twice that of PDA/PTFE films. It is also evident that the wear progression of PDA/PTFE + Cu films decreased significantly after 60 rubbing cycles. This became apparent through the cross-section profile of the wear tracks which showed little increase in wear depth between 60 and 1000 cycles. On the contrary, the PDA/PTFE film showed a significant increase in wear depth between 60 and 1000 cycles. This phenomenon is explained

by the formation of a transfer film on the ball rubbed against the PDA/PTFE + Cu film, which was observed in the optical images in Figure 9.11. It is clear that the presence of Cu nanospheres aids in the formation of a transfer film on the counterface, resulting in a self-lubricating effect. Once a robust film is established on the counterface, the wear progression of the sample surface slows down. This is also supported by the results of the scratch test which reveal that the PDA/PTFE + Cu nanosphere film can withstand significantly higher loads without rupture or detachment of the film.

Chapter 10

Conclusion and future direction

The goal of this investigation was to find a solution to the issue of wear in PTFE thin films. One of the appeals of solid lubricants is the ability to form maintenance-free mechanical assemblies. For this to be achievable it is essential to find solid lubricants that do not only exhibit a low COF, but also high durability/wear life. This constraint precludes the use of PTFE films unless a method to improve the wear resistance can be found. This investigation has done just that. Table 10.1 shows the durability and dynamic COF results for the four studies carried out in this investigation.

Table 10.1: Summary of processing parameters, dynamic COF, and durability of the 4 studies presented in this investigation.

Film Composition	PTFE wt.%	Film thickness	Heating 2	Heating 3	Avg. COF	Wear life
PTFE	40	1.80 µm	300 °C, 5 min	337 °C, 10 min	0.09	21 cycles
PTFE + 3.30 wt.%SiO_2	40	1.00 µm	300 °C, 5 min	337 °C, 10 min	0.08	482 cycles
PTFE	40	0.45 µm	300 °C, 5 min	337 °C, 10 min	0.09	174 cycles
PTFE + 0.023 wt.%Au	40	0.47 µm	300 °C, 5 min	337 °C, 10 min	0.07	263 cycles
PTFE	40	0.58 µm	250 °C, 10 min	-	0.08	7.3 cycles
PDA/PTFE	40	0.72 µm	250 °C, 10 min	-	0.07	4,690 cycles
PDA/PTFE	40	1.32 µm	300 °C, 4 min	372 °C, 4 min	0.07	10,082 cycles
PDA/PTFE + Cu	40	1.17 µm	300 °C, 4 min	372 °C, 4 min	0.07	19,854 cycles
PDA/PTFE	45	1.20 µm	300 °C, 4 min	372 °C, 4 min	0.05	22,983 cycles
Emralon 333	-	25 µm	-	-	0.08	14,000 cycles

The first attempt at a solution was the use of a hard ceramic nanoparticle. SiO_2 nanoparticles were selected because of their accessibility, low cost, and proven ability to enhance the mechanical properties of bulk PTFE. As shown in Table 10.1, in the friction test performed using a 50 g normal load, the pure PTFE film exhibited an average dynamic COF of 0.09 and an average durability of 21 cycles. On the other hand, the PTFE + 3.3 wt.% SiO_2 composite film

showed an average dynamic COF of 0.09 and an average durability of 482 cycles. These result indicate that a 3.3 wt.% concentration of SiO_2 can increase the durability of PTFE by 23x. Although the COF for the composite film did not rise above 0.4 after 1000 rubbing cycles, surface chemical analysis and cross-sectional profiles of the wear tracks confirmed that after 1000 rubbing cycles under a 50 g normal load the film was sufficiently removed from the surface to allow the stainless steel substrate to be abraded.

The second attempt was to use a soft metallic nanoparticle. Au was selected because of its low shear strength which allows it to exhibit a relatively low friction. AFM images of the coated surfaces showed that the PTFE + Au nanoparticle films formed a fibrillar network due to a higher degree of melting. This enhanced the film's adhesion to the substrate, resulting in improved durability. The results of the friction test performed using a 50 g normal load showed that even at a low Au concentration of 0.023 wt.%, the PTFE + Au film was able to withstand up to 1.5x the number of rubbing cycles of pure PTFE. As shown in Table 10.1, PTFE withstood an average of 174 cycles whereas PTFE + Au withstood an average of 263 cycles. Furthermore, the COF for the PTFE + Au film was 22% lower than pure PTFE for the 50 g friction test. Analysis of the wear tracks revealed that the dominant wear mechanism differed between the two films. While the pure PTFE film underwent delamination and adhesive wear as was evident from the large build up on the edges of the wear track which showed corrugations and tearing of the film, the PTFE + Au film was compacted and polished by the chrome steel ball.

Because of PTFE's nonstick nature and consequent susceptibility to delamination, the next solution was naturally to incorporate an adhesive primer to aid with PTFE film to substrate adhesion. Polydopamine, a synthetic polymer that attempts to mimic the adhesive proteins secreted by mussels, was selected because studies have shown that PTFE sheets can be coated

with this polymer to produce functional surfaces that demonstrate strong adhesion to the PTFE substrate. Frictional tests on a PDA/PTFE dual layer film showed unprecedented results. Within this study, the durability of PTFE was increased by 600x without producing negative effect on the COF. As shown in Table 10.1, PTFE withstood 7.3 cycles whereas PDA/PTFE withstood 4690 cycles. Surface chemical analysis and cross-sectional profiles of the wear tracks revealed that a tenacious layer of PTFE was strongly adhered to the PDA and not easily removed, contributing to the durability of the film.

It is important to note that the heat treatment for the PDA/PTFE study presented in Chapter 9 was carried at only 250 °C to prevent degradation of the PDA film. As a result, the PTFE only film showed lower durability for this study compared to those in Chapter 6 and 7. It was thus necessary to perform an optimization of the heat treating conditions. Chapter 9 presented a study which utilized an optimized heat treating condition. The optimal treatment was to first heat at 120 °C for 3 min, followed by 300 °C for 4 min, and finally 372 °C for 4 min. The study in chapter 9 evaluated the combination of a PDA primer coat and Cu nanospheres as fillers in PTFE to further enhance the durability of the film. The combination of these two factors produced remarkable results, exhibiting an average durability of up to 19,854 cycles.

Compared to the values obtained initially, using Dupont's suggested heat treatment method for PTFE, the added materials and optimized processing of the PTFE composite films used in this investigation have enhanced PTFE's durability by over 940x. While PDA/PTFE + Cu had an average durability of 19,854 cycles, the PTFE only film produced in Chapter 6, using Dupont's suggested heating conditions, had an average durability of only 21 cycles.

Much work is still necessary to optimize the fabrication process of this new coating. The heating procedure and dip coating conditions still require tweaking to produce better quality

films. In addition, other deposition methods may prove to enhance the properties of the film even further. Spray coating of PTFE is of particular interest. Also, because of time constraints, the combined effects of other nanoparticle materials in PDA/PTFE were not explored. However, recent progress made by other members of the Nanomechanics and Tribology lab in the use of PDA/PTFE films with fillers such as graphite, has shown much promise. The invention of this film is currently patent pending and steps are being taken for commercialization.

References

[1] M. E. Campbell, J. B. Loser, E. Sneegas, Solid lubricants, (1966) 115.

[2] A.Y. Albagachiev, B.E. Gurskii, Y.M. Luzhnov, A.T. Romanova, A.V. Chichinadze, Economic and ecological issues in tribology, Russian Engineering Research. 28 (2008) 959-964.

[3] B. Bhushan, Modern Tribology Handbook, CRC Press, Boca Raton, FL, 2001.

[4] J. Lee, D. Lim, Tribological behavior of PTFE film with nanodiamond, Surface and Coatings Technology. 188-189 (2004) 534-538.

[5] C. Mateus, S. Costil, R. Bolot, C. Coddet, Ceramic/fluoropolymer composite coatings by thermal spraying-a modification of surface properties, Surf. Coat. Technol. 191 (2005) 108-118.

[6] M. Nishimura, M. Watanabe, R. Yoshimurs, Friction and wear of sputtered PTFE films, (1989) 213-222.

[7] Y. S. Huang, X. T. Zeng, I. Annergren, F. M. Liu, Development of electroless NiP-PTFE-SiC composite coating, Surf. Coat. Technol. 167 (2003) 207-211.

[8] N.L. McCook, D.L. Burris, G.R. Bourne, J. Steffens, J.R. Hanrahan, W.G. Sawyer, Wear resistant solid lubricant coating made from PTFE and epoxy, Tribology Letters. 18 (2005) 119-124.

[9] D. L. Burris, Effects of Nanoparticles on the Wear Resistance of Polytetrafluoroethylene, Dissertation submitted to the University of Florida. (2007).

[10] A.J. Howard, R.R. Rye, A.J. Ricco, D.J. Rieger, M.L. Lovejoy, L.R. Sloan, M.A. Mitchell, New Methods for Circuit Fabrication on Poly(tetrafluoroethylene) Substrates, J. Electrochem. Soc. 141 (1994) 3556-3561.

[11] B. J. Basu, V. D. Kumar, Fabrication of Superhydrophobic Nanocomposite Coatings Using Polytetrafluoroethylene and Silica Nanoparticles, ISRN Nanotechnology. (2011),

[12] T.W. Scharf, S.V. Prasad, Solid lubricants: A review, J. Mater. Sci. 48 (2013) 511-531.

[13] D. Tabor, Friction: The Present State of Our Understanding, Trans. ASME: J. Lub. Technol. 103 (1981) 169-179.

[14] Noria Corporation, Choosing a High-temperature Lubricant, Machinery Lubrication. http://www.machinerylubrication.com/read/29371/high-temperature-lubricant. (2013) accessed on 11/4/2014.

[15] Y.M. Chong, Q. Ye, Y. Yang, W.J. Zhang, I. Bello, S.T. Lee, Tribological study of boron nitride films, Diamond and Related Materials. 19 (2010) 654-660.

[16] DuPont Fluoroproducts, Teflon PTFE TE3859 product information, http://www2. dupont. com/Teflon_Industrial/en_US/assets/downloads/k10918.pdf. (2006) accessed 12/5/2014.

[17] B. Bhushan, Principles and Applications of Tribology, 2nd ed., Wiley, 2013, var. pages.

[18] M.E. Campbell, Dry-Lubrication: Self-Lubricating Composites Versus Bonded Thin-Film Lubricants, American Chemical Society, Division of Organic Coatings and Plastics Chemistry, Preprints. 34 (1) (1974) var pages.

[19] B. Podgornik, J. Vizintin, Tribology of thin films and their use in the field of machine elements, Vacuum. 68 (2002) 39-47.

[20] C. Donnet, A. Erdemir, Historical developments and new trends in tribological and solid lubricant coatings, Surf. Coat. Technol. 180-181 (2004) 76-84.

[21] K. Holmberg, A. Matthews, Coatings tribology : properties, mechanisms, techniques and applications in surface engineering / Kenneth Holmberg, Allan Matthews, in: Anonymous Amsterdam ; Boston ; London : Elsevier Science, 2009, var. pages.

[22] M. Fundus, H. Knoch, Diamond like carbon coatings - tribological possibilities and limitations in applications on sintered silicon carbide bearings and seal faces, Proceedings of the 14th international pump users symposium. 93-98.

[23] R.F. Deacon, J.F. Goodman, Lubrication by Lamellar Solids, Proceedings of the Royal Society of London. Series A. Mathematical and Physical Sciences. 243 (1958) 464-482.

[24] L.W. McKeen, Fluorinated Coatings and Finishes Handbook: The Definitive User's Guide and Databook, 18th ed., William Andrew Pub., Norwich, NY, 2006.

[25] V.A. Bely, A.I. Sviridenok, M.I. Petrokovets, V.G. Savkin, Friction and Wear in Polymer-Based Materials, Pergamom Press, Oxford, 1982.

[26] B.J. Briscoe, D. Tabor, The sliding wear of polymers: a brief review,
Fundam. Tribol. Proc. Int. Conf. (1980) 733-758.

[27] B.J. Briscoe, S.K. Sinha, Wear of polymers, Proceedings of the Institution of Mechanical Engineers, Part J: Journal of Engineering Tribology. 216 (2002) 401-413.

[28] J.H. Lee, G.H. Xu, H. Liang, Experimental and numerical analysis of friction and wear behavior of polycarbonate, Werar. 251 (2001) 1541-1556.

[29] H. Unal, A. Mimaroglu, U. Kadioglu, H. Ekiz, Sliding friction and wear behaviour of polytetrafluoroethylene and its composites under dry conditions, Materials and Design. 25 (2004) 239-245.

[30] W.G. Sawyer, D.L. Burris, Improved wear resistance in alumina-PTFE nanocomposites with irregular shaped nanoparticles, Wear. 260 (2006) 915-918.

[31] M. Minami, M. Suzuki, M. Nishimura, Evaluation of tribological characteristics of PTFE composite transfer films in ultra-high vacuum, S T L E Tribology Transactions. 36 (1993) 95-103.

[32] O. Olabisi, Handbook of thermoplastics, Marcel Decker, New York (1997)

[33] J. F. Visjager, Ultra-high molecular weight polymers processing and properties of polyethylene and poly(tetrafluoroethylene), Eidgenössische Technische Hochschule Zürich. 1-132.

[34] S.K. Biswas, K. Vijayan, Friction and wear of PTFE - a review, Wear. 158 (1992) 193-211.

[35] M.A. Karnath, Q. Sheng, A.J. White, S. Muftu, Frictional characteristics of ultra-thin polytetrafluoroethylene (PTFE) films deposited by hot filament-chemical vapor deposition (HFCVD), Tribol. Trans. 54 (2011) 36-43.

[36] D.L. Burris, W.G. Sawyer, Tribological behavior of PEEK components with compositionally graded PEEK/PTFE surfaces, Wear. 262 (2007) 220-224.

[37] M.H. Cho, S. Bahadur, A.K. Pogosian, Friction and wear studies using Taguchi method on polyphenylene sulfide filled with a complex mixture of MoS2, Al2O3, and other compounds, Wear. 258 (2005) 1825-35.

[38] X. Cheng, Y. Xue, C. Xie, Friction and wear of rare-earth modified glass-fiber filled PTFE composites in dry reciprocating sliding motion with impact loads, Wear. 253 (2002) 869-877.

[39] S.E. McElwain, T.A. Blanchet, L.S. Schadler, W.G. Sawyer, Effect of particle size on the wear resistance of alumina-filled PTFE micro- and nanocomposites, Tribol. Trans. 51 (2008) 247-253.

[40] D. Xiang, K. Li, W. Shu, Z. Xu, On the tribological properties of PTFE filled with alumina nanoparticles and graphite, J Reinf Plast Compos. 26 (2007) 331-339.

[41] S. Bahadur, The development of transfer layers and their role in polymer tribology, Wear. 245 (2000) 92-99.

[42] W.G. Sawyer, K.D. Freudenberg, P. Bhimaraj, L.S. Schadler, A study on the friction and wear behavior of PTFE filled with alumina nanoparticles, Wear. 254 (2003) 573-580.

[43] Y. Chen, H. Lin, Y. Lee, The Effects of Filler Content and Size on the Properties of PTFE/SiO2 Composites, Journal of Polymer Research. 10 (2003) 247-258.

[44] J.A. Joyce, P.J. Joyce, The Fracture Toughness of Polytetrafluoroethylene, ECF15, Stockolm. (2004).

[45] J.K. Lancaster, The effect of carbon fibre reinforcement on the friction and wear of polymers, Journal of Physics D: Applied Physics. 1 (1968) 549.

[46] J.K. Lancaster, The effect of carbon fibre reinforcement on the friction and wear of polymers, Brit J Appl Phys. 1 (1968) 549.

[47] J. Lee, D. Lim, Tribological behavior of PTFE film with nanodiamond, Surface and Coatings Technology. 188-189 (2004) 534-538.

[48] J.-Y. Lee, D.-P. Lim, D.-S. Lim, Tribological behavior of PTFE nanocomposite films reinforced with carbon nanoparticles, Composites Part B. 38 (2007) 810-816.

[49] T. Hui, J. Hui-Juan, Shao Jun-Peng, Structure and micro-tribological properties of PTFE/Al2O3 micro-assembling film, Transactions of the Nonferrous Metals Society of China. 13 (2003) 1381-1384.

[50] M. Nishimura, Y. Miyakawa, H. Furukawa, E. Hikima, S. Maekawa, M. Watanabe, SEM Built-In Friction Tester And Its Application To Observing The Wear Process Of Solid Lubricant Films. (1984) 50-65.

[51] V. Eustathios, Fluoropolymer primer having improved scratch resistance, United States Patent. 4,049,863 A (1977).

[52] H. P. Tannenbaum, Non-stick coating system with PTFE-FEP for concentration gradient, United States Patent. 5,230,961 A (1993).

[53] H. Lee, Bioadhesion of Mussels and Geckos : Molecular Mechanics, Surface Chemistry, and Nanoadhesives, Dissertation submitted to Northwestern University, 2008.

[54] D.J. Crisp, G. Walker, G.A. Young, A.B. Yule, Adhesion And Substrate Choice In Mussels And Barnacles, J. Colloid Interface Sci. 104 (1981) 40-50.

[55] J.H. Waite, Adhesion à la Moule, Integrative and Comparative Biology. 42 (2002) 1172-1180.

[56] H. Lee, N.F. Scherer, P.B. Messersmith, Single-molecule mechanics of mussel adhesion, Proc. Natl. Acad. Sci. U. S. A. 103 (2006).

[57] T. Akter, W.S. Kim, Reversibly stretchable transparent conductive coatings of spray-deposited silver nanowires, ACS Applied Materials and Interfaces. 4 (2012) 1855-1859.

[58] L.A. Burzio, J.H. Waite, Cross-linking in adhesive quinoproteins: Studies with model decapeptides, Biochemistry (N. Y.). 39 (2000) 11147-11153.

[59] S. Haemers, G.J.M. Koper, G. Frens, Effect of oxidation rate on cross-linking of mussel adhesive proteins, Biomacromolecules. 4 (2003) 632-640.

[60] J. Monahan, J.J. Wilker, Cross-linking the protein precursor of marine mussel adhesives: Bulk measurements and reagents for curing, Langmuir. 20 (2004) 3724-3729.

[61] M. Yu, J. Hwang, T.J. Deming, Role of L-3,4-dihydroxyphenylalanine in mussel adhesive proteins, J. Am. Chem. Soc. 121 (1999) 5825-5825.

[62] J.H. Waite, Surface chemistry: Mussel power, Nature Materials. 7 (2008) 8-9.

[63] S. Hong, Y.S. Na, S. Choi, I.T. Song, W.Y. Kim, H. Lee, Non-Covalent Self-Assembly and Covalent Polymerization Co-Contribute to Polydopamine Formation, Advanced Functional Materials. 22 (2012) 4711-4717

[64] F. Yu, S. Chen, Y. Chen, H. Li, L. Yang, Y. Chen, Y. Yin, Experimental and theoretical analysis of polymerization reaction process on the polydopamine membranes and its corrosion protection properties for 304 Stainless Steel, J. Mol. Struct. 982 (2010) 152-161.

[65] C. Muller, A. Luders, W. Hoth-Hannig, M. Hannig, C. Ziegler, Initial bioadhesion on dental materials as a function of contact time, pH, surface wettability, and isoelectric point, Langmuir. 26 (2010) 4136-4141.

[66] Q. Wang, Q. Xue, W. Shen, The friction and wear properties of nanometre SiO2 filled polyetheretherketone, Tribol. Int. 30 (1997) 193-197.

[67] Y. Zheng, Y. Zheng, R. Ning, Effects of nanoparticles SiO2 on the performance of nanocomposites, Mater Lett. 57 (2003) 2940-2944.

[68] Y. Miyakawa, Friction And Wear Performance Of Gold And Gold Alloy Films, Gold bulletin. 13 (1980) 21-30.

[69] O. Olea-Mejia, W. Brostow, L. Escobar-Alarcon, E. Vigueras-Santiago, Tribological properties of polymer nanohybrids containing gold nanoparticles obtained by laser ablation, Journal of Nanoscience and Nanotechnology. 12 (2012) 2750-2755.

[70] X.B. Yan, T. Xu, G. Chen, X.B. Wang, H.W. Liu, S.R. Yang, Preparation and characterization of amorphous hydrogenated carbon films containing Au nanoparticles from heat-treatment of polymer precursors, Applied Physics A (Materials Science Processing). A81 (2005) 197-203.

[71] S.R. Puniredd, K.W. Yong, N. Satyanarayana, S.K. Sinha, M.P. Srinivasan, Tribological properties of nanoparticle-laden ultrathin films formed by covalent molecular assembly, Langmuir. 23 (2007) 8299-8303.

[72] S.J. Kim, J.Y. Lee, J.M. Han, Y.C. Kim, H.D. Park, S.H. Sung, J.J. Lee, J.H. Cha, J.H. Jo, H. Jang, The Role of Copper on the Friction and Wear Performance of Automotive Brake Friction Materials, SAE International Journal of Materials and Manufacturing. 5 (2012) 9-18.

[73] Y. Zhang, J. Yan, L. Sun, G. Yang, Z. Zhang, P. Zhang, Friction reducing anti-wear and self-repairing properties of nano-Cu additive in lubricating oil, Jixie Gongcheng Xuebao/Journal of Mechanical Engineering. 46 (2010) 74-79.

[74] Z. Yong, X. Zhao, H. Qiang, J. Ye, Q. Niu, Experimental study of nanoparticle as oil additives, 230-232 (2011) 288-292.

[75] Z.N. Jia, C.Z. Hao, Y.L. Yang, Tribological performance of hybrid PTFE/ serpentine composites reinforced with nanoparticles, Tribology - Materials, Surfaces and Interfaces. 8 (2014) 139-145.

[76] Y. Yan, Z. Jia, Y. Yang, Preparation and mechanical properties of PTFE/nano-EG composites reinforced with nanoparticles, 10 (2011) 929-935.

[77] B. Bhushan, Introduction to Tribology, John Wiley & Sons, New York, 2002, var. pages.

[78] H. Hertz, On the contact of firm elastic bodies, J. Reine Angewandte Mathematik. 92 (1882) 156-171.

[79] B. Bhushan, Adhesion and stiction: mechanisms, measurement techniques, and methods for reduction, Journal of Vacuum Science & Technology B (Microelectronics and Nanometer Structures). 21 (2003) 2262-2296.

[80] F.P. Bowden, D. Tabor, Friction and Lubrication of Solids, Oxford University Press, New York, NY, United States, 1950.

[81] N.P. Suh, Delamination Theory Of Wear, Wear. 25 (1973) 111-124.

[82] M. Faustini, B. Louis, P.A. Albouy, M. Kuemmel, D. Grosso, Preparation of sol-gel films by dip-coating in extreme conditions, Journal of Physical Chemistry C. 114 (2010) 7637-7645.

[83] Kyowa Interface Science Co., Ltd., Operation manual for triboster: Automatic friction abrasion analyzer, 106 (2009) 1-51.

[84] Bruker Coorporation, UMT-2 overview, 2014 (2014) 1.

[85] Bruker Coorporation, Introduction to Bruker's ScanAsyst and PeakForce tapping AFM technology, AN133 (2011) 1-12.

[86] Bruker Coorporation, Dimension icon with ScanAsyst instruction manual 004-1023-000, 2014 (2011) 1-487.

[87] G. Fantner, Advanced Bioengineering methods laboratory: Atomic force microscopy, Ecole Polytechnique Federale De Lausanne. 2014 1-34.

[88] Michigan State University, Techniques for surface chemical composition, http://www.cem.msu.edu/~cem924sg/Topic09.pdf 2014 (2001) 9.1-9.40.

[89] C. R. Brundle, J. F. Watts, J. Wolstenholme, X-ray photoelectron and auger electron spectroscopy, Marcel Dekker, 2005 399-403.

[90] Chalmers University of Technology, Introduction to energy dispersive X-ray spectrometry http://micron.ucr.edu/public/manuals/EDS-intro.pdf (EDS), 2014 11.

[91] R.F. Egerton, Physical Principles of Electron Microscopy: An Introduction to TEM, SEM, and AEM, Springer, New York, NY, 2005.

[92] Nissan Chemical, Snowtex, http://Www.nissanchem-usa.com/snowtex.php, 2014 accessed on 1/10/2011.

[93] M. Cai, Y. Liang, M. Yao, Y. Xia, F. Zhou, W. Liu, Imidazolium ionic liquids as antiwear and antioxidant additive in poly(ethylene glycol) for steel/steel contacts, ACS Applied Materials and Interfaces. 2 (2010) 870-876.

[94] T.A. Blanchet, F.E. Kennedy, D.T. Jayne, XPS analysis of the effect of fillers on PTFE transfer film development in sliding contacts, S T L E Tribology Transactions. 36 (1993) 535-544.

[95] K.G. McLaren, D. Tabor, Viscoelastic properties and the friction of solids. Friction of polymers and influence of speed and temperature. Nature. 197 (1963) 856-858.

[96] J. Sanchez-Lopez, M.D. Abad, L. Kolodziejczyk, E. Guerrero, A. Fernandez, Surface-modified Pd and Au nanoparticles for anti-wear applications, Tribology International. 44 (6) (2011) 720-726.

[97] J. Turkevich, P. Stevenson, J. Hillier, A Study of the Nucleation and Growth Processes in the Synthesis of Colloidal Gold, Discuss. Faraday Soc. 11 (1951) 55-75.

[98] G. Frens, Controlled nucleation for the regulation of the particle size in monodisperse gold suspensions, Nature (Physical Science). 241 (1973) 20-22.

[99] S.K. Biswas, K. Vijayan, Friction and wear of PTFE-a review, Wear. 158 (1992) 193-211.

[100] I.S. Bayer, V. Caramia, D. Fragouli, F. Spano, R. Cingolani, A. Athanassiou, Electrically conductive and high temperature resistant superhydrophobic composite films from colloidal graphite, Journal of Materials Chemistry. 22 (2012) 2057-2062.

[101] O.A. Yeshchenko, I.M. Dmitruk, K.P. Grytsenko, V.M. Prokopets, A.V. Kotko, S. Schrader, Influence of interparticle interaction on melting of gold nanoparticles in Au/polytetrafluoroethylene nanocomposites, Journal of Applied Physics. 105 (2009) 094326-094328

[102] H. Wang, X. Feng, L. Mu, X. Lu, Different Nano-Fillers on the Tribological Properties of PTFE Nanocomposites, Advanced Tribology: Proceedings of CIST2008 & ITS-IFToMM2008. (2010) 392-395.

[103] J. Ou, J. Wang, Y. Qiu, L. Liu, S. Yang, Mechanical property and corrosion resistance of zirconia/polydopamine nanocomposite multilayer films fabricated via a novel non-electrostatic layer-by-layer assembly technique, Surf. Interface Anal. 43 (2011) 803-808.

[104] J. Ou, L. Liu, J. Wang, F. Wang, M. Xue, W. Li, Fabrication and tribological investigation of a novel hydrophobic polydopamine/graphene oxide multilayer film, Tribology Letters. 48 (2012) 407-415.

[105] H. Lee, S.M. Dellatore, W.M. Miller, P.B. Messersmith, Mussel-inspired surface chemistry for multifunctional coatings, Science. 318 (2007) 426-430.

[106] K. C. Ludema, Friction, wear, lubrication: A textbook in tribology, (1996) 259.

[107] L. Li, F.T. Zi, Y.F. Zheng, The characterization of fluorocarbon films on NiTi alloy by magnetron sputtering, Appl. Surf. Sci. 255 (2008) 432-434.

[108] H. Rubahn, G. Horowitz, Interface controlled organic thin films, 129 (2009) 230.

[109] D.L. Burris, W.G. Sawyer, A low friction and ultra low wear rate PEEK/PTFE composite, Wear. 261 (2006) 410-418.

[110] S. Beckford, M. Zou, Wear resistant PTFE thin film enabled by a polydopamine adhesive layer, Appl. Surf. Sci. 292 (2014) 350-356.

[111] J. Chen, Copper nanospheres and nanowires synthesized by reduction of copper precursors using amines, Department of Chemistry. 2014 (University of Arkansas).

[112] Henkel Coorporation, Bonderite S-Fn 333 Dryfilm Coating Acheson, http://www. henkelna. com/adhesives/product-search-1554. htm?nodeid=8798045601793. accessed 12/5/2014 (2014).

[113] Acheson, Product data sheet: Emralon 333, http://www. silitech. ch/upload/fiche_technique_D/343. PDF. Accessed 12/5/2014 (2007).

Appendix A: Description of Research for Popular Publication

Knovel Dry Lubricant for Extreme Conditions

Imagine never having to change the oil in your car again; imagine not only saving money and saving yourself the hassle of driving to the mechanic, but at the same time lowering you carbon foot print and extending the life of your vehicle. Traditionally, petroleum based oils and greases have played a dominant role in lubrication. However, new technology is being developed to produce lubricants that can perform in extreme conditions such as high temperatures, low temperatures, high pressure, maintenance free systems, low emission systems, and use in high vacuum. The lubricants that have shown the best potential to meet these needs are solid lubricants which can be coated onto mechanical component's surfaces. These films have the potential of being used for applications in micro-electro-mechanical devices, biomedical devices, and machine components in general to reduce energy losses due to friction and wear, as well as reducing corrosion, stiction and surface fouling.

This investigation presents a method for the fabrication of a durable solid lubricant composed of polydopamine (PDA), Teflon (PTFE), and copper nanoparticles. This novel solid lubricant exhibits exceptional lubricity and a durability of more than 940 times what is typically observed in Teflon based lubricants and up to two times higher than the top of the line solid lubricants currently available on the market. What is more, it also exhibits frictional values that are as much as 50% lower than what is seen in many solid lubricants today. These properties make PDA/PTFE+copper nanoparticles an ideal lubricant to replace both fluid lubricants and currently available solid lubricants.

One particular application for which it is being explored is the aerospace industry. In space, because it is a vacuum, most lubricants will change states from a fluid to a gas or from a solid to a gas. However, polytetrafluoroethylene (PTFE) does not. The only issue with using PTFE in space is that it is not very durable; it wears away very easily. However a solid lubricant like PDA/PTFE+copper nanoparticles could pose a solution to this issue. The adhesion and wear issues of PTFE are solved by incorporating a biomimetic polymer, polydopamine, as an adhesive layer to bond PTFE films to various substrates. Increased adhesion of the PTFE film to the substrate in turn significantly increases the wear resistance of the film. The copper nanoparticles enhance the durability even further by improving the mechanical properties of PTFE.

It doesn't stop there. The low friction, wear resistant, PDA/PTFE+copper coating can be used as a low friction coating on syringe needles, catheters, and stents to reduce pain in patients. Although more research is needed to study the behavior of PDA/PTFE+copper nanoparticles in these specific applications, the ball is rolling. Current plans are on the way to test this new lubricant in these applications.

Appendix B: Potential Patent and Commercialization

B.1. Patentability

1. Polytetrafluoroethylene lubricant thin film with a polydopamine adhesive layer: improves adhesion of Teflon-coatings to improve durability in lubrication applications.
2. Polytetrafluoroethylene composite lubricant incorporating SiO_2 nanoparticles as a filler to reduce the wear rate while maintaining the low coefficient of friction observed in PTFE.
3. Polydopamine coating of cylinders to increase adhesion of PTFE additives in fluid lubricants.

B.2. Commercialization Applications

1. Marine equipment - antifouling coatings
    a) Polydopamine can be used to improve the adhesion of PTFE films used as antifouling coatings in marine applications.
2. Lock assemblies – lubricant
    a) PDA/PTFE can be used as a solid lubricant in automotive lock assemblies
3. Valves – lubricant
    a) PDA/PTFE can be used as a solid lubricant in automotive lock assemblies
    b) PTFE+SiO_2 can also be used as a solid lubricant in this application; however, it is less promising due the relatively low durability it has, compared to commercially available coatings.
4. Aerospace parts - lubricant
    a) PDA/PTFE would require testing in vacuum and extreme temperatures to evaluate its potential uses in aerospace applications; however, based on the properties of the materials which compose the coating and the arrangement of the two layer coating, it is a promising candidate for further investigation under these conditions.

B.3. Possible Prior Disclosures

Presetation in Society of Tribologists an Lubrication Engineers annual meeting May 2014

- *Cu Nanoparticle Filled PTFE Thin Film Modified With a Polydopamine Adhesive Layer*

Publication of paper in Applied Surface Science

-*Wear resistant PTFE thin film enabled by a polydopamine adhesive layer*

Publication of paper in Tribology Transactions

- *Wear Resistant PTFE/Silica Nanoparticle Composite Film*

Appendix C: Broader Impact of Research

C.1. Applicability of Research Methods to Other Problems

Although the focus of this investigation is on the development of a lubricating thin film, the knowledge gained about the interaction of PTFE and PDA can be used to improve the adhesion of PTFE to various substrates/films, for a wide range of applications. For example, PTFE is currently being investigated as a material for use in integrated circuits due its low dielectric constant. The adhesion of metallic coatings to PTFE in this application has been an issue of great concern. PTFE is also used as a coating to produce self-cleaning surfaces; wear of such coatings is also a problematic issue. The results from this investigation may help to reduce wear issues in such films.

C.2. Impact of Research Results on U.S. and Global Society

At least one third of all energy produced is lost to friction and wear annually [1]. A successful lubricant can reduce a significant amount of cost in fuel and maintenance in industrial equipment, commercial transportation, vehicles, and electro-domestic appliances.

C.3. Impact of Research Results on the Environment

The solid lubricant discussed in this investigation presents an alternative to petroleum based lubricants and also can help decrease CO_2 emissions by lowering friction losses and thus lowering energy consumption.

Appendix D: Microsoft Project for MicroEP Degree Plan

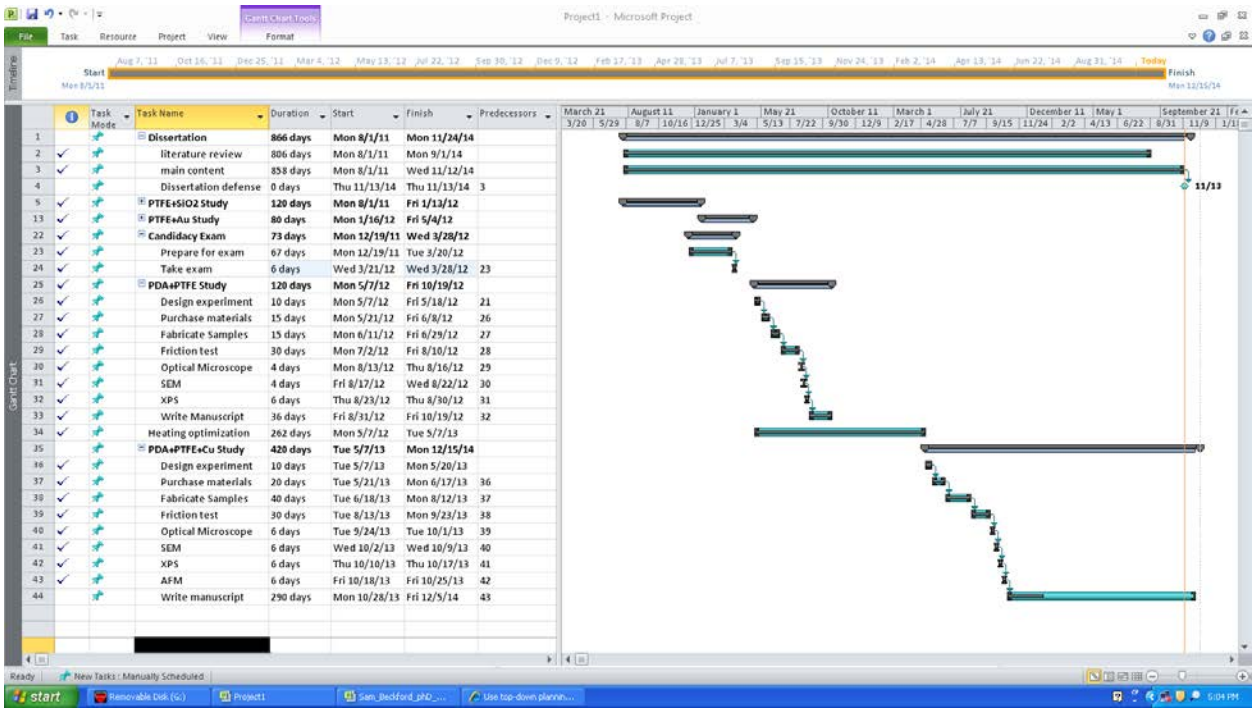

	Task Mode	Task Name	Duration	Start	Finish	Predecessors
1		**Dissertation**	**866 days**	**Mon 8/1/11**	**Mon 11/24/14**	
2	✓	literature review	806 days	Mon 8/1/11	Mon 9/1/14	
3	✓	main content	858 days	Mon 8/1/11	Wed 11/12/14	
4		Dissertation defense	0 days	Thu 11/13/14	Thu 11/13/14	3
5	✓	**PTFE+SiO2 Study**	**120 days**	**Mon 8/1/11**	**Fri 1/13/12**	
13	✓	**PTFE+Au Study**	**80 days**	**Mon 1/16/12**	**Fri 5/4/12**	
22	✓	**Candidacy Exam**	**73 days**	**Mon 12/19/11**	**Wed 3/28/12**	
23	✓	Prepare for exam	67 days	Mon 12/19/11	Tue 3/20/12	
24	✓	Take exam	6 days	Wed 3/21/12	Wed 3/28/12	23
25	✓	**PDA+PTFE Study**	**120 days**	**Mon 5/7/12**	**Fri 10/19/12**	
26	✓	Design experiment	10 days	Mon 5/7/12	Fri 5/18/12	21
27	✓	Purchase materials	15 days	Mon 5/21/12	Fri 6/8/12	26
28	✓	Fabricate Samples	15 days	Mon 6/11/12	Fri 6/29/12	27
29	✓	Friction test	30 days	Mon 7/2/12	Fri 8/10/12	28
30	✓	Optical Microscope	4 days	Mon 8/13/12	Thu 8/16/12	29
31	✓	SEM	4 days	Fri 8/17/12	Wed 8/22/12	30
32	✓	XPS	6 days	Thu 8/23/12	Thu 8/30/12	31
33	✓	Write Manuscript	36 days	Fri 8/31/12	Fri 10/19/12	32
34	✓	Heating optimization	262 days	Mon 5/7/12	Tue 5/7/13	
35		**PDA+PTFE+Cu Study**	**420 days**	**Tue 5/7/13**	**Mon 12/15/14**	
36	✓	Design experiment	10 days	Tue 5/7/13	Mon 5/20/13	
37	✓	Purchase materials	20 days	Tue 5/21/13	Mon 6/17/13	36
38	✓	Fabricate Samples	40 days	Tue 6/18/13	Mon 8/12/13	37
39	✓	Friction test	30 days	Tue 8/13/13	Mon 9/23/13	38
40	✓	Optical Microscope	6 days	Tue 9/24/13	Tue 10/1/13	39
41	✓	SEM	6 days	Wed 10/2/13	Wed 10/9/13	40
42	✓	XPS	6 days	Thu 10/10/13	Thu 10/17/13	41
43	✓	AFM	6 days	Fri 10/18/13	Fri 10/25/13	42
44		Write manuscript	290 days	Mon 10/28/13	Fri 12/5/14	43

Appendix E: Software Used in Research and Dissertation Generation

Computer #1:

Model #: Dell Inspiron 15R

Serial #: 4NKFWA00

Location: Home

Owner: Sam Beckford

Software:

Name: Microsoft Office 2010

Purchased by: University of Arkansas

Software:

Name: Inkscape 0.48.5

Purchased by: Open source software

Software:

Name: ImageJ 1.46r

Purchased by: Open source software

Computer #2:

Model #: Bruker CPU

Serial #: 313060-004

Location: ENRC 3414

Owner: Min Zou

Software:

Name: Bruker Nanoscope Suite

Purchased by: Min Zou

Computer #3:

Model #: Dell Precision T7500

Serial #: 1ML1PS1

Location: ENRC 3414

Owner: Min Zou

Software:

Name: Microsoft Office 2010

Purchased by: Mechanical Engineering Department

Computer #4:

Model #: Dell Vostro 220

Serial #: BG23JL1

Location: NANO 131

Owner: Min Zou

Software:

Name: ToupView

Purchased by: Min Zou

Computer #5:

Model #: Dell Vostro 220

Serial #: CG23JL1

Location: NANO 131

Owner: Min Zou

Software:

Name: Microsoft Office 2010

Purchased by: Min Zou

Software:

Name: ImageJ 1.46r

Purchased by: Open source software

Computer #6:

Model #: Dell Dimension 2400

Serial #: 3F5TK71

Location: NANO 132

Owner: Min Zou

Software:

Name: SGServer

Purchased by: Min Zou

Appendix F: All publications Published, Submitted, and Planned

F.1. Published Papers

Beckford, S., Langston, N., Zou, M., 2011, "Fabrication of Durable Hydrophobic Surfaces through Surface Texturing," Applied Surface Science, **257**(13) pp. 5688-5693.

Zou, M., Beckford, S., Wei, R., 2011, "Effects of Surface Roughness and Energy on Ice Adhesion Strength," Applied Surface Science, **257**(8) pp. 3786-92.

Beckford, S., and Zou, M., 2011, "Micro/nano Engineering on Stainless Steel Substrates to Produce Superhydrophobic Surfaces," Thin Solid Films, **520**(5) pp. 1520-1524.

Beckford, S., Wang, A., Zou, M., 2011, "Wear-Resistant PTFE/SiO_2 Nanoparticle Composite Films," Tribology Transactions, 54, pp. 849-858.

Beckford, S., Zou, M., 2014, "Wear resistant PTFE thin film enabled by a polydopamine adhesive layer," Applied Surface Science, 292, pp. 350-356.

Beckford, S., Cai, J., Chen, J., Zou, M., 2014, "Use of Au Nanoparticle-Filled PTFE Films to Produce Low-Friction and Low-Wear Surface Coatings," Tribology Letters, 56, pp. 223-230.

Beckford, S., Cai, J., Chen, J., Zou, M., 2014, "Use of Au Nanoparticle-Filled PTFE Films to Produce Low-Friction and Low-Wear Surface Coatings," Tribology Letters, 56, pp. 223-230.

F.2. Planned Papers

Combined effect of incorporating polydopamine as an adhesive layer and Copper nanoparticle filler in PTFE

Appendix G: Permission to use copywrited material

ELSEVIER LICENSE
TERMS AND CONDITIONS
Dec 01, 2014

This is a License Agreement between Samuel Beckford ("You") and Elsevier ("Elsevier") provided by Copyright Clearance Center ("CCC"). The license consists of your order details,
the terms and conditions provided by Elsevier, and the payment terms and conditions.

All payments must be made in full to CCC. For payment instructions, please see information listed at the bottom of this form.

Supplier Elsevier Limited
The Boulevard,Langford Lane
Kidlington,Oxford,OX5 1GB,UK
Registered Company Number 1982084
Customer name Samuel Beckford
Customer address Nano 104
FAYETTEVILLE, AR 72701
License number 3520280422829
License date Dec 01, 2014
Licensed content publisher Elsevier
Licensed content publication Wear
Licensed content title Friction and wear of PTFE — a review
Licensed content author S.K. Biswas,Kalyani Vijayan
Licensed content date 15 October 1992
Licensed content volume number
158
Licensed content issue number
12
Number of pages 19
Start Page 193
End Page 211
Type of Use reuse in a thesis/dissertation
Intended publisher of new work
other
Portion figures/tables/illustrations
Number of figures/tables/illustrations
1
Format both print and electronic
Are you the author of this Elsevier article?
No

Will you be translating? No
Title of your thesis/dissertation

Wear Resistant Polydopamine/PTFE Nanoparticle Composite Coating for Dry Lubrication Applications
Expected completion date Dec 2014
Estimated size (number of pages)
198
Elsevier VAT number GB 494 6272 12
Permissions price 0.00 USD
VAT/Local Sales Tax 0.00 USD / 0.00 GBP
Total 0.00 USD
Terms and Conditions

JOHN WILEY AND SONS LICENSE
TERMS AND CONDITIONS

Dec 01, 2014

This is a License Agreement between Samuel Beckford ("You") and John Wiley and Sons
("John Wiley and Sons") provided by Copyright Clearance Center ("CCC"). The license consists of your order details, the terms and conditions provided by John Wiley and Sons, and the payment terms and conditions.

All payments must be made in full to CCC. For payment instructions, please see information listed at the bottom of this form.

License Number 3520280050891
License date Dec 01, 2014
Licensed content publisher John Wiley and Sons
Licensed content publication Advanced Functional Materials
Licensed content title NonCovalent SelfAssembly and Covalent Polymerization CoContribute to Polydopamine Formation
Licensed copyright line Copyright © 2012 WILEYVCH Verlag GmbH & Co. KGaA, Weinheim
Licensed content author Seonki Hong,Yun Suk Na,Sunghwan Choi,In Taek Song,Woo Youn Kim,Haeshin Lee
Licensed content date Jul 5, 2012
Start page 4711
End page 4717
Type of use Dissertation/Thesis
Requestor type University/Academic
Format Print and electronic
Portion Figure/table
Number of figures/tables 1
Original Wiley figure/table number(s) Scheme 1
Will you be translating? No
Title of your thesis / dissertation Wear Resistant Polydopamine/PTFE Nanoparticle Composite Coating for Dry Lubrication Applications
Expected completion date Dec 2014
Expected size (number of pages) 198
Total 0.00 USD
Terms and Conditions

JOHN WILEY AND SONS LICENSE
TERMS AND CONDITIONS
Dec 01, 2014
This is a License Agreement between Samuel Beckford ("You") and John Wiley and Sons
("John Wiley and Sons") provided by Copyright Clearance Center ("CCC"). The license consists of your order details, the terms and conditions provided by John Wiley and Sons, and the payment terms and conditions.
All payments must be made in full to CCC. For payment instructions, please see information listed at the bottom of this form.
License Number 3520290229046
License date Dec 01, 2014
Licensed content publisher John Wiley and Sons
Licensed content publication Wiley Books
Licensed content title Introduction to Tribology
Book title Introduction to Tribology
Licensed copyright line Copyright © 2002, John Wiley and Sons
Licensed content author Bharat Bhushan
Licensed content date Aug 1, 2002
Type of use Dissertation/Thesis
Requestor type University/Academic
Format Print and electronic
Portion Figure/table
Number of figures/tables 1
Original Wiley figure/table number(s)
3.2.1
Will you be translating? No
Title of your thesis / dissertation
Wear Resistant Polydopamine/PTFE Nanoparticle Composite Coating for Dry Lubrication Applications
Expected completion date Dec 2014
Expected size (number of pages)
198
Total 0.00 USD

NATURE PUBLISHING GROUP LICENSE TERMS AND CONDITIONS

Dec 04, 2014

This is a License Agreement between Samuel Beckford ("You") and Nature Publishing Group ("Nature Publishing Group") provided by Copyright Clearance Center ("CCC"). The license consists of your order details, the terms and conditions provided by Nature Publishing Group, and the payment terms and conditions.

All payments must be made in full to CCC. For payment instructions, please see information listed at the bottom of this form.

License Number	3522201090921
License date	Dec 04, 2014
Licensed content publisher	Nature Publishing Group
Licensed content publication	Nature
Licensed content title	Friction and Transfer of Polytetrafluoroethylene
Licensed content author	K. RACHEL MAKINSON, D. TABOR
Licensed content date	Feb 1, 1964
Volume number	201
Issue number	4918
Type of Use	reuse in a dissertation / thesis
Requestor type	academic/educational
Format	print and electronic
Portion	figures/tables/illustrations
Number of figures/tables/illustrations	1
Figures	Figure 3
Author of this NPG article	No
Your reference number	None
Title of your thesis / dissertation	Wear Resistant Polydopamine/PTFE Nanoparticle Composite Coating for Dry Lubrication Applications
Expected completion date	Dec 2014
Estimated size (number of pages)	198
Total	0.00 USD
Terms and Conditions	

Samuel Beckford <sbeckfor@email.uark.edu>

permission to use figure

PNAS Permissions <PNASPermissions@nas.edu> Tue, Dec 2, 2014 at 4:12 PM
To: Samuel Beckford <sbeckfor@email.uark.edu>

Permission is granted for your use of the figure as described in your message. Please cite the PNAS article in
full, and include "Copyright (2006) National Academy of Sciences, U.S.A." as a copyright note. Because this
material published between 1993 and 2008, a copyright note is needed. Let us know if you have any questions.

Best regards,
Kay McLaughlin for
Diane Sullenberger
Executive Editor
PNAS

From: Samuel Beckford [mailto:sbeckfor@email.uark.edu]
Sent: Monday, December 01, 2014 5:55 PM
To: PNAS Permissions
Subject: permission to use figure

I would like to request permission to use Fig. 1 in "Singlemolecule
mechanics of mussel adhesion" for use in
my dissertation, "Wear Resistant Polydopamine/PTFE Nanoparticle Composite Coating for Dry Lubrication
Applications".

1. My name is Samuel Beckford, University of Arkansas, graduate research assistant
2. My address is: 731 W Dickson St., Fayetteville, AR 72701; 4792636922; sam.beckford@gmail.com
3. The article to be used is: volume number 103, issue number 35, and issue date July 3, 2006
4.Article title "Singlemolecule mechanics of mussel adhesion"
5. Authors: Haeshin Lee, Norbert F. Scherer, and Phillip B. Messersmith
6. page 12999
7. Figure 1

Following information is about the intended use of the material:

1. Used in a dissertation: "Wear Resistant Polydopamine/PTFE Nanoparticle Composite Coating for Dry
Lubrication Applications"
2. Samuel Beckford
3. N/A it is a dissertation
4. N/A it is a dissertation
5. 4 copies
6. Intended audience is academic professors
7. work is nonprofit

regards,
Sam Beckford